



INSTITUTO POLITÉCNICO NACIONAL

ESCUELA SUPERIOR DE INGENIERÍA MECÁNICA Y ELÉCTRICA
UNIDAD ZACATENCO
SECCIÓN DE ESTUDIOS DE POSGRADO E INVESTIGACIÓN
LABORATORIO DE INGENIERÍA TÉRMICA E HIDRÁULICA APLICADA

“THEORETICAL AND NUMERICAL ANALYSIS OF EROSION IN STEAM TURBINE BLADES”

THESIS

FOR THE DEGREE OF

DOCTOR OF MECHANICAL ENGINEERING SCIENCE
ENERGETIC OPTION

PRESENTED BY:

M. C. FERNANDO RUEDA MARTÍNEZ

THESIS DIRECTOR:

DR. MIGUEL TOLEDO VELÁZQUEZ



MÉXICO, D.F., DECEMBER 2011



INSTITUTO POLITÉCNICO NACIONAL
SECRETARÍA DE INVESTIGACIÓN Y POSGRADO

SIP-14

ACTA DE REVISIÓN DE TESIS

En la Ciudad de México, D.F. siendo las 18:00 horas del día 2 del mes de Diciembre del 2011 se reunieron los miembros de la Comisión Revisora de la Tesis, designada por el Colegio de Profesores de Estudios de Posgrado e Investigación de E. S. I. M. E. para examinar la tesis titulada:

“THEORETICAL AND NUMERICAL ANALYSIS OF THE EROSION IN STEAM TURBINE BLADES”.

Presentada por el alumno:

RUEDA
Apellido paterno

MARTÍNEZ
Apellido materno

FERNANDO
Nombre(s)

Con registro:

A	0	8	0	5	7	1
---	---	---	---	---	---	---

aspirante de:

DOCTOR EN CIENCIAS EN INGENIERIA MECÁNICA

Después de intercambiar opiniones los miembros de la Comisión manifestaron **SU APROBACIÓN DE LA TESIS**, en virtud de que satisface los requisitos señalados por las disposiciones reglamentarias vigentes.

LA COMISIÓN REVISORA

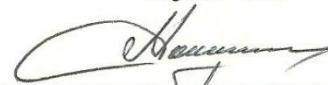
Director(a) de tesis


DR. MIGUEL TOLEDO VELÁZQUEZ

Presidente



DR. SAMUEL ALCÁNTARA MONTES

Segundo Vocal


DR. GEORGIY POLUPAN

Secretario

Tercer Vocal


DR. FLORENCIO SÁNCHEZ SILVA


DR. IGNACIO CARVAJAL MARISCAL

EL PRESIDENTE DEL COLEGIO


DR. JAIME ROBLES GARCÍA





**INSTITUTO POLITECNICO NACIONAL
SECRETARIA DE INVESTIGACION Y POSGRADO**

CARTA CESION DE DERECHOS

En la Ciudad de México, D. F., el día **6** del mes de **diciembre** del año **2011**

el(la) que suscribe **Fernando Rueda Martínez** alumno (a) del Programa de

Doctorado en Ciencias de la Ingeniería Mecánica opción Energética

con número de registro **A080571** adscrito a la Sección de Estudios de Posgrado e Investigación de la E.S.I.M.E. Unidad Zacatenco, manifiesta que es autor(a) intelectual del presente Trabajo de Tesis

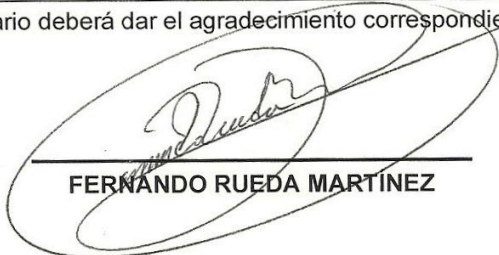
bajo la dirección del **Dr. Miguel Toledo Velázquez** y cede los derechos del

trabajo intitulado: **"Theoretical and Numerical Analysis of the Erosion in Steam Turbine Blades"** al

Instituto Politécnico Nacional para su difusión, con fines Académicos y de Investigación.

Los usuarios de la información no deben reproducir el contenido textual, graficas o datos del trabajo sin el permiso expreso del autor y/o director del trabajo. Este puede ser obtenido escribiendo a la siguiente dirección: **ing.fernandorueda@yahoo.com**

Si el permiso se otorga, el usuario deberá dar el agradecimiento correspondiente y citar la fuente del mismo.



FERNANDO RUEDA MARTÍNEZ

Dedicatoria

A mis padres **Fernando Rueda López** y **Petra Martínez Barreiro**, y a mis hermanos **Aldo Antonio Rueda Martínez** y **Claudia Patricia Rueda Martínez** que siempre me han dado todo su inagotable amor, cariño, apoyo, sacrificio, paciencia y confianza. También los miembros de la familia que ya no están con nosotros.

AGRADECIMIENTOS

Un sincero agradecimiento a mi director de tesis, el Dr. Miguel Toledo Velázquez, por su valioso asesoramiento, sus consejos y el estímulo de seguir creciendo intelectualmente.

A los miembros de la Comisión Revisora de este trabajo:

Dr. Miguel Toledo Velázquez,
Dr. Florencio Sánchez Silva,
Dr. José Ángel Lodegario Ortega Herrera,
Dr. Samuel Alcántara Montes
Dr. Georgiy Polupan,
Dr. Ignacio Carvajal Mariscal,

y a todos los profesores que integran el Laboratorio de Ingeniería Térmica e Hidráulica Aplicada, que con su excelente consejo, profesionalismo y enseñanza me han instruido desde el inicio del posgrado y hasta la terminación de este trabajo.

Al personal administrativo del LABINTHAP y de Control Escolar del IPN, gracias por su apoyo y paciencia.

DEDICATORIA

Un agradecimiento al Lic. Jesús Espinosa Morales por su invaluable comprensión y apoyo, y que al tenderme la mano depositó en mí el ánimo de no claudicar y seguir adelante.

Al Consejo Nacional de Ciencia y Tecnología y al Programa Integral de Formación de Investigadores, por el apoyo que he recibido y que ha sido destinado para culminar mis estudios.

A mi amigo Diego Rodrigo Flores Galindo y a mis compañeros de estudios de posgrado. Gracias por compartir su valioso tiempo conmigo.

Quiero agradecer:

Especialmente a Maria Elena Hernández Castillo, por ser mi inspiración y ocupar un lugar único en mi corazón.

A mis amigos y compañeros profesores en el atletismo Víctor Manuel González Cruz y Rogelio Gaytan Monroy. A mis alumnos, en especial a Kevin Gaytan Becerra, Israel Sánchez Castillo y Jorge Arturo Alonzo Pech y a todo el equipo de Burros Negros del IPN, y a mis amigos de competencia y de la vida Carlos y David Juárez Santiago, a Humberto Alfredo Opazo Pérez, a Juan José Reyes Vázquez y su hermosa familia, a José Alejandro Varela Guizar. Al Director de Desarrollo y Fomento Deportivo del IPN, el Ing. Rodolfo Alejandro Romo Mexía Gutiérrez por su invaluable apoyo y confianza. A todos mis amigos en el deporte, de Coatzacoalcos, Ver., y del Instituto Politécnico Nacional.

A mis amigos y profesores de la Esc. Sec. y de Bach. Gral. Miguel Alemán González, por darme parte de los mejores recuerdos de mi vida.

A las personas que con su amistad sincera, sus oraciones, su ayuda incondicional y su motivación influyen en mi vida de manera positiva.

GENERAL INDEX	i
Index of figures	iii
Index of tables	iv
Nomenclature	v
Objective	vii
Justification	viii
Resumen	ix
Abstract	x
Introduction	xi
Chapter I Droplet Formation in Steam Turbine	1
1.1 Droplet Formation	3
1.2 Thermodynamics	7
1.3 Cluster Formation	11
1.4 Spherical Cluster as a Drop	13
1.5 Collision Process	15
1.6 Compressible Droplet Impact	20
1.7 Wet in Steam Turbines	24
Chapter II Numerical Modeling Procedure in the Stator Blade Cascade	30
2.1 Conditions for Calculation of Drop Movement	32
2.2 Transonic Stream in the Mesh	32
2.3 Velocity Fields	35
2.4 Conservation Laws	37
2.4.1 Dimension of the Conservation Laws	39
2.5 Condition Periodicity in the Profile	41
2.5.1 Boundary Condition in Inlet and Outlet Plane	43
2.5.2 Boundary Condition for the Profile Outline	44
2.5.3 Condition in Discharge in the Trailing Edge	45
2.5.4 Direction of Flow within the Stagnation Point	46

2.6 Numerical Approximation of the Balance Equations	47
2.7 Criterion to Stop the Computing Method	48
2.8 Transformation Coordinates	49
2.8.1 Conditions to Mesh	51
2.8.2 Mesh Organization	51
2.9 Balance Equations for Turbulent Boundary Layer	52
2.9.1 Integral Condition for the Impulse	53
2.10 Drop Movement for Individual Drop	54
2.11 Interpolation of Flow Parameters Between the Mesh Points	60
2.12 Drop Distribution in the Mesh Outlet Plane	60
2.13 Particular Data of Stator Blade in the Last Stage of Low Pressure	63
2.14 Calculation and Control of the Transonic Stream	69
2.15 Diagram of Calculations for Flow Pattern with Liquid Droplets	71
Chapter 3 Results Analysis	73
3.1 Flow Calculations	75
3.2 Mach Distribution	78
3.3 Pressure Distribution	80
3.4 Velocity Distribution Calculation	82
3.5 Enthalpy Calculation	85
3.6 Impulse Calculation	87
3.7 Displacement Thickness Calculation	89
3.8 Calculation of Energy Thickness	93
3.9 Calculation of Friction Coefficient	95
3.10 Presence of Droplets in the Flow	98
3.11 Comparison with other Works	99
Conclusions	103
Bibliography	106
Annex	113
Papers Generated	121

Index of Figures

Figure 1.1: Water phase diagram in the pressure-temperature plane.	4
Figure 1.2 According to the Stillinger definition.	5
Figure 1.3 Dependence of the droplet radius of the Gibbs free energy.	9
Figure 1.4: Work of cluster formation.	10
Figure 1.5: Determination of the surface area of a liquid droplet.	12
Figure 1.6: Cluster formed in a collision of liquid drops.	14
Figure 1.7: Collision of a drop with a wall.	17
Figure 1.8: Impact of liquid drop on solid surface.	18
Figure 1.9: Impact of a spherical liquid drop on a rigid surface.	21
Figure 1.10: Scheme of impact of the drop against a plane rigid surface.	22
Figure 1.11: Mollier diagram, with regions of impurity.	25
Figure 1.12: Topology of phase transition in a LP steam turbine.	26
Figure 1.13: Cross section of a turbine with locations of erosion.	28
Figure 1.14: Vortices that are generated in the exit of the stage.	29
Figure 2.1: Designation of the zone of flow by mesh.	33
Figure 2.2: Range of periodicity and direction of flow.	42
Figure 2.3: The net indices.	47
Figure 2.4: Rotation in Cartesian coordinate system.	50
Figure 2.5: Representation of the boundary layer thicknesses.	54
Figure 2.6: Mesh indices.	60
Figure 2.7: Nomenclature for the moisture distribution in the mesh.	61
Figure 2.8: Stator blade 980BE23 of low pressure section.	67
Figure 2.9: Mesh flow channel.	67
Figure 2.10: Flow chart of the methodology.	71
Figure 3.1: Suction and pressure side of stator blade.	75
Figure 3.2: Graphic that shows the Mach values.	78
Figure 3.3: Graphic that shows the pressure values.	81
Figure 3.4: Graphic that shows the behavior of the velocity distribution.	83
Figure 3.5: Graphic that shows the behavior of the velocity distribution.	84

Figure 3.6: Graphic that shows the total enthalpy calculation.	85
Figure 3.7: Graphic that shows the enthalpy calculation in the suction.	85
Figure 3.8: Levels of reference in the blade channel.	87
Figure 3.9: Graphic that shows the impulse calculation in the suction.	88
Figure 3.10: Graphic that shows the behavior of boundary layer.	91
Figure 3.11: Graphic that shows the behavior of boundary layer.	92
Figure 3.12: Graphic that shows the behavior of loss of energy.	93
Figure 3.13: Graphic that shows the behavior of loss of energy.	94
Figure 3.14: Graphic that shows the behavior of friction coefficient.	96
Figure 3.16: Graphic that shows the boundary layer parameters.	100
Figure 3.17: Graphic that shows the surface pressure distributions	101

Index of Tables

Table 3.1: Coordinates of suction and pressure side of stator blade.	76
Table 3.2: Mach number throughout stator blade channel.	79
Table 3.3: Pressure throughout stator blade channel.	81
Table 3.4: Velocity distribution on the suction side.	83
Table 3.5: Velocity distribution on the pressure side.	84
Table 3.6: Enthalpy throughout stator blade channel.	86
Table 3.7: Impulse values throughout stator blade channel.	88
Table 3.8: Boundary layer thickness values.	91
Table 3.9: Boundary layer thickness values throughout pressure.	92
Table 3.10: Loss energy thickness values throughout suction side.	94
Table 3.11: Loss energy thickness value throughout pressure side.	95
Table 3.12: Friction coefficient values throughout suction side.	96
Table 3.13: Friction coefficient values throughout pressure side stator.	98

Nomenclature

\vec{A} : Lift strength.

A_1, A_2, A_3, A_4 : Borders of the contact line.

B: Stream width.

C_f : Friction coefficient.

c_{DO} : Drop velocity.

$\bar{c}_{D1,i}$: Steam medium velocity

c_{TO} : Steam velocity.

c_x : Field velocity in x

c_y : Field velocity in y

d_T Drop diameter

\vec{G} : Gravity force.

h_{tot} : Total enthalpy.

\vec{K}_E : Electrostatic forces.

K_κ : Volume of the element.

K_n : Knudsen number

\vec{K}_P : Field strength due to a pressure gradient.

m_T : Drop mass

M_δ : Local Mach number.

n : Polytropic exponent

P: Pressure.

R_c Radius of cluster.

Re Reynolds number

r_{drop} Radius of drop.

r_{str} Radius of the stream of the contact line.

r_3 Radius of the contact line.

S_{ij} : Length of the element.

t: Time.

\vec{T} : Force of inertia.

U: Axial Velocity.

V: Peripheral Velocity.

w : Impact velocity of the drop.

w_{Dx} : Relative velocity in x

w_{Dy} : Relative velocity in y

\vec{W} : Strength.

We: Weber number.

\vec{W}_M : Strength due to additional movement along steam mass.

w_{rel} Relative velocity

x: Quality.

β_{2is} : Theoretically exit angle.

$\Delta\tau$: Time interval.

ΔV_k Volume in hexagonal space k.

δ_1 : Displacement thickness.

δ_2 : Pulse loss thickness.

δ_2 : Energy thickness.

Φ : Friction Force.

$\psi_{T,i}$ Drop course

λ Mean free path of the molecules

σ : Surface Tension

ρ : Density

η_p : Polytropic efficiency.

Objective

To develop a procedure of calculation for the flow pattern with liquid droplets those cause the problem of erosion in the exit plane of the stator crown of the last stages, in order to have the knowledge of the behavior of the stator blades geometry, like the channels of the steam flow and the drops as a set in the low pressure steam turbine.

The previous thing is necessary to the exit of the stator crown, since the phenomenon of the erosion as a set also makes its appearance in the following crown of blades, well-known as rotor crown, being observed damages in the surface of these.

An analysis will become of the different foundations, like mass, impulse and enthalpy, for the bidimensional calculation of the analysis of transonic flow in the crown of turbine blades, in condition of which the behavior of the flow is stationary and free of friction.

Justification

The estator-rotor crown of the last stages is selected, since the damages by erosion are here remarkably and the phenomenon of condensation of the steam flow is analyzed with the nucleation theory, to know more thorough the causes than they bring about his wearing down due to the origin of drops, and to have more information about the erosion problems, according to the data of design of the turbine.

Resumen

En la sección de baja presión de las turbinas de vapor los daños debido a la erosión son pronunciados, llegando a observarse en todas las etapas, puesto que la generación de micropartículas de líquido implica el impacto sobre los álabes, ocasionando mayores problemas de erosión en los últimos pasos por el incremento de la humedad.

Se establece una metodología de cálculo de la distribución de velocidad y de presión en base a un flujo sin fricción, bidimensional, estacionario, homogéneo y transónico. También se presentan las condiciones que gobiernan la sección de baja presión de las turbinas de vapor en los últimos pasos en relación al movimiento aproximado de las gotas que fluyen a través del vapor y su acumulación en la cascada de álabes estatores.

Este estudio se utiliza para desarrollar un código en lenguaje Fortran que calcula la distribución de presión y velocidad en la salida de los álabes estatores que tienen condiciones de flujo de vapor húmedo, para entender las causas que origina el fenómeno de erosión sobre los álabes de los últimos pasos en la sección de baja presión de las turbinas de vapor.

Abstract

In the low pressure section of the steam turbines the damages due to the erosion are pronounced becoming remarkable in all the stages, since the generation of water liquid microparticles implies the impact on the blades having majors problems of erosion in the last stages by the increase of the humidity.

The methodology of calculation of the velocity and pressure distribution on the basis of the frictionless, two-dimensional, stationary, transonic and homogenous flow is established. The knowledge of conditions that govern the low pressure section of steam turbines in the last stage to have an approximate movement of the droplets in the blade cascades and the accumulation of droplets on the stator blades, flowing through the steam, is presented.

This study is used for developing a code in Fortran about the pressure and velocity and pressure distribution in the output of stator blades that have flow conditions of wet steam, in order to understand the causes that originate the erosion on the blades of the last stages in the low pressure section of steam turbines.

Introduction

The cycle of steam in a thermoelectrical power plant begins when the feed water enters to the steam generator. There it happens, due to of the process of combustion and heat transference, the conversion of the water to steam by means of the auxiliary equipment. Normally, when exists units of great power or small power in the turbine of high pressure, intermediate pressure and low pressure, it occurs the process of expansion of the steam, as is shown in Fig.(I.1), in the part of equipment and its enthalpy-entropy diagram.

If the enthalpy-entropy diagram is observed carefully, it is had that the expansion crosses in a certain moment the line of saturation in the diagram of Mollier, as it is known to date. By the information in literature articles and corresponding books, it is known that the steam has another behavior when crossing the saturation line in the last stage passages of the expansion turbine.

In these stages the steam flow contains liquid water particles and their impact against the blades causes different problems, for example, vibrations, changes in the flow velocities, imbalance in the meridian line, corrosion and erosion. These liquid water particles are originated by a phenomenon that in technical literature is known like nucleation. This entails to define to the nucleus like a particle set (atoms, ions, molecules, etc.) ready in ordinate form, so that they can serve as antecedent of growth of the drops (Benavente, 2002). The nucleation of drops will have origin when its temperature is reduced below the condensation point; this is, minor to 90°C. According to the nucleation theory, when the formation of the drops begins and they achieve to surpass their critical radius (of the order of 10^{-3} μm), these grow until reaching a stable size (0,1 to 100 μm ; Gerber & Mousavi, 2007), and they are united with others forming a molecular group denominated conglomerate, as is illustrated in Fig.(I.2).

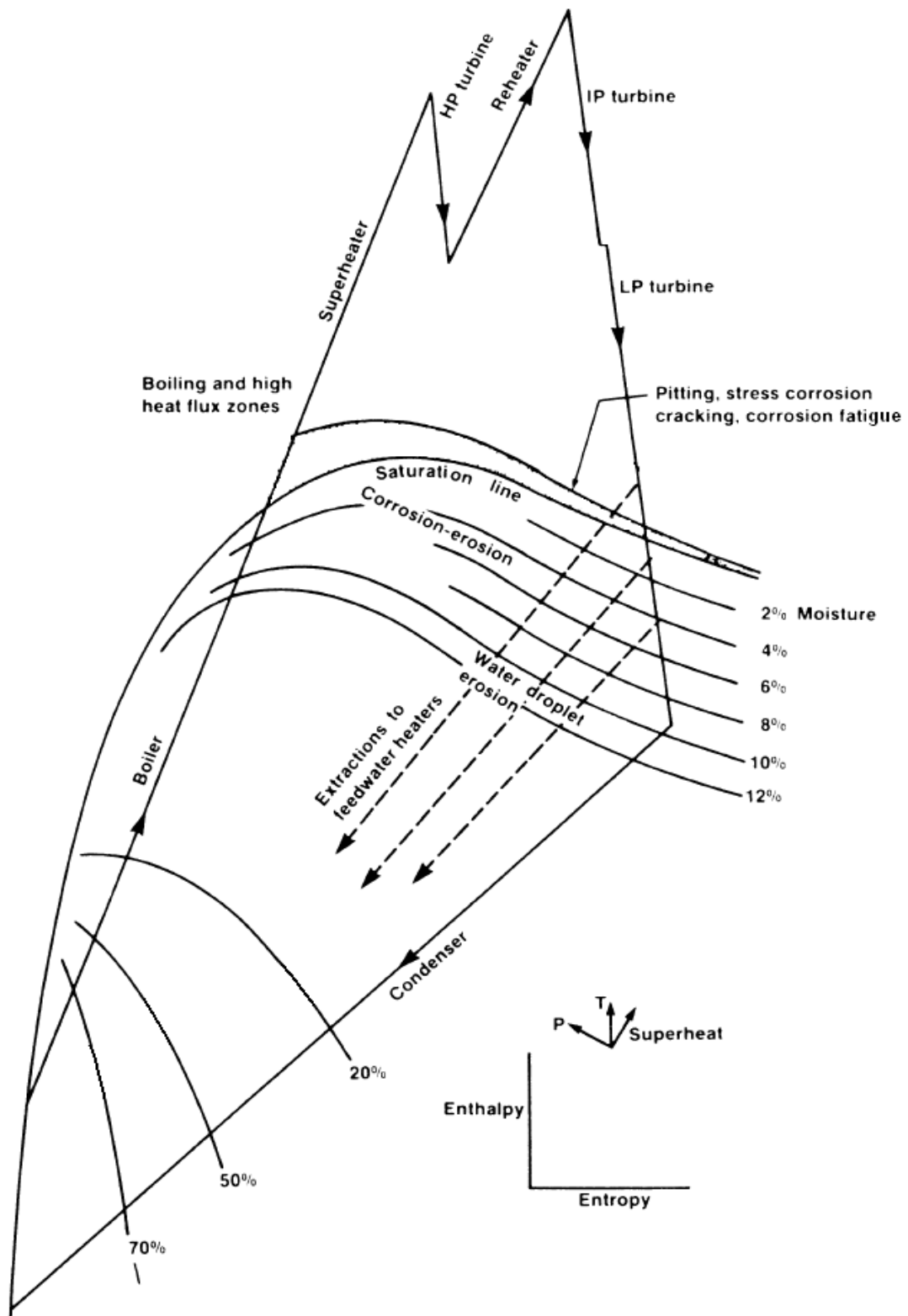


Figure I.1: Diagram of Mollier shows the equipment that takes part in the cycle of steam with overheating and illustrates the regions where it concentrates the corrosion and the erosion by drops of water (Jonas, 2001).

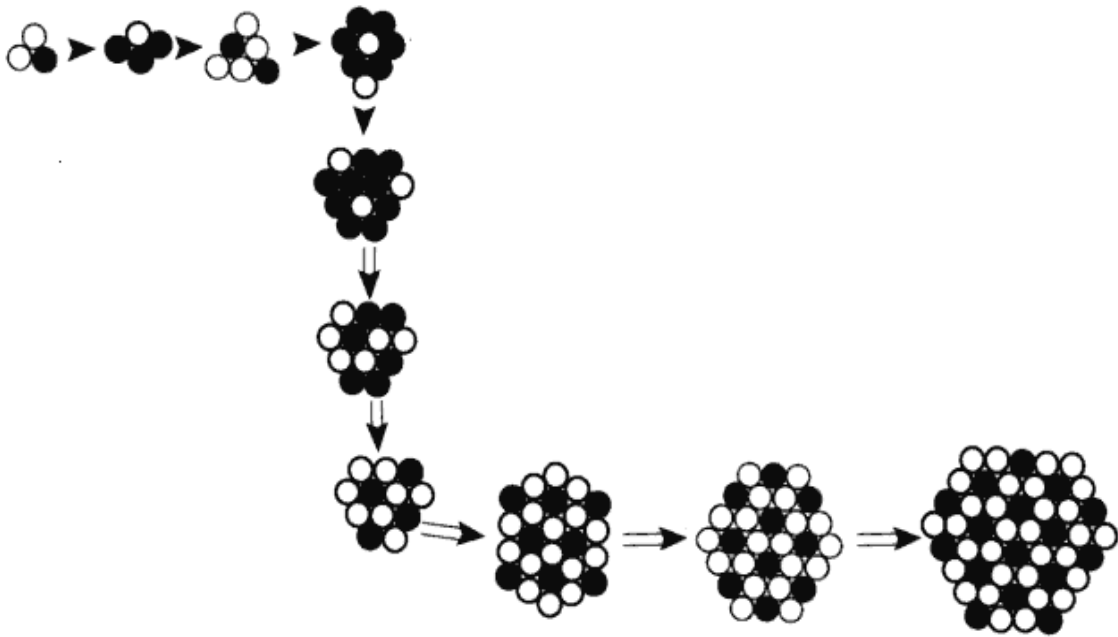


Figure I.2: Formation of a molecular conglomerate (Schmelzer, 2005).

Some researchers mention that, during the transition of the dry steam to the wet one, the union between the molecular conglomerates exists, that is, coalescences (Ford, 2004; Bakhtar, Schmelzer, 2005). The coalescences are majors when the conglomerate reaches a critical dimension that will allow to make them stable and homogenous, being the properties of these molecular conglomerates the center of the theory of nucleation of origin of liquid microparticles.

The effect of this phenomenon in the steam flow has consequences in the performance of the turbomachinery, since the interactions of the set of the wet steam with the blades gradually originate a wearing down in the surface of the same; so that appear tracks of roughness and, sometimes, phenomena of erosion very pronounced, that it is normal to observe in the blades of the last stages of the steam turbines, as well as losses, as much in the leading edge, like in the suction side, pressure side and trailing edges. So that the material of the blades is diminished and the rotor stability in the turbine is lost, and consequently it is had in the maintenances that make decisions to change blades or complete crowns.

Examples in Fig.(I.3) and Fig.(I.4) show to crowns of blades with erosion in their pressure side and their peripheral zone in the leading edges (pictures taken to the rotor crown of the last stage of the steam turbine installed in the Thermoelectrial Power Station Valley of Mexico; Rueda, 2006).



Figure I.3: Blades damaged by erosion in the low pressure section (Rueda, 2006).



Figure I.4: Wearing in the peripheral zone (Rueda, 2006).

In the low pressure section of the steam turbines the damages are pronounced becoming remarkable in all the stages, since the generation of liquid microparticles implies the impact on the blades having majors problems of erosion in the last stages by the increase of the humidity.

The necessity to understand the transition of the dry steam to the wet one in the steam turbines and the technological problems that appear it is what motivates to this study. This work implies a calculation procedure at the outlet of a set of blades when the flow has a certain wet degree, in order to have the knowledge of the behavior of the stator blades geometry, like the channels of the steam flow and the drops as a set in the low pressure steam turbine.

CHAPTER

DROPLETS FORMATION IN STEAM
TURBINES

1

One of the most important properties of matter is its capacity to take different physical forms for different values of parameters such as temperature or pressure; for example, the condensation of the vapor by nucleation of droplets. Such changes are fundamentally characterized on the part of physical systems to minimize their free energy by any available means.

A practical situation where the existence of water droplets creates problems is the behavior of steam in turbines. The temperature and pressure gradients are such that these droplets might nucleate with undesirable effects on the performance of the machine, including the erosion of the turbine blades due to the repeated impact on them. On the other hand the steam must be expanded as much as possible to extract the most work from it. The need for an understanding of the transition from dry to wet steam in turbines has motivated this thesis.

Being the liquid impact erosion a major technological problem in steam turbines, the interaction of drops, droplets or clusters, plays an important role in the low pressure section. The understanding of drops collision is pertinent to a broad range of processes including nucleation, growth and cluster coalescence. The erosion that appears on the blades due to repetitive impact of the great droplets causes damage in the surface of them and, therefore, changes in the flow conditions of the stage.

In this chapter an analysis about the formation of droplets in the steam turbines and their impact on the rigid surface of blades is presented. The treatment of the cluster of droplets as one small liquid droplet is based on the assumption that these droplets are spherical, equal in size with others and water chemistry issues are not considered. The impact of a droplet of radius r , moving with a velocity V towards the rigid surface considering the compression of the liquid adjacent to the surface, is examined. The subject is concentrated on the droplets that cause the erosion on blades of steam turbines, which constitutes also a matter of investigation.

1.1 Droplet formation

A phase transition or phase change is the transformation of a thermodynamic system from one phase to another. There are some phase transitions which occur when experimental conditions change such that a new phase becomes stable, for example, the evaporation from the surface of a pure liquid. However, there are other phase transitions for which this is not the case. An example of phase change is condensation of a gas. Gases supersaturated need to nucleate before a new phase can be formed. Melting and boiling (i.e., phase changes which almost always occur at equilibrium) [1] differ from condensation and crystallization because they occur at free surfaces (stable).

In general, a phase is defined as a set of states of a macroscopic physical system that have relatively uniform chemical composition and physical properties (i.e. density, crystal structure, and so forth). The different phases of a system can be represented using a phase diagram, where the axes of the diagram are the relevant thermodynamic variables, like temperature and pressure. The phase diagram of a typical case of water is sketched in Fig. (1.1). In this diagram, the open spaces correspond to the stable phases, which are separated by lines corresponding to the phase boundaries, or coexisting lines.

When a system passes from one stable phase to another, crossing a phase boundary, a change in its physical properties occurs. In this case the system is said to undergo a phase transition. However, in some cases a phase can be stable for a relatively long time even beyond the line of coexistence, in a region of the phase diagram where a different phase would have lower free energy [2]. These systems are said metastable with respect to the equilibrium stable phase, concept which describes state of delicate equilibrium; in other words, a system is in a metastable state when it is in equilibrium (not changing with time) but is susceptible to fall into lower-energy states with only slight interaction.

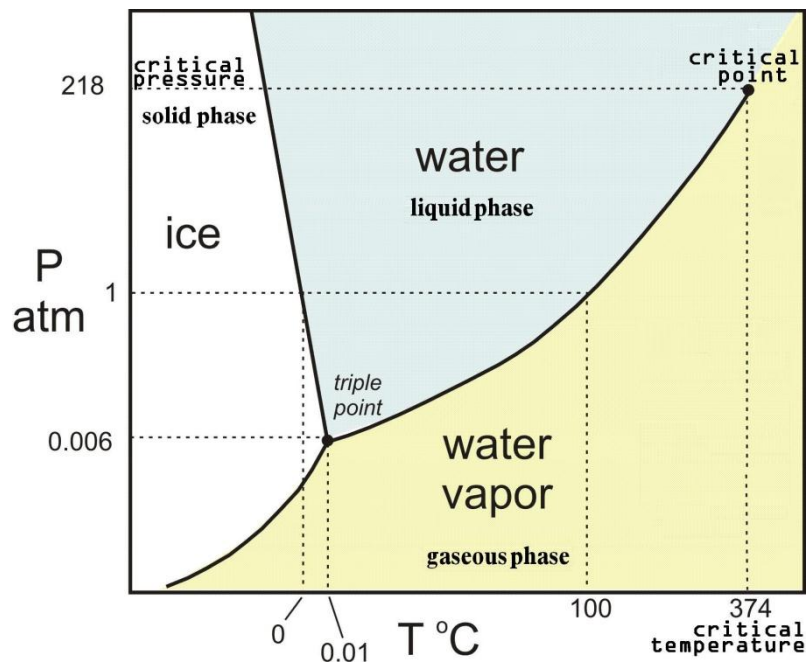


Figure 1.1: Water phase diagram in the pressure-temperature plane, showing the boundaries between solid, liquid and gas phases.

To microscopic level, phase fluctuations occur as random events due to the thermal vibration of atoms (collisions). In terms of nucleation, the spontaneous fluctuations lead to the formation of small nuclei droplet that can grow beyond some critical radius, being possible overcome this barrier and sustain spontaneous growth; that is, it can only survive and grow if there is a reduction in free energy; once the nuclei reach the critical size, the phase transition practically occurs. However, if the energy barrier to spontaneous growth is large and the droplet cannot achieve the critical size, it remains unstable and with all possibility will be evaporated. As a result of this energy barrier, the state is prevented from escaping to the equilibrium state [3], being possible that the system exists in a metastable state with unfavorably high supersaturation levels being maintained in the gas phase [4].

It is just this mechanism of energy necessary to form a stable nuclei of a new phase [5], caused by random phase fluctuations in the metastable phase, which is called nucleation. In this picture the critical nucleus is assumed spherical.

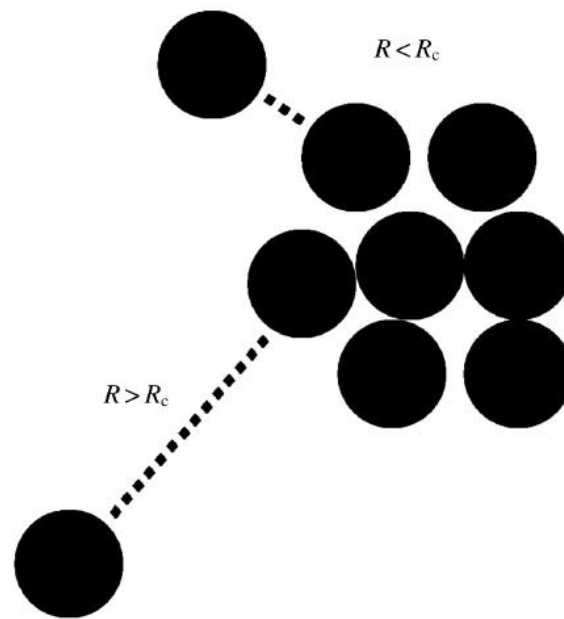


Figure 1.2 According to the Stillinger definition, a molecule is considered part of a cluster if it lies closer than a distance R_c from a constituent molecule of the cluster.

When a change of phase takes place, the repositioning of molecules (monomers) happens on a grand scale. Phase transformations are the statistical consequences of the ability of large physical systems (and any environment with which they interact) to explore a huge range of microscopic configurations. The principal idea is that there exists a bottleneck in the transformation, which is passed through only by fragments, or molecular clusters, of the new phase. The bottleneck is narrowest when the clusters reach a critical size [6]. Any molecular nucleation requires a definition of a cluster. Unfortunately nature does not provide an automatic definition of which molecular configurations form a single physical cluster, and one is forced to introduce an artificial definition instead. Here is occupied the Stillinger definition, according to the connectivity between cluster molecules [7]. It states that a cluster molecule cannot be separated by more than a Stillinger distance R_c (see Fig.(1.2)) from another cluster molecule, and that a cluster is formed by a single network of connected molecules. The Stillinger radius chosen in the specialized literature typically varies between values of 1.2σ and 1.8σ [8], where σ is the surface tension.

The first considerations of the nucleation phenomena were presented by Thomson (1870, 1871) (later Lord Kelvin), followed by the work of Gibbs (1906) on thermodynamics of curved surfaces during 1876-1878. The theory that is nowadays known as the classical nucleation theory was evolved from the joint works by Volmer and Weber (1925), Farkas (1927), Becker and Döring (1935), Zeldovich (1942), and Frenkel (1946).

In this chapter will be exposed the nucleation by homogeneous condensation from the vapor phase and its intervention on the steam turbines. The basic distinction between homogeneous and heterogeneous nucleation is that the heterogeneous nucleation is formed by suspended and dissolved impurities, as well as imperfectly wetted solid boundaries that provide preferential sites for the formation of the new phase; while for homogeneous nucleation the nuclei of the new phase are formed throughout a homogeneous sample in absence of impurities and occurs when there are no heterogeneous nuclei present, involving only the material and so it is intrinsic to the material [9].

1.2 Thermodynamics

As already pointed out, the first detailed description of the phenomenon of nucleation was given by Gibbs [10]. In its original treatment, the nuclei that are formed in the volume of supersaturated ambient phase, have the same properties as the corresponding bulk phase (unstructured system) with the only exception of being their small sizes. This approach treats a microscopic problem (surface tension) in terms of macroscopic thermodynamic variables [11]. According to it, if the radius of the curvature of the interface between an object and its surrounding is large with respect to its molecular dimension, the object is treated as being macroscopic.

Considering the formation of liquid nuclei in the bulk of a vapor phase, the surface free energy of the liquid droplet is treated equal to the surface tension σ of the liquid bulk, which, being isotropic, the form will be the one that requires a minimum of energy of formation and allows to equilibrium of the spherical shape of the small liquid entities. It is considered that the nuclei have a structure, equal composition and properties, identical to that one of the future phase (in this case, liquid) and they are not different between them more than by the form and the size. Now, it is considered a volume containing n_v molecules of a vapor with chemical potential μ_v (tendency of a component to escape of a certain phase) which is a function of the temperature T and pressure P . The thermodynamic potential (energy available from a thermodynamic system) of the initial state of the system at $T = \text{constant}$ and $P = \text{constant}$ is given by:

$$G_1 = n_v \mu_v. \quad (1.1)$$

When a droplet of a liquid with bulk chemical potential μ_l is formed from n molecules of the vapor phase, the thermodynamic potential of the system vapor-liquid droplets reads:

$$G_2 = (n_v - n)\mu_v + G_n, \quad (1.2)$$

where G_n is the thermodynamic potential of a cluster containing n molecules. The work of formation (equilibrium and spontaneity condition at $T = \text{const}$ and $P = \text{const}$) of a cluster consisting of n atoms is then given by the difference $\Delta G_n = G_2 - G_1 = G(n) - n\mu_v$. From the previous equation, it follows that the work of formation of the cluster represents the difference of the thermodynamic potential of the cluster and the thermodynamic potential of the same amount of material (number of molecules) but in the parent (vapor) phase.

The thermodynamic potential of the liquid droplet is given by the sum of the chemical potential of the constituent atoms in the infinitely large liquid phase $n\mu_l$ and the surface energy $4\pi r^2\sigma$ necessary to obtain the nuclei [12]:

$$G(n) = n\mu_l + 4\pi r^2\sigma, \quad (1.3)$$

In this equation σ is the surface energy as measured for a flat surface. Now if it is substituted Eq.(1.3) into Eq.(1.2), and n is evaluated with the expression $n = 4\pi r^3 / 3v_l$ (v_l being the molecular volume of the liquid), then is obtained the expression for the work of formation as a function of the radius of the droplet:

$$\Delta G(r) = -\frac{4}{3} \frac{\pi r^3}{v_l} \Delta\mu + 4\pi r^2\sigma, \quad (1.4)$$

where $\Delta\mu = \mu_v - \mu_l$ is the supersaturation. Thus in the simplest case of a droplet formation in vapor, ΔG consists of two terms: the free energy by the nuclei compared to the same volume to the liquid phase, $4\pi r^3\Delta\mu / 3v_l$, which is negative when the liquid phase is stable (see Fig.(1.3)), and a surface term $4\pi r^2\sigma$, to obtain the nuclei with radio r , which is always positive. The increase of the thermodynamic potential of the system is due to the formation of the interface between the liquid droplet and the surrounding vapor. Then ΔG displays a maximum at some critical size r^* given by:

$$r^* = -\frac{2\sigma v_l}{\Delta\mu}, \quad (1.5)$$

Under this condition the system is in unstable equilibrium. Indeed, any infinitesimal deviation of the size of the nucleus from the critical one leads to a decrease of the thermodynamic potential of the system. In this sense the cluster with size r^* is a critical nucleus of the new phase.

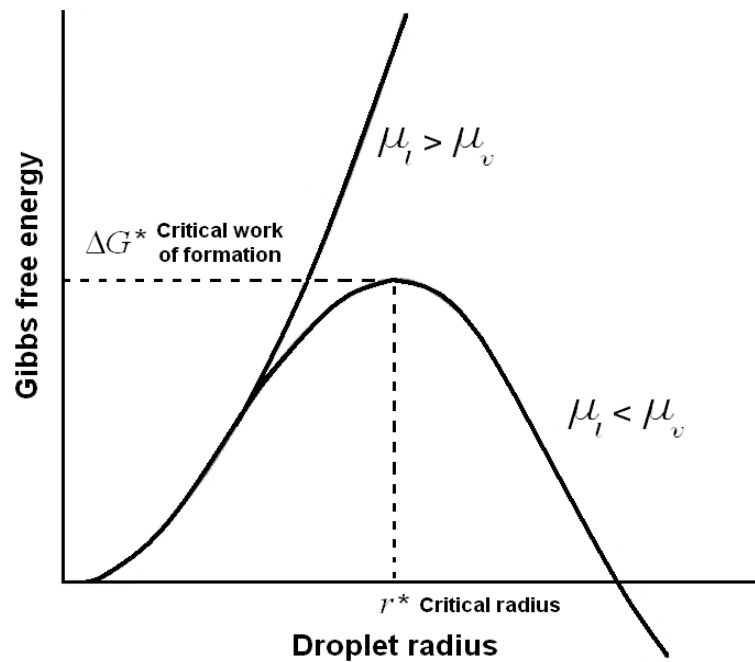


Figure 1.3 Dependence of the droplet radius of the Gibbs free energy change ΔG in relation to the formation of liquid nuclei from a supersaturated vapor phase. When the liquid phase is stable ($\mu_l < \mu_v$), ΔG displays a maximum at some critical radius r^* . This maximum is the work of formation of the critical nucleus; beyond the critical size, growth of the nucleus leads to a decrease of the Gibbs free energy of the system. When vapor phase is stable ($\mu_l > \mu_v$) both terms in Eq.(1.4) are positive and the formation of nuclei capable of unlimited growth is thermodynamically forbidden (it would lead to an infinite increase of the Gibbs free energy).

The maximal value of ΔG is obtained by substituting the expression of r^* into Eq. (1.4), thus obtaining [13]:

$$\Delta G^* = \frac{16\pi}{3} \frac{\sigma^3 v_l^2}{\Delta\mu^2}, \quad (1.6)$$

This expression gives the height of the free energy barrier which should be overcome for condensation takes place. It is inversely proportional to the square of the supersaturation and increases steeply near the phase equilibrium, i.e. at small supersaturation, thus imposing great difficulties for the phase transition to occur.

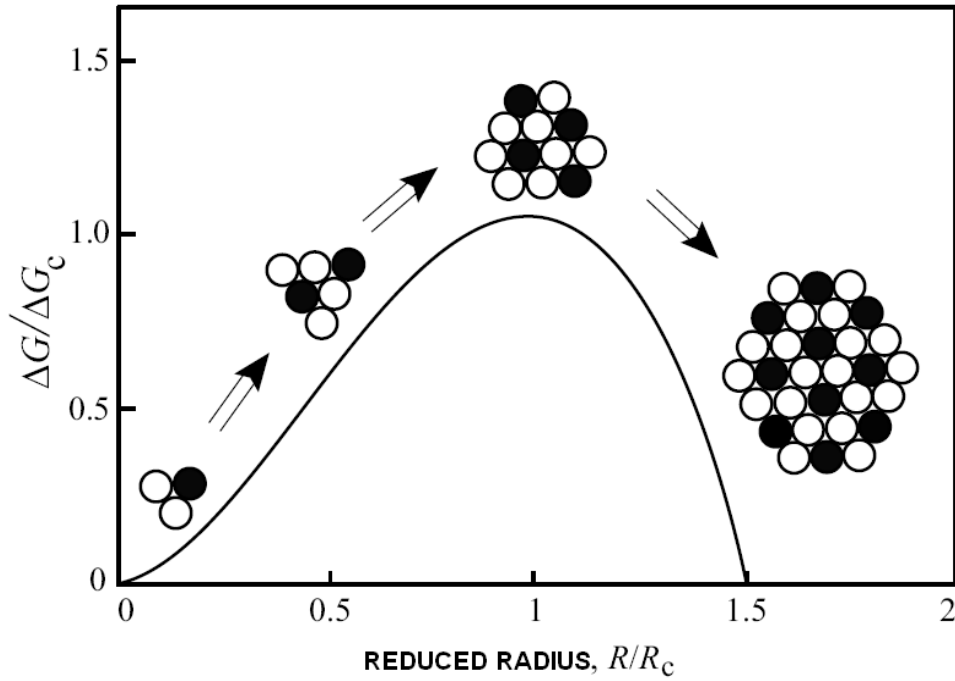


Figure 1.4: Work of cluster formation (change in Gibbs free energy, ΔG) in dependence on cluster size (R is the radius of the cluster). The subindex denotes the critical size.

Useful expressions for $\Delta\mu$ could be obtained if is substituted the expression for the radius of the critical nucleus, Eq.(1.5), into Eq.(1.4), and is used the Eq.(1.6):

$$\Delta G^* = \Delta G(r)^* \left[3 \left(\frac{r}{r^*} \right)^2 - 2 \left(\frac{r}{r^*} \right)^3 \right], \quad (1.7)$$

or in terms of the number n^* of atoms in the nucleus (from $v_l n = 4\pi r^3 / 3$):

$$\Delta G(n) = \Delta G^* \left[3 \left(\frac{n}{n^*} \right)^{2/3} - 2 \left(\frac{n}{n^*} \right) \right], \quad (1.8)$$

where

$$\Delta G^* = \frac{4}{3} \pi r^{*2} \sigma, \quad (1.9)$$

and has been obtained substituting the expression for $\Delta\mu$ from Eq.(1.5) into Eq.(1.6). The Eq.(1.8) can be shown in the Fig.(1.4) in function to the ratio of the cluster and the radius of the critical cluster R_C . The process of formation of supercritical clusters will be with sizes $R > R_C$ capable of a further growth. The bulk and surface properties of the clusters are widely same as the respective properties in the newly macroscopic phase [14].

1.3 Cluster formation

The kinetic interpretation can be taken assuming that the only important transition processes of evolution clusters are those involving the addition or loss of single molecules to or from the cluster. For the critical size, the probabilities of growth and decay are equal. Since growth and decay are stochastic, an individual cluster can reach the critical size through improbable sequences of molecular acquisitions [15]. According to this scheme (see Fig.(1.5)), cluster of class n (i.e. consisting of n atoms), are formed by the attachment of one molecule to a cluster of class $n-1$ and detachment of a molecule from a cluster of class $n+1$ and disappear by the attachment and detachment of one molecule respectively to the cluster of class n , giving rise to a cluster of class $n+1$ and $n-1$ respectively.

In fact, the growth of a cluster of class $n-1$ to form a cluster of class n , is given by the number of collisions of atoms from the vapor phase on the surface of the droplets.

According to Volmer, the number of atoms leaving a cluster of class n , in equilibrium with the vapor phase, in a fixed interval of time, is equal to the number of atoms arriving at its surface. Hence the flux of atoms leaving the cluster is equal to the equilibrium flux of atoms arriving at its surface.

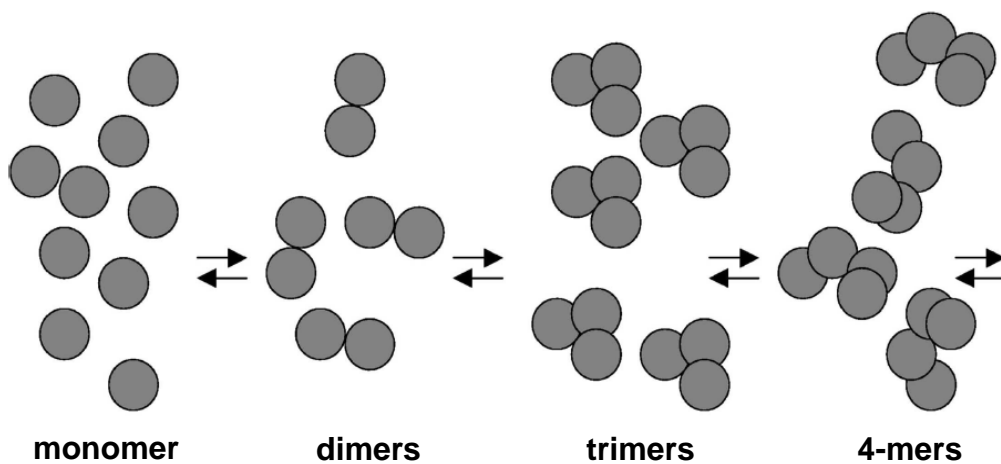


Figure 1.5 The scheme of birth and death of clusters. Addition of a monomer to a cluster will take it up the chain, towards the right, while the loss of a monomer will take it in the opposite direction.

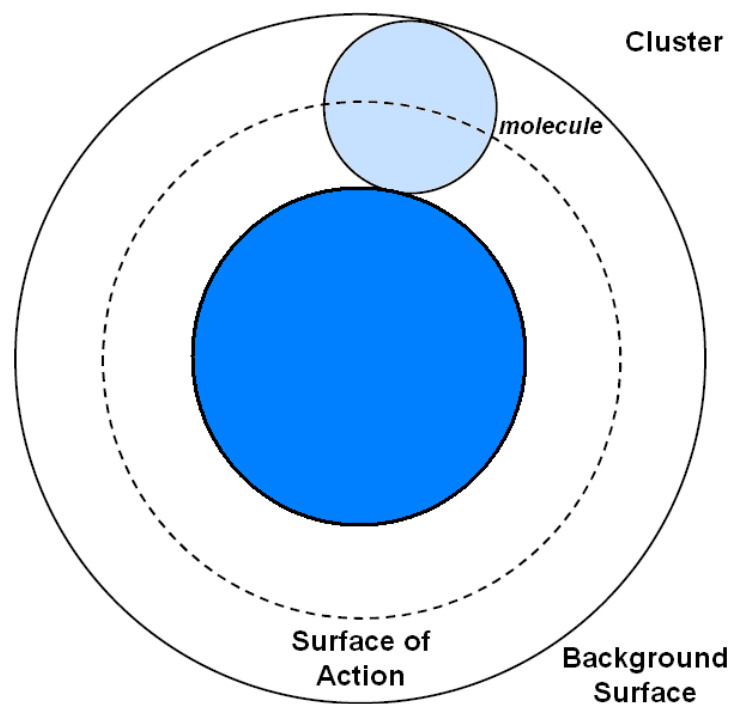


Figure 1.5: Determination of the surface area of a liquid droplet containing n molecules upon detachment of a single molecule shown by the small circle. The molecule leaves the droplet when its center of mass crosses the surface of action of the intermolecular forces given by the dashed circle. Precisely at that moment the surface area of the droplet becomes S_{n-1} as given by the solid circle.

Condensation takes place when the center of mass of a molecule (joining the droplet) crosses a sphere of action of the interatomic forces, and the radius of the droplet increases just after that event (see Fig.(1.5)). Similarly, the evaporation of a molecule takes place when its center of mass crosses the same sphere of action and at that moment the droplet shrinks and the radius of the droplet decreases.

1.4 Spherical cluster as a drop

It has often been argued that from the thermodynamic point of view, a cluster of drops behaves in fact as one large drop of the same dimension as the cluster. The physical picture of the cluster of drops as an equivalent large drop is not supported by results obtained with models coupling dynamics and thermodynamics of interacting drops. Nucleation theory builds on the treatment of droplets, according to which small droplets are considered to have the same properties as bulk condensed phases, with bulk surface properties [16] and whereby the critical cluster, however small, is considered as a scaled-down macroscopic droplet of the condensed phase.

Generally speaking, the drops are closely approximated by spheres if carried by an inviscid fluid [17]. Here, in this model, the cluster is considered using the concept of the "sphere of influence". By definition, each drop is surrounded by a fictitious sphere of influence centered at the drop's center and having for radius the half distance between the centers of two adjacent drops (all droplets having equal separation distances). Thus, the cluster volume is the volume of all spheres of influence plus the volume between the spheres of influence. The drops have both an axial velocity in the direction of the motion of the entire cluster with respect to a frame of reference located outside of the cluster, and a radial velocity with respect to the center of the cluster [18].

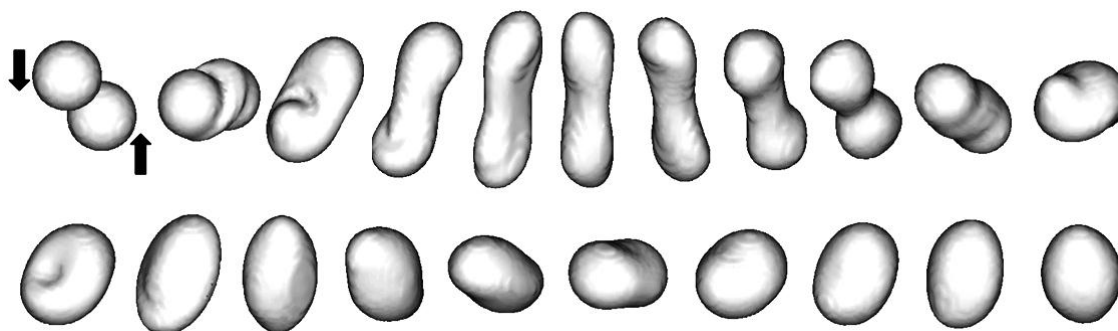


Figure 1.6: Cluster formed in a collision of liquid drops (supposed as a one drop).

A snapshot of the molecules present in a supersaturated state shows small clusters of the new phase containing two, three, or more molecules. There also would be occasional clusters containing a larger number of molecules; however, a motion picture of these larger clusters would show that most are very short lived; they grow rapidly and then shrink rapidly. Nucleation occurs when a cluster of two, three, four, grows (fluctuates in size) to a size large enough that it then continues to grow rather than shrink [19]. Eventually, agglomeration by coalescence (see Fig.(1.6)) of large clusters enters until thermodynamic equilibrium [20].

A cluster formed in a collision [21] has a size probability to live long enough to undergo another collision and grow further before it breaks up. This probability is determined by the formation free energy of the cluster. In a nucleating vapor, a distribution of clusters of different sizes is presented. Clusters collide with each other and form larger clusters [22]. During the collision of a molecular cluster with a solid substrate, the initially directed kinetic energy of the cluster will be thermalized (thermal equilibrium) rapidly by collisions of the molecules of the cluster with each other and with the atoms of the solid surface. This sudden, impact-induced redistribution of the cluster translational energy may lead to a variety of processes, including the collision-induced dissociation of inter- and intramolecular bonds. The cluster-surface collisions have received considerable attention, because can provide internal excitations to the impacting clusters, on a sub-picosecond time-scale [23].

The ability of the target cluster to absorb the monomer depends primarily on the state of the cluster at the moment of the collision, however, the water molecules with the smaller force constant seem to be able to absorb some of the kinetic energy in the collision, and thus the clusters have considerably longer lifetimes.

When the bonds in the cluster increases their flexibility, the molecules stabilizes the cluster and increases the ability of cluster molecules to transform part of the kinetic energy of the incident monomer into intramolecular vibration, resulting to a slowing down of both the translational and rotational movements of molecules [24].

1.5 Collision process

The collisions of particles can occur at different scales, ranging from macroscopic particles, such as raindrops, down to nanosized particles, i.e., clusters and nanodroplets. In the context of macroscopic scales, collisions of droplets have been the subject of extensive investigations over the last few decades. Collision fragments that are formed during the collision process are classified according to their size. Depending on the collision dynamics, there may be one or two main fragments. In some cases it may also include satellite droplets.

Experimental studies have identified four main collision modes: coalescence, reflexive separation, stretching separation, and shattering. The outcome of a collision for a given set of initial conditions is developed and enhanced using experimental results. However, the details of the collision processes are difficult to be obtained through experiments, especially at small length [25].

The attracting interatomic forces cause the coalescence of the two clusters, which takes place through two distinguishable stages: initially a neck forms between the clusters. The neck disappears later and one particle is formed. Generally, the coalescence prevails at low velocities and/or small impact. Common to all collisions belonging to this mode is the formation of one main cluster or a droplet that is created by the two original clusters.

The particles of smaller dimensions change of direction by consequence of reflection [26]. The temporarily formed cluster separates after being stretched, thus the mode is referred to as stretching separation labeled. The shattering label (total disintegration) corresponds to the destruction of clusters and occurs for high velocities.

In the formation of a larger cluster, these are flattened at impact and the initial contact point evolves to a flat circular interface. The heat generated at the contact interface liquefies the material in this region and a liquid layer with reduced friction is formed acting as a cushion between the clusters facilitating sliding along each other. Eventually, the interface locks and the sliding motion completely stop leaving behind a rotating cluster.

The clusters' trajectories after the initial contact are parallels to each other, while symmetry is preserved throughout. As it was mentioned above, the friction increases when the trajectories enter a circular motion and the contact interface is locked, thus not permitting further sliding of the clusters. The distance of the mass centers is closest approach immediately after the clusters have come in contact. This distance increases during the sliding phase. The initial kinetic energy is transformed into internal potential energy, causing deformation and increasing pressure. Increasing the faster and longer sliding motion, eventually leads to the separation of both clusters; this is the transition to stretching separation mode. The translational motion is transformed into rotation. The shape of the resulting cluster depends mainly on the extent of flattening and sliding of the original cluster.

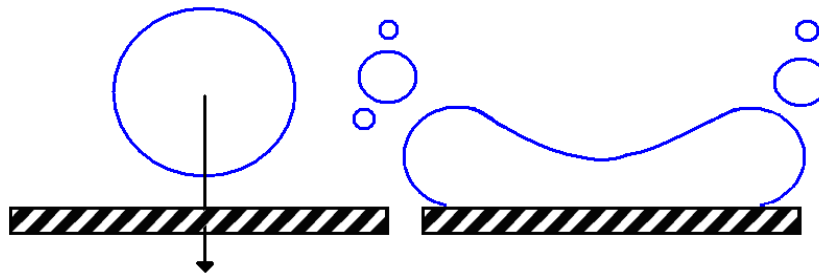


Figure 1.7: Collision of a drop with a wall. Original drop and ejection of satellite droplets.

With respect to dense clusters of drops, cannot sustain slip velocities with respect to the vapor due to the large surface area that they expose to the flow (since the drop number density is large). An important implication of particle collisions with walls is erosion. The literature on erosion by liquid impact dates back to the start of the last century when the velocities of the rotating blades of steam turbines became sufficient to cause erosion. At first the suggested mechanisms for turbine blade erosion (Coles 1904) included almost every possibility except liquid drop impact.

Finnie (1972) developed a quantitative model for the mass of material removed from a surface because of collisions of particles. He predicted that the maximum rate of erosion, defined as the rate of mass of material removed from the surface, would occur at a direction that is almost normal to the surface (13°). Erosion is of significance when drops impact a wall. The continuous impact of drops will form a liquid film on the wall surface, which would attenuate the forces during the impact at subsequent times and, hence, the long-term wear on the surface [27]. The perpendicular impact of liquid drops on solid surfaces gives like result that the drops flatten and spread on the wall. When an initially spherical drop of radius on the order of millimeters spreads out at impact, the maximal spreading radius is on the order of a centimeter [28]. Zaleski (1998) and Carles (2001) demonstrated that the impact causes very large deformations on the drop and creates a radial jet at the early stages of the impact, which finally induces the ejection of fluid at the sides of the flattened drop and formation of several smaller satellite droplets. The qualitative details of this process have been depicted schematically in Fig.(1.7).

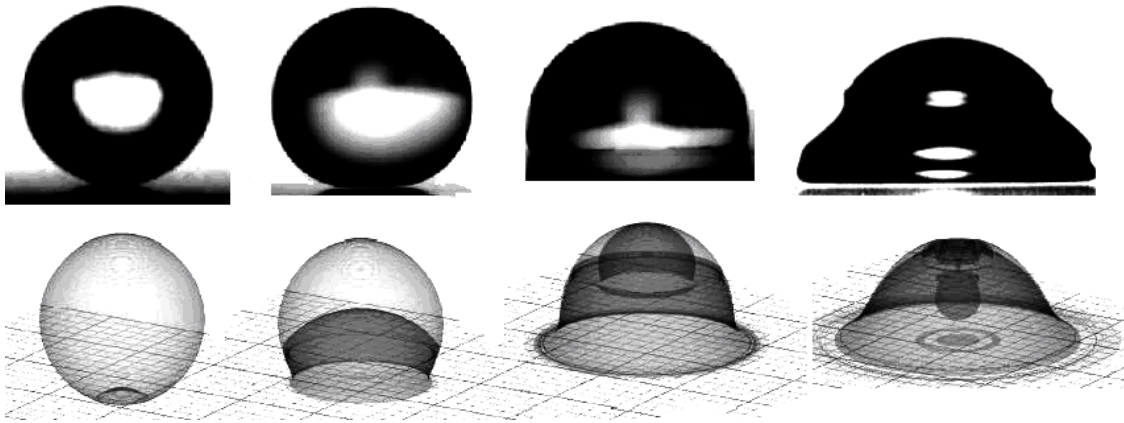


Figure 1.8: Impact of liquid drop on solid surface. In this picture is shown the evolution of compression of the liquid and the propagation of pressure waves.

The impact phenomenon is characterized by the compression of the liquid adjacent to the solid surface, whereas the rest of the liquid droplet remains unaware of the impact. Initially, the area of compressed liquid is assumed to be bounded by a shock envelope, which propagates both laterally and upwards into the bulk of the motionless liquid. Compression of the liquid in a zone defined by a shock wave envelope, lateral jetting of very high velocity and expansion waves in the bulk of the medium are the most important mechanisms identified.

When a liquid drop impacts against a rigid surface, is expected to see a number of flow regimes. The impact involves compression of the liquid, triggering the propagation of pressure waves outward from the point of first contact (see Fig.(1.8)) being all wave propagation velocities smaller than the contact line velocity. At a certain point, the radial velocity of the contact line decreases below the shock velocity and the shock wave overtakes the contact line, starting to travel along the droplet free surface. The resulting high pressure difference across the free surface at the contact line region triggers an eruption of intense lateral jetting. The pressure waves travel through the bulk of the droplet, interacting with the free surface. In the final state of the contact, when the compressible effects are expected to die away, the drop spreads out over the rigid surface.

The behaviour during impact depends mainly on the impact velocity V , or more precisely on the Weber number We , which is the ratio of kinetic energy to surface tension [29]:

$$We = \frac{\rho V^2 r_{drop}}{\sigma}. \quad (1.10)$$

Here, r_{drop} denotes the radius of a sphere with the same volume as the drop, and ρ and σ denote the density and surface tension of the liquid, respectively. The Weber number We it can be defined as the ratio between average dynamic pressure and the drop, and the surface tension, under the hypothesis that the drop has a spherical form. Assuming that the breakage of the drop takes place when the dynamic pressure of the steam exceeds to the pressure surface tension [30], then the number of critical Weber goes bound to the maximum number of Weber that allows the stable existence of the drop in the steam flow, stability that comes given by the equality from the dynamic pressures and surface tension [31].

For $We < 1$, drop deformation during impact is small, and the drop retains an oval shape (Richard & Quéré 2000). For $We > 1$, the deformation becomes significant (of the order of the drop radius), and the drop spreads over the solid, with a well-defined maximal extension. Above a threshold Weber number ($We \sim 4$), capillary waves travel to the top without being damped. This structure can also occur for a normal solid surface; indeed, it should exist on normal solids because it takes place in the inertial regime of spreading, where the wetting properties do not play a major role.

The liquid is described by its thermodynamic state, surface tension, viscosity and compressibility. Depending on impact velocity, drop and target geometries as well as the physical properties of both, there might exists a regime in which effects such as viscosity and surface tension do not play a role.

Numerous studies have been published on low velocity impact (e.g. 1 m/s), where the compression effects have been assumed negligible. The fluid flow associated with impinging drops is rather complex and not understood in detail. The high-speed impact involves compressibility patterns, whose both analytical and numerical modeling cause significant difficulties.

1.6 Compressible droplet impact

The problem geometry is boarded of a spherical liquid droplet impacting at high speed onto a perfectly rigid surface (Fig.(1.9)). The droplet is assumed to move with a velocity normal V to the wall and to have an initial density ρ under pressure p . Then, the angle between the shock wave and the plane wall, β , as depicted in Fig.(1.9). During the first phase of the impact, liquid adjacent to the contact zone is highly compressed whereas the rest of the liquid droplet remains unaware of the impact. The two regions are separated by a shock front which travels into the bulk of the liquid remaining joined to the surface at very early times due to the outward motion of the contact line [32]. The most frequently used approximations to the pressure developed in liquid-solid impact are based on one-dimensional elastic impact theory.

According to this model, the generated pressures in the compressed region are of the order of water-hammer pressure:

$$P_{wh} = \rho_0 s V \quad (1.11)$$

where s are the shock velocity with respect to the unaffected bulk of the liquid, respectively. The pressure in the compressed area is not uniform and reaches its highest values just behind the contact line. A temporal maximum will be reached at the instant when the shock wave overtakes the contact periphery.

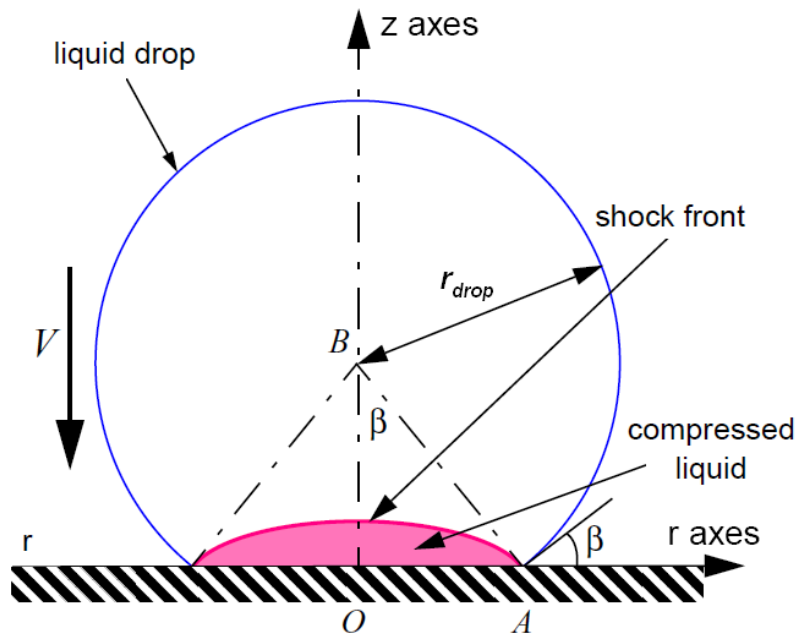


Figure 1.9: Impact of a spherical liquid drop (blue) on a rigid surface. The zone of the high compressed liquid (red) is bounded by the shock front and rigid surface.

The damage caused by liquid impact and particularly the damage threshold velocities required to initiate failure, are convincing evidence that compressible behavior occurs during impact. As in mentioned previously, once the shock detaches and moves up the free surface of the drop, release waves travel into liquid and jetting commences [33].

For the calculation of the velocities of the contact line of the drop against the surface without movement, the maximum radius and the beginning and duration of the extension of the drop deformed against the surface can be obtained through following analysis [34].

At the first moment of time τ_1 , when the drops makes contact with the surface (Fig.(1.10)), only in the point A_1 a contact line propagates in the wave with a velocity a' . Simultaneously the expansion of the contact line of the drop takes place (in the plane) in the region of point A_1 . The velocity c_B as a result of the points in the circumference of the contact line move by the surface of the impact from point A_1 is equal a:

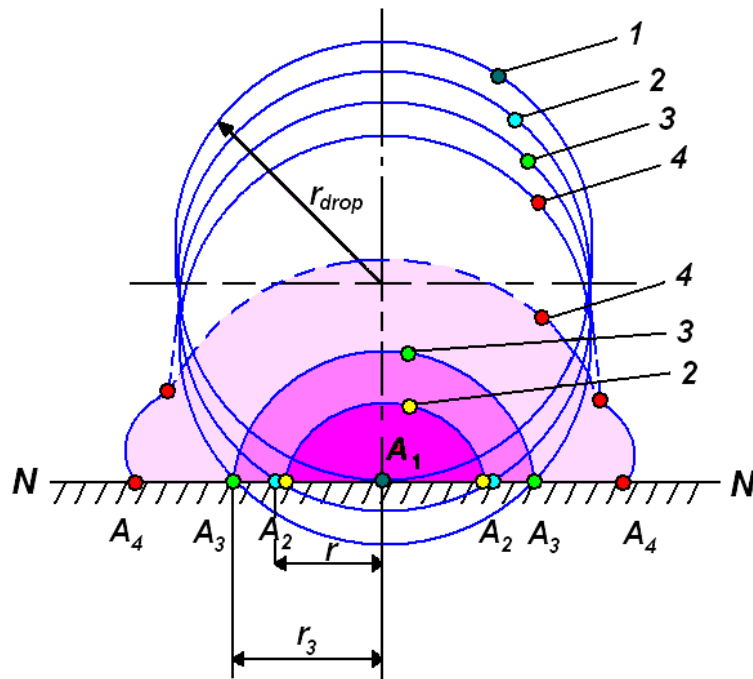


Figure 1.10: Scheme of impact of the drop against a plane rigid surface NN ; ——— contours of the drop; - - - - - borders of the shock wave; A_1, A_2, A_3, A_4 borders of the contact line with the surface of contact, respectively, in the moments of time $\tau_1, \tau_2, \tau_3, \tau_4$; r_{drop} radius of drop; r_{str} radius of the stream of the contact line; r_3 radius of the contact line that corresponds at the moment τ_3 of the beginning of the extension.

$$c_B = w \frac{r_{drop}}{r_{str}} \quad (1.12)$$

where w is the impact velocity of the drop, in m/s; r_{drop} is the radius of the drop and r_{str} is the radius of stream in μm . In the initial period, being small the values of the radius r_{str} , speed c_B overtakes the speed of propagation of the contact line a . In this case the particles on the surface of the droplet enter in contact with the impact plane NN faster than the propagation of the disturbance in the interior of the drop. In the Fig.(1.10) the moment of time τ_2 is shown by means of the points A_2 that are the borders of the contact line.

Meanwhile the contact line that is shown by the dots line 2, does not leave of the limits of this spot. Only in the time τ_3 , when the velocity $c_B = a$, the extension of the drop begins throughout the impact surface. The borders of contact line at this moment are designated with points A_3 , and the shock wave, with the dots line 3. The later extension of the drop ($\tau_4 > \tau_3$) is with the help of points A_4 . The maximum radius of contact line r_3 corresponds at moment τ_3 of the beginning of the extension, and it is determined with:

$$r_3 = r_{\max} = r_{drop} \frac{W}{a}. \quad (1.13)$$

The duration of the time interval in the period of action in which the elastic deformation of the drop takes place, can calculate by means of the equation:

$$\tau = \tau_3 - \tau_1 = \frac{W \cdot r_{drop}}{2(a\hat{\gamma})^2}. \quad (1.14)$$

The time in which the impulse ($\tau_3 - \tau_1$) in seconds acts is proportional to the c_B and the dimension of the drop.

The existence of water droplets formation presents practical difficulty concerning the behavior of steam in turbines. Following the conditions of flow and the type of design of the turbine it will be the size of the drop, for example, the humidity degree, the geometric conditions, the velocities of the blades altogether with the velocity of the flow, the conditions of pressure and temperature in the stage to analyze, etc., they will determine the influence of erosion. Therefore, the impact of the drops on rigid surface is one of the causes that will carry out the deterioration of the blades [35].

1.7 Wet in Steam Turbines

Development of the nucleation is of considerable help in the study of wetness problems in turbines. It has been observed that on the low pressure section occurs a decrease of the quality, beginning with values without greater risks ($x = 98\%$), till reaching lower qualities ($x = 90\%$) in the last stage [36]. Steam turbines are designed to extract thermal energy from steam and convert it into rotary work. The thermodynamicists conceive the expansion work of turbines on an enthalpy-entropy diagram, called a Mollier Chart. The pressure and temperature conditions of the steam at various points in the turbine are shown on this chart and called the expansion line [37].

Fig.(1.11) shows the expansion line for a turbine, the corrosion and impurity behavior zones [38]. Once supersaturated, the fluid begins to nucleate and the supercritical droplets will grow, but the nucleation is initially negligible and steam remains in a metastable state. As the expansion continues, eventually supercritical droplets formed are sufficient to return the system to thermodynamic equilibrium [39].

The heterogeneous droplets are formed earlier and the expansion and grow to a larger size and their presence can often be detected before the steam has nucleated homogeneously. The surface offered by the heterogeneously formed droplets is sufficient to affect the flow, and the fluid will supercool with further expansion until it nucleates homogeneously to return to near-equilibrium.

The steam thus becomes supercooled with further expansion such that homogeneous nucleation is usually the dominant mechanism [40]. Wet steam thus formed consists of a very large number of extremely small droplets that are suspended in, carried by, and interact with the parent vapor, affecting its subsequent behavior.

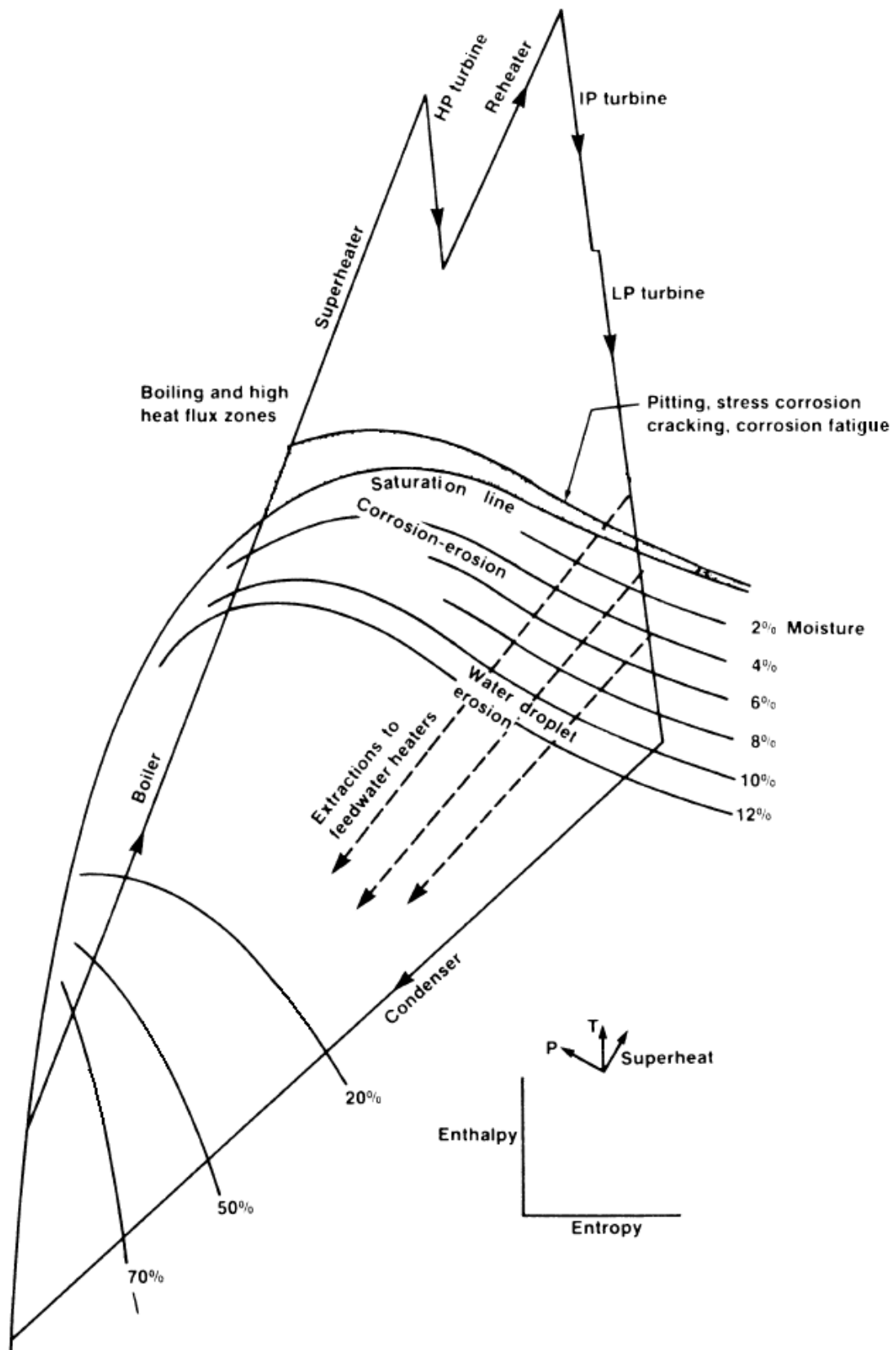


Figure 1.11: Mollier diagram, with regions of impurity concentration, corrosion and erosion by drops of water.

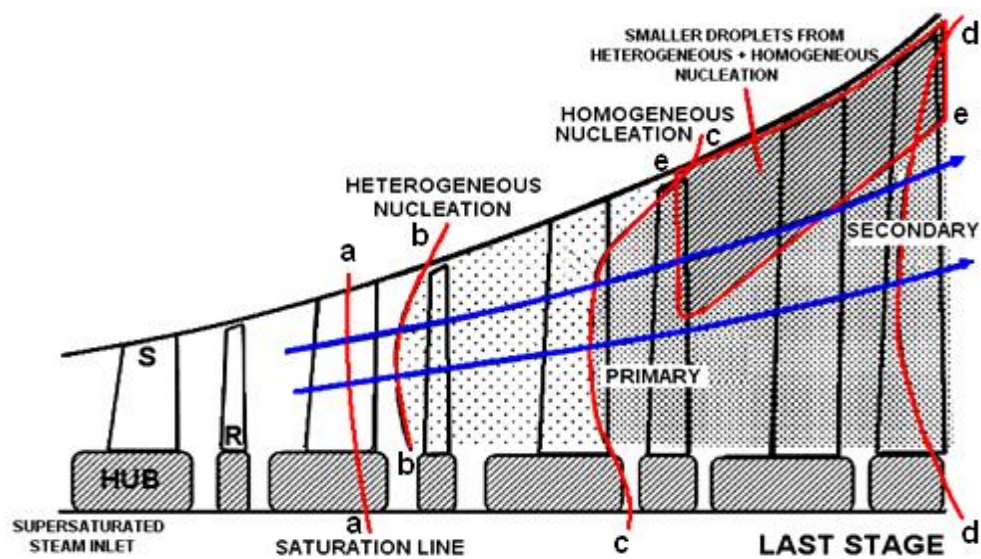


Figure 1.12: Topology of phase transition in a LP steam turbine: *a-a*, saturation line; *b-b*, heterogeneous nucleation transition; *c-c*, primary homogeneous nucleation transition; *d-d*, secondary primary homogeneous nucleation transition; *e-e*, secondary droplet region originating from trailing edges of rotating blades. Stator and rotor components labeled with S and R, respectively.

Because the last stages of low-pressure steam turbines are directly connected with the condenser having necessarily low values of pressure and temperature, the working fluid starts already to condense flowing through the last blade passages [41]. Within a few microseconds, the temperature of the vapor decreases below the equilibrium saturation limit. This is because the phase change proceeds at a finite rate and there is no sufficient time for equilibrium condensation to occur.

Fig.(1.12) is provided to assist in further describing the two-phase flow behavior in a LP turbine [42]. The solid lines, with letters at the beginning and ending, denote typical nonequilibrium phase transition lines or zones of secondary droplet behavior. Dashed lines indicate equilibrium phase transition. The first transition line (*a-a*) denotes the saturation line where, under equilibrium assumptions phase transition would appear. Transition line *b-b* denotes heterogeneous nucleation transition, which occurs on contaminants in the flow, and is generally insufficient in number to bring the flow to equilibrium conditions.

Typical sizes for droplets generated in this manner are 0.01-0.1 μm . Under rapid expansion, supercooling continues up to line *c-c*, where primary homogeneous nucleation occurs, creating droplet sizes in the range of 0.001-0.01 μm and following with the reversion of the flow to near equilibrium conditions.

Note that transition line *c-c* can be highly curved such that primary nucleation toward the shroud occurs in the following stage component (the third rotor). As flow expansion continues into the final stage, significant supercooling is again possible, leading to further secondary homogeneous nucleation along line *d-d*. Finally, smaller droplets generated along lines *b-b* and/or *c-c* can collect on blades and be re-entrained, as secondary droplets, into the flow at the trailing edges of rotating components, in particular. Centrifugal action generally confines these droplets toward the shroud as shown by boundary *e-e*. Droplets in region *e-e* are entrained at sizes that are generally greater than 100 μm and have a considerable slip relative to the vapor; therefore, water drops tend to move more slowly than the vapor; they strike the rotor blades at unfavorable velocities and exert a braking effect [43]. These droplets have a significant influence on blade erosion, and the fact that the small nucleated droplets provide the source for entrainment of large droplets into region *e-e* describes a highly coupled two-phase flow system. Erosion is only one consequence of the presence of water in steam.

A tangible wetness effect is erosion of blading. The nucleated droplets are generally too small to cause erosion damage but some of the droplets are collected by the stator and rotor blades to form films and streams on the blade and casing walls. In Fig.(1.13) it can see the locations of erosion problems in a low pressure section of a steam turbine. On reaching the trailing edges or the tips of blades, the liquid streams are re-entrained into the flow in the form of coarse droplets and are these larger droplets that cause the erosion damage and braking loss.

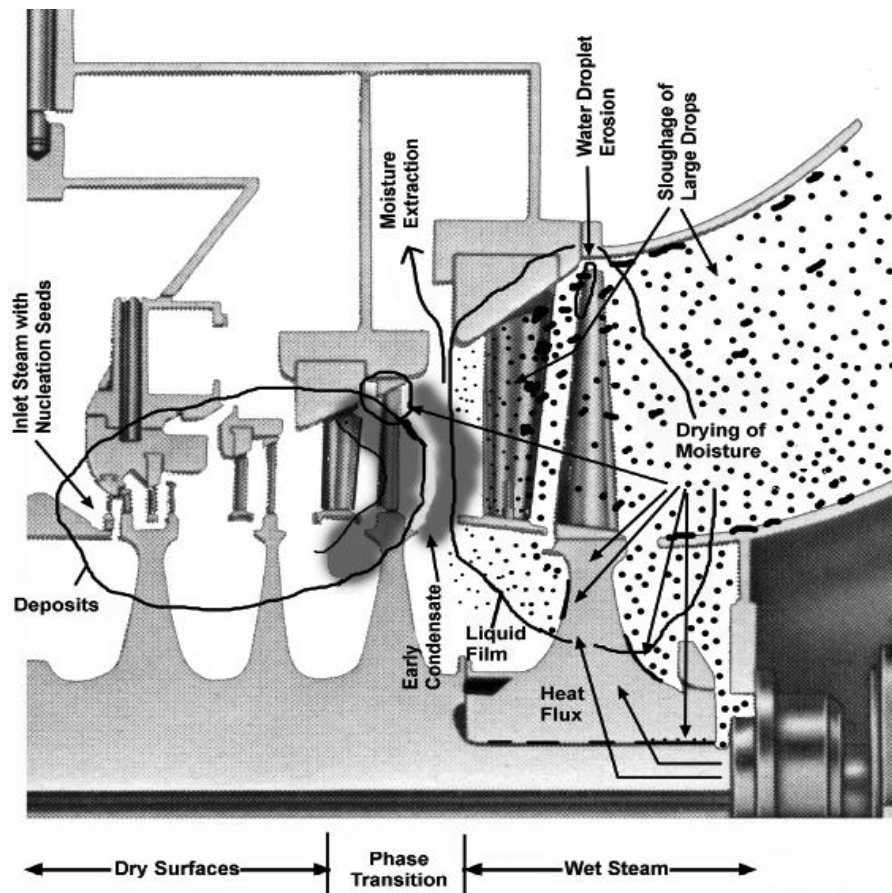


Figure 1.13: Cross section of a turbine with locations of erosion in low pressure section.

After nucleation, the flow behavior of the wet vapor (formed by a polydispersed system of droplets [44]) is strongly dependent on the size distribution of the droplets present and hence on the conditions under which nucleation occurred. Understanding the nucleation process is thus central to know the behavior of wet steam [45].

The formation of the vortices (Fig.(1.14)) takes place in the zones of separation of the flow, for example, in the roughness of the trailing edges. In the center of the vortices that leave of the trailing edge, there is a zone of low temperature, where ΔT of mean takes place, which is essential condition for the formation of the violent condensation of the steam, and the drops which they form are expelled from the vortex to the nucleus of the flow. The nuclei of condensation grow until dimensions that overpass the critics, passing to be the condensation centers for steam weakly supercooled of the main flow.

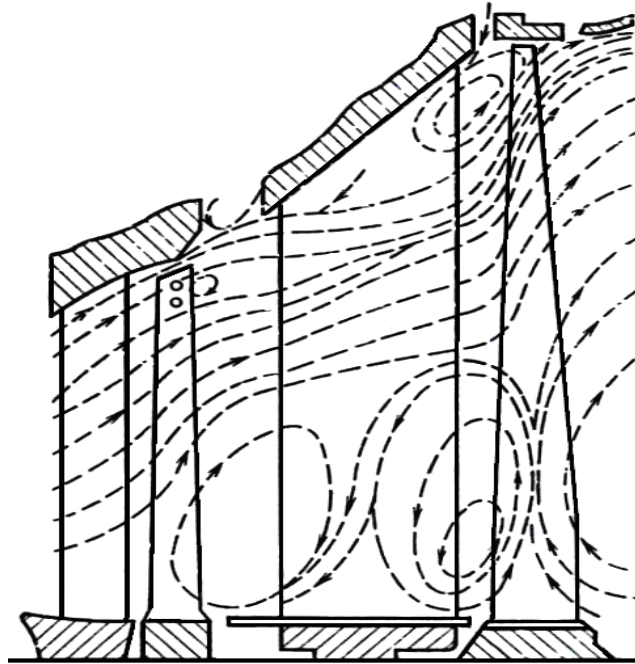


Figure 1.14: Vortices that are generated in the exit of the stage of the low pressure section.

The effect of the interaction of the boundary layer and the condensation is localized in the outer part of the turbulent boundary layer where considerably larger droplets appear in the inviscid core flow of the same cross section. The reason for this effect is that in the outer part of the boundary layer fewer droplets are formed. However, these droplets grow faster and get therefore larger since the reduction of the supersaturation, i.e. the driving force of the growth, decreases slower. This is, because the faster growth of the lower number of droplets produces less condensate than the weaker growth of the larger number of droplets in the core flow and thus causes a slower reduction of the supersaturation [46]. It may also be added that, in turbine flows, the droplets formed by heterogeneous nucleation are relatively few in number and usually grow to a sufficient size to deposit on the blade and casing surfaces. They provide a mechanism for the transfer of chemical species and water to the metallic surfaces, and cause erosion in the phase transition zone. However, condensation on these droplets and on the blade and casing surfaces is too small in magnitude to affect the behaviour of the main flow. The dominant mechanism for condensation in high-speed flows is therefore homogeneous nucleation.

CHAPTER

NUMERICAL MODELING PROCEDURE
IN THE STATOR BLADE CASCADE

2

This work implies a calculation procedure at the outlet of a set of blades when the flow has a certain wet degree. The main detail is to know the behavior and the influence in the geometry that can have this type of damages on blades in normal operation.

In blade cascades the flow of saturated steam is a nebula of droplets. Due to the accumulation that is formed on the stator blade, the erosion features in the following rotor blades is the consequence. The impact of droplets on the blade surfaces is essentially based in the range of particles with sizes affected by the forces of inertia. These droplets cannot follow the path of the steam flow in the blade cascade.

Particularly, the effects of the saturated steam are clears by the occurrence of remarkably erosion damage. In turbines the water becomes to escape from the stator blades in form of large drops, generally toward the suction side of the following rotor blade, causing there erosion problems.

Erosion and reduction in efficiency are in relationship with the accumulation of the fine nebula drops on the blade profiles. Only the accumulation leads to the generation of large drops, which cause flow losses and erosion damage directly.

The observations show that is of practical importance an approximated calculation of the drop movement in a mesh configuration for a turbine, of the saturated steam and, in particular, of the accumulation of drops on the stator blades, if with the calculation procedure the fundamental characteristics of the drops distribution are qualitative and quantitatively detectable.

The analysis of the influence of the water in the flow is had, seeing itself as loss due damage of the wet steam.

2.1 Conditions for calculation of drop movement

The movement of water on the blade channel is the distribution velocity and local density of steam. As a condition for the calculation of the drop movement, first the velocity field of the steam in the blade cascade must be calculated. For calculation of the velocity distribution in the subsonic region the procedure which permits the treatment of the mesh in the curvature is used.

Frequently the blade cascades with supercritical pressure ratio and transonic velocities in the last stages of steam turbines are used. In these cases, for the calculation of the velocity field in the mesh, an appropriate procedure for transonic conditions is needed. In the following section a two-dimensional time step procedure is described in detail.

With the velocities in the profile surface and in the mesh, the motion equations of individual drop were calculated by Gyarmathy [46] and the drop trajectories already calculated were used for the calculation of the local drops distribution in the mesh.

For the computer model the stream of frictionless flow is divided on the blade surface. Here, real conditions are given in order to determine quantitatively the water accumulation in the symmetric stator blade cascade mesh.

2.2 Transonic stream in the mesh

For the calculation of the compressible-subsonic stream in blade cascades, generally the method of singularities is used. For calculating the transonic stream, the time step procedure is suitable.

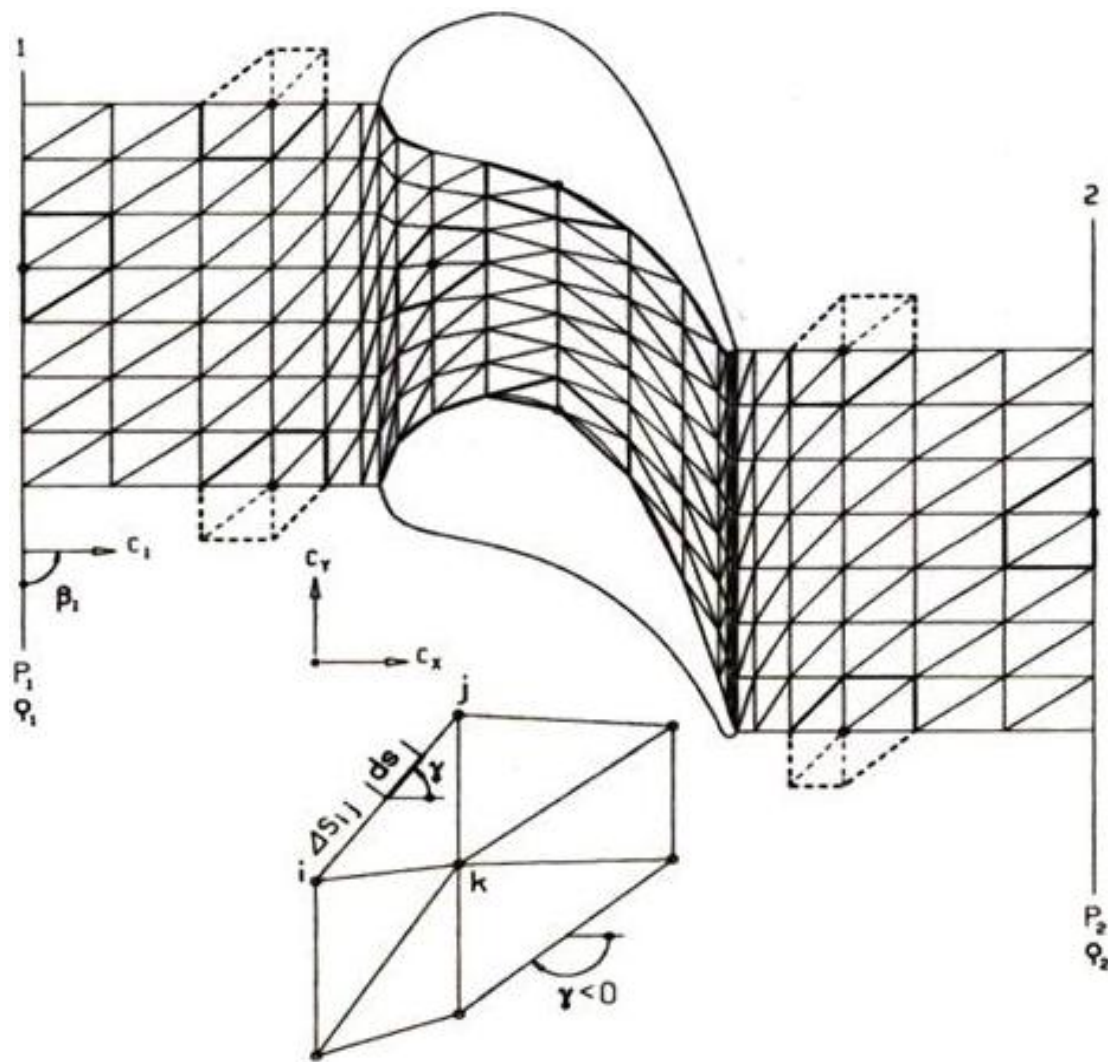


Figure 2.1: Designation of the zone of flow by mesh.

With the arrangement according to Fig.(2.1) the starting point of the calculation of the estimated field velocity c_x , c_y , is does not agree with the zone of flow which can be calculated yet; however, the boundary conditions of the problem are fulfilled. In future, the ideal gas with constant relationship of the specific thermal capacities k is accepted for the medium flow.

With the polytropic law, the pressure and density are in each point of well-known field for this approximation. Any kind of field can be treated in a compressible fluid regarded as a possible momentary condition within an unsteady procedure.

If this condition prevails at time $t = 0$ and if is kept as constant $t > 0$, then an iterated transition adjusts itself to a stationary condition, which is the flowing state searched. The theory determines this temporal transition, which offers the advantage that the problem receives a parabolic character everywhere in the field, since the solution in the time $t + \Delta t$ from the time t , until is sufficiently closed at the final state. The parabolic character makes the treatment of subsonic and supersonic problems possible.

In order to solve the problem, a mesh configuration is made, suggested as in Fig.(2.1). The point of mesh k surrounding hexagonal space, whose volume is ΔV_k is in the Fig.(2.1), is still drawn separately. The simplifying accepts that in the points k of the existing values c_{xk} , c_{yk} , ρ_k , p_k as average values of the components of the velocities and the condition over the whole ΔV_k are regarded at the same time to be allowed. It is possible formulate the conservation laws for these spaces.

However, first the law of the change of state may be indicated, which is accepted as polytropic, in accordance with

$$P_k = P_1 \left(\frac{\rho_k}{\rho_1} \right)^n \quad (2.1)$$

whereby index 1 always refers about flow condition.

The polytropic exponent n is given by the Eq.(2.1). In the practice, the most important case of the adiabatic procedure is with the definition over the polytropic efficiency η_p

$$\frac{n}{n-1} = \frac{1}{\eta_p} \frac{\kappa}{\kappa-1} \quad (2.2)$$

2.3 Velocity Fields

The base factors serve to the Mach number and speed of sound in the flow, which provide the index 1, and the quantities with the index R.

$$a_1 = \sqrt{\kappa \frac{P_1}{\rho_1}} \quad (2.3)$$

$$M_1 = \frac{c_1}{a_1} \quad (2.4)$$

$$\rho_R = \rho_1 \left(1 + \frac{\kappa - 1}{2} M_1^2 \right)^{-\frac{\kappa}{\kappa - 1}} \quad (2.5)$$

$$\rho_R = \rho_1 \left(\frac{P_R}{P_1} \right)^{\frac{1}{\kappa}} \quad (2.6)$$

A condition for the application of the Eq.(2.6) is that the function of the mesh and the leading edge crossing compression shocks must be weak. This condition is very well fulfilled with the turbine mesh.

It is accepted that in the flow, the angle β_1 takes place. In the zone of flow of the mesh profile the velocities of the compressible stream with the given variables of state become pressure and density of inlet and outlet plane after the relationship

$$c^2 = \frac{2\kappa R}{\kappa - 1} \left[1 - \left(\frac{P}{P_1} \right)^{\frac{\kappa - 1}{\kappa}} \right] \quad (2.7)$$

is calculated.

In the outline of the profile the condition is fulfilled if the velocity is tangential. Thus it is possible if the velocity, pressure and density of the fields regarding the size in the inlet and outlet plane linear can be interpolated.

In the closest section l_{min} the exit angle β_2 in the following form can be written:

$$\sin \beta_2 = \frac{l_{min}}{t} \left(\frac{\kappa + 1}{2} \right)^{-\frac{1}{2\kappa-1}} \left[M_2 \left(1 + \frac{\kappa - 1}{2} M_2^2 \right)^{-\frac{1}{2\kappa-1}} \right]^{-1} \quad (2.8)$$

$$\sin \beta_2 = \frac{l_{min}}{t} \quad \text{für} \quad M_2 = 1.0 \quad (2.9)$$

with

$$M_2 = \sqrt{\frac{2}{\kappa - 1} \left[\left(\frac{P}{P_0} \right)^{\frac{\kappa}{\kappa - 1}} - 1 \right]} \quad (2.10)$$

Thus, a theoretically exit angle β_{2is} of the mesh turbine results in the case of isentropic expansion on a given pressure side. The velocities in x and y-direction toward the trailing edge are calculated

$$c_x = c \cdot \cos \left(\beta_2 - \frac{\pi}{2} \right) \quad (2.11)$$

$$c_y = c \cdot \sin \left(\beta_2 - \frac{\pi}{2} \right)$$

The estimated parameters, e.g. velocity, pressure and density fields are introduced as initial values for the iterative methods. The pressure p_1 and p_2 are well-known from the given state of flow. Also is known c_1 and c_2 in each case with p_1 and p_2 from the Eq.(2.7).

2.4 Conservation laws

In Eq.(2.2) the polytropic efficiency η_p considers the friction in summary way. It allow to understand the friction strength constantly distributed in the area.

It can suppose the field strength per mass unit, in the direction of the increasing meridian coordinate against the points n' . Then is

$$\delta F = \eta_p \frac{dh}{dn'} \quad (2.12)$$

$$dh = \eta_p \frac{dp}{\rho} \quad (2.13)$$

$$\delta F = \eta_p (1 - \eta_p) \frac{dp}{dn'} \quad (2.14)$$

If these equations are divided by dn' , dp/dn' is replaced in such a way by the developed $\Delta p/\Delta n'$, where Δp and $\Delta n'$ are the total differences from inlet to outlet, then follows finally

$$\delta F = (1 - \eta_p) \frac{\Delta p}{\bar{\rho} \Delta n'} \quad (2.15)$$

whereby $\bar{\rho}$ is an average value of the density. Thus the polytropic exponent n and the friction force δF can be determined for a given η_p .

For the transition the continuity equation applied on the volume element ΔV_k reads

$$\rho_1 V_1 = \rho_2 V_2 \quad (2.16)$$

The circulation is extended in that way over the whole element.

For a list of the impulse equation in meridional direction is considered the following: A is the impulse stream entering in the area, B is the pressure force, C is the ideal friction force. Then is valid

$$A = \int \rho (c_x \sin \gamma - c_y \cos \gamma) c_x \delta s$$

$$B = \int p \sin \gamma \delta s$$

$$C = -\Delta V_{ir} \rho \delta F$$

Thus the impulse equation is written



therefore 

In the same way the impulse equation in tangential direction is deduced itself. It reads



The circulations can be represented as sums of the connecting distances Δs_{ij} in the Fig.(2.1), in each case are multiplied by the average value integrating along the distance. For example, in the Eq.(2.16) then the integral is read



where γ_{ij} is the angle of inclination of the side that connects the points designated with i and j . The summation is extended over all sides.

2.4.1 Dimension of the conservation laws

For the representation of the appropriately calculation procedure, the dimensionless formulation may be introduced in addition of the following definition:

$$B = \frac{\delta b}{\delta b_1} \quad : \text{Stream width}$$

$$S_{ij} = \frac{\Delta s_{ij}}{l_a} \quad : \text{Length of the element}$$

$$K_\kappa = \frac{\Delta V_\kappa}{l_a^2 \delta b_1} \quad : \text{Volume of the element}$$

$$r = \frac{a_1 t}{l_a} \quad : \text{Time}$$

$$P = \frac{P}{\rho_1^2 M_1} \quad : \text{Pressure} \quad (2.19)$$

$$\sigma = \frac{\rho}{\rho_1} \quad : \text{Density}$$

$$\Phi = \frac{l_a \mathcal{F}}{c_1^2} \quad : \text{Friction Force}$$

$$U = \frac{\rho_x}{\rho_1 c_1} \quad : \text{Axial Velocity}$$

$$V = \frac{\rho_y}{\rho_1 c_1} \quad : \text{Peripheral Velocity}$$

Here, index 1 refers to the inlet level, with dependence of time $t = 0$. The axial length of the mesh is l_a . Then the Eq.(2.16), (2.17), (2.18) and (2.1) are represented in the following way:



$$(2.20)$$



$$-\sigma_\kappa M_1 \Phi \quad (2.21)$$



$$(2.22)$$

$$P_\kappa = P_1 \sigma_\kappa^n \quad (2.23)$$

On the basis of U, V, P and σ into all points in the mesh in a stream value τ the temporal derivatives Eq.(2.20) - (2.22) can be calculated



$$(2.24)$$



$$(2.25)$$

$$\text{[Diagram showing a grid of points with arrows indicating flow direction and variables } U_k, V_k, \sigma_k \text{ associated with points } P_k \text{]} \quad (2.26)$$

the magnitude of U_k , V_k and σ_k in the time $\tau + \Delta\tau$ and the Eq.(2.23) are associated to P_k . The consequence to receive the function values is the smooth, in order to avoid instabilities in the calculation, on which the calculation around a further interval of $\Delta\tau$. It is terminated, if the function values with increasing τ do not change substantially.

2.5 Condition of periodicity in the profile

The edges which can be treated simply represent the upper and lower delimitations of the profile blade range. Here the condition of periodicity must be fulfilled. It demands that the sizes in the place (i, j_s) are equal to those in the place (i, j_p) , like are represented in Fig.(2.2).

The inclusion of two additional points in the cascade reaches the actual boundary lines (i, j_s-1) and (i, j_p+1) to internal points. The values on these border lines can be determined by means of the normal differential equations. The sizes of the two additional lines are according for periodicity from internal grid points.

$$f(i, j_s-1) = f(i, j_p+1) \quad (2.27)$$

$$f(i, j_p+1) = f(i, j_s-1) \quad (2.28)$$

The function f does not correspond to the function character σ , P , U and V . In fact, is guaranteed the values on the lines (i, j_s) and (i, j_p) corrects. In order to exclude these deviations additionally, in the area of the profile of blades the values of (i, j_s) in the grid of the mesh are assigned or turned around with (i, j_p) .

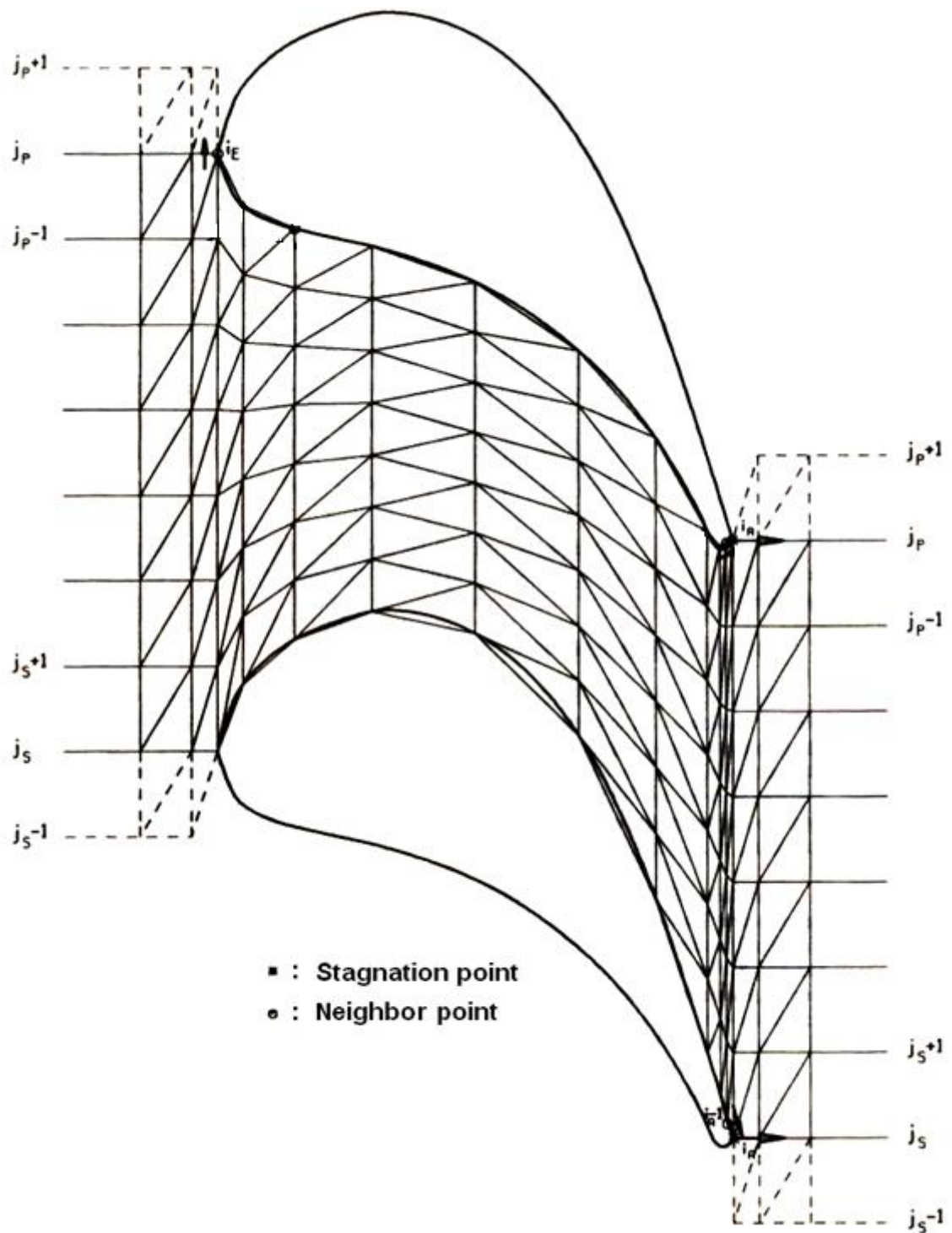


Figure 2.2: Range of periodicity and direction of flow in the stagnation point.

2.5.1 Boundary Condition in Inlet and Outlet Plane

The two dimensional elements have there only five sides considering the points, and the examples are indicated in Fig.(2.1). For the calculation of the elements, equal to the others, only the sizes with index k appear under the sigma sign.

The boundary lines 1 and 2 must be arranged at least for a division far away from the mesh. Then P and σ as independent of place and time are prescribed. With the pressure on the boundary lines 1 and 2 reads the associated quantities P and σ

$$P(1) = \frac{P_1}{R_1^2 M_1}$$

$$\sigma(1) = 1.0$$

$$P(2) = \frac{P_2}{R_2^2 M_2}$$

$$\alpha(2) = \left(\frac{P_2}{P_1} \right)^{\frac{1}{n}}$$

$$W = \sqrt{U^2 + V^2}$$

$$U = W \left(\alpha_1 \frac{r_1}{2} \right)$$

$$V = W \left(\alpha_2 \frac{r_2}{2} \right) \quad (2.29)$$

$$U_2^* = U_1^*$$

$$V_2^* = V_1^*$$

Here, refers index (1) on the inlet level, index (2) on the following level and index (n) in each case on the outlet plane. The symbol * shows the size with the inflow angle β_1 formulated for the conditions of the inlet level. Thus, one receives U and V in the level 2, therefore the exit angle.

$$\beta_2 = \tan^{-1} \frac{V_2}{U_2} \quad (2.30)$$

Index 1 and 2 refer the deflection condition.

2.5.2 Boundary Condition for the Profile Outline

With a frictionless stream the velocity vector \vec{c} must be zero on the blade surfaces.

$$\vec{n} \cdot \vec{c} = 0 \quad (2.31)$$

with five-lateral in two dimensional elements at the blade surfaces. The summations are simplified as polygon sides, the dimensionless function size disappear of the part of the blade surface, with which the impenetrability condition for the suction and pressure side [46] of the blade surface is expressed.

$$U \sin \alpha + V \cos \alpha \quad (2.32)$$

With the blade geometry also the angle θ is given on the blade surfaces. The associated velocity components are expressed in the blade surfaces

$$W = \sqrt{U^2 + V^2}$$

$$U^* = W \cos \theta \quad (2.33)$$

$$V^* = W \sin \theta$$

The symbol * shows the magnitude with the resulting velocity component and with the angle, formulated for the conditions of the blade surfaces.

2.5.3 Condition of discharge in the trailing edge

The trailing edge in Fig.(2.2) requires a certain reasoning. Same pressure in the pressure and suction side of the blade is demanded in its direct proximity. Then is represented the function values in the following way.

$$\sigma (i_A - 1, j_S) = \sigma (i_A - 1, j_P)$$

$$P (i_A - 1, j_S) = P (i_A - 1, j_P)$$

$$W_S = \sqrt{U (i_A - 1, j_S)^2 + U (i_A - 1, j_S)^2}$$

$$U^* (i_A - 1, j_P) = W_S \cdot \cos \theta (i_A - 1, j_P)$$

$$V^* (i_A - 1, j_P) = W_S \cdot \sin \theta (i_A - 1, j_P) \quad (2.34)$$

$$W_P = \sqrt{U (i_A - 1, j_P)^2 + U (i_A - 1, j_P)^2}$$

$$U^* (i_A - 1, j_S) = W_P \cdot \cos \theta (i_A - 1, j_S)$$

$$V^* (i_A - 1, j_S) = W_P \cdot \sin \theta (i_A - 1, j_S)$$

Here, $\theta (i_{a-1}, j_s)$ and $\theta (i_{a-1}, j_p)$ are the tangential angle in the associated place (i_{a-1}, j_s) and (i_{a-1}, j_p) . The symbol * shows the reformulated magnitude with the angle θ .

2.5.4 Direction of flow within the stagnation point

For the determination of the stagnation points in the time step procedure does not exist accurate solution. Depending of the blade profile, the direction of flow must be accepted in the stagnation points as in Fig.(2.2). Thus, is defined the direction of flow and the neighbor point, in order to complete the physical conditions in the blade profile. During the calculation method the accepted stagnation points remain unchanged, because their positions do not result from the calculation.

The velocity components directly on the stagnation point (j_E, j_P) and (i_A, j_S) follow the impulse equations (2.21) and (2.22). The determination of the velocity direction at the points of neighbor is described as a function of the blade profile in the direction of flow in the section 2.5.2.

If the resulted with the accepted stagnation points are not real, this acceptance must improve and the calculations must be repeated. The stagnation point refers in each case to the joint of the mesh.

The angle of inclination γ of the element is already defined (see Fig. (2.1)), does not have influence on this stagnation point, since the angle γ is a geometrical size of the element.

2.6 Numerical Approximation of the Balance Equations

For the smoothing procedure of the balance equations, a method of numeric approximation is examined. The smoothing absorbs practically the ripples of the solution functions resulted from computing inaccuracies. The equations takes place according to time (t) works on ($t + \Delta t$). In the Fig.(2.3) i and j are the net indices in x and y direction.

The smoothing is accomplished by σ , U and V . The function f means in each case a function before the smoothing, g the same function after the smoothing. After the smoothing the Eq.(2.33) for the character function U and V in the blade surface must be used, thus the Eq.(2.32) is fulfilled. Anyhow the Eq.(2.23) with P and σ is fulfilled in the entire range. ϕ is an empirical constant. For the absorption the product of ϕ and the time step value Δt is determined. Small values result in a strong absorption. According to the exactitude of the calculation it can be selected the magnitude of ϕ , which is adapted to the desired computational accuracy with approximately 100.

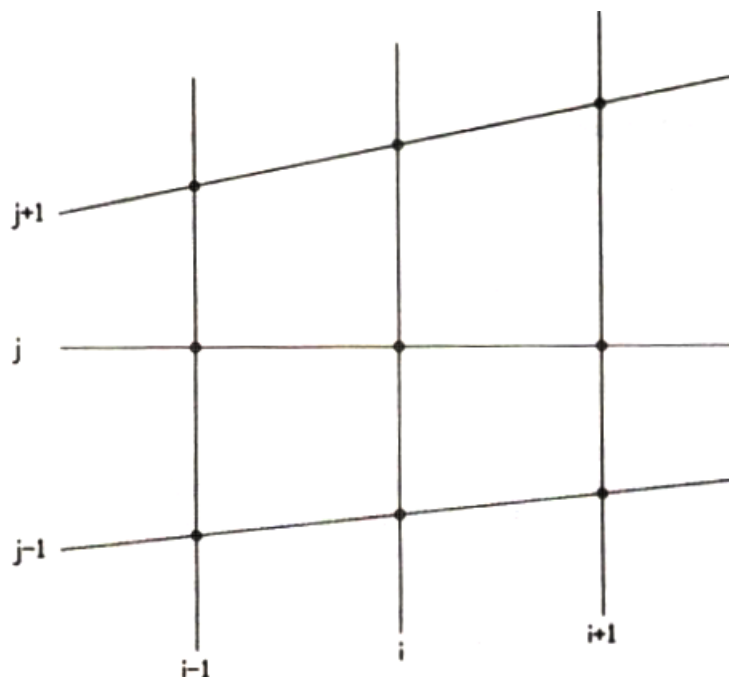


Figure 2.3: The net indices.

$$\frac{1}{\Delta t} \left(\frac{\partial \phi}{\partial t} \right)_{i,j,k} = \dots \quad (2.35)$$

$$\frac{1}{\Delta t} \left(\frac{\partial \phi}{\partial t} \right)_{i,j,k} = \dots \quad (2.36)$$

Where a is the local speed of sound. The computer cost depends of the time step magnitude Δt . For the organization of a more finely mesh, Δt must be selected smaller, in order to secure stability.

2.7 Criterion to Stop the Computing Method

As stop criterion is used the deviation of the function size at all points and should be below a border which can be specified.

The total enthalpy in the output pressure after certain number of time steps, presents convergence in the control. A simplification of the equation system is possible by introduction of a constant specific total enthalpy for the entire computing area. This is from the first law of thermodynamic for stationary systems and taking or adding work. The energy equation in differential form can be replaced therefore by an algebraic equation [47].

$$h_{tot} = \dots \quad (2.38)$$

The replacement of the energy equation in differential form by the expression for the constant total enthalpy results in a restriction in the case of the application of the equation system. The total enthalpy is constant only in a stationary system. If is inserted $h_{tot} = const.$ into the energy equation, then this is simplified to the expression

$$\frac{\partial p}{\partial t} = 0 \quad (2.39)$$

i. e. the pressure must be constant. The total enthalpy takes the simple form



$$(2.40)$$

Further control is accomplished by the comparison of inlet and outlet mass stream and the mass density of the stream $\rho \cdot c$ in inlet and outlet plane as well as in the closest cross section. The theory is not suitable for high supersonic speed. In addition, with very small Mach number it fails, as the structure of the Eq.(2.17a,b) and (2.18). Indeed, the output condition is invalidated in the border line of the incompressibility for any velocity field. This difficulty makes itself noticeably as instability of the calculation, for a long time before this border line is reached.

2.8 Transformation of coordinates

The coordinates of one point in the X_1 - X_2 system through PX_1 and PX_2 in Fig.(2.4) are given. From turn around the angle ϕ is developed a new system where Y_1 - Y_2 results. When is written an instruction sequence, is calculated the new coordinates PY_1 and PY_2 . The new coordinates result from the transformations equation

$$\begin{aligned} Y_1 &= X_1 \cos \phi + X_2 \sin \phi \\ Y_2 &= X_1 (-\sin \phi) + X_2 \cos \phi \end{aligned} \quad (2.41)$$

In order to program this equation of transformation, the transformation matrix T is used, multiplied by the column vector PX and the column vector PY is received.

$$T \begin{bmatrix} t_1 & t_2 \\ b_1 & b_2 \end{bmatrix} = \begin{bmatrix} \cos\phi & \sin\phi \\ -\sin\phi & \cos\phi \end{bmatrix} \quad (2.42)$$

It can be written then:

$$\begin{bmatrix} t_1 & t_2 \\ b_1 & b_2 \end{bmatrix} \begin{bmatrix} P_1 X_1 \\ P_2 X_2 \end{bmatrix} = \begin{bmatrix} P_1 Y_1 \\ P_2 Y_2 \end{bmatrix} \quad (2.43)$$

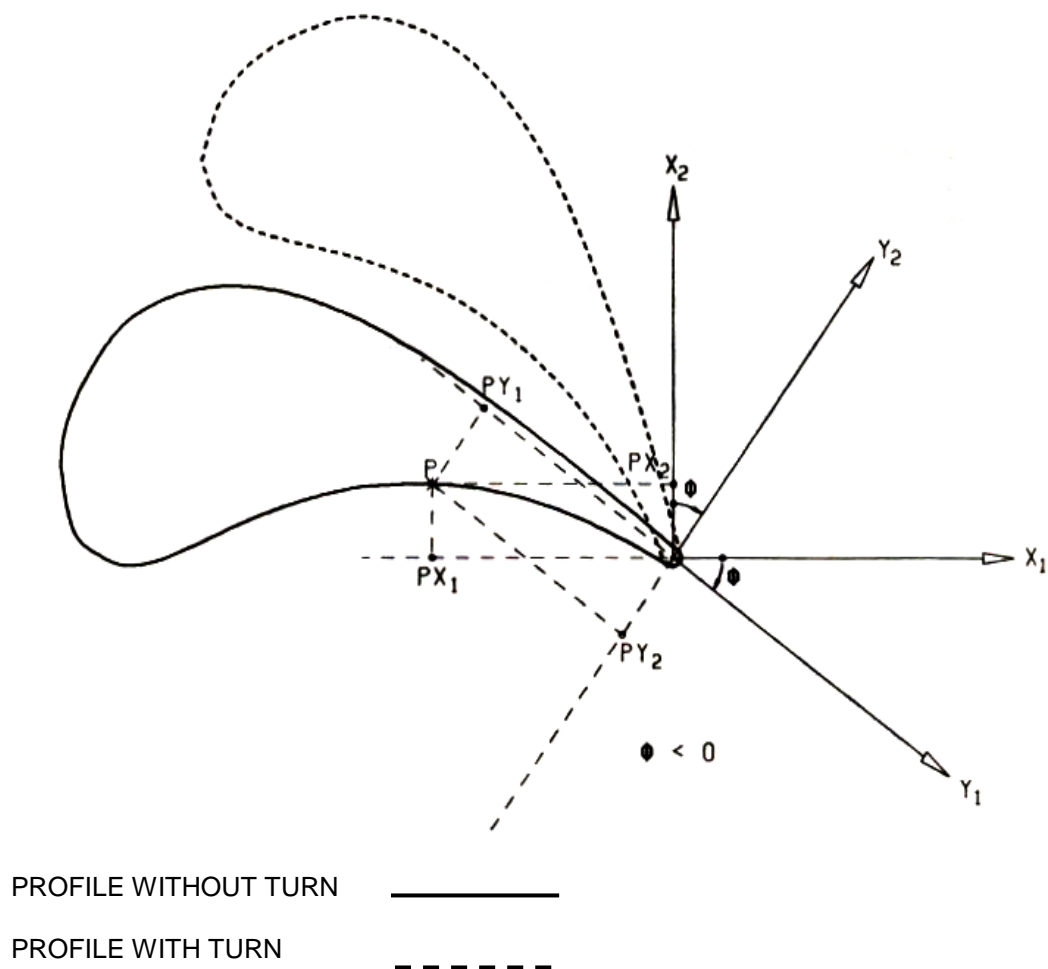


Figure 2.4: Rotation in Cartesian coordinate system.

The arithmetic rule for the elements of the column vector reads:

$$P_i = \sum_{j=1}^n t_{ij} P_j \quad (2.46)$$

Thus, is transformed the profile coordinates with the given progressive rate angle ϕ into the new coordinates, with the corresponding angle $\beta_s - \pi/2$.

2.8.1 Conditions to mesh

The periodicity of the cascade flow (when all blades are identical in shape and equally spaced from each other) can be guaranteed in the calculation, which covers only one blade channel and the outflow, only by periodic boundary conditions on the lateral delimitations of the computing area. Also, this requires geometrically periodic bounds in diverting range.

In addition, the computing mesh is divided in such a way that the respective arithmetic procedures with the smooth do not become strongly affected by the neighbor points and without loss of physical characteristics evenly balanced, in order to avoid instabilities of the calculation. Sharp profile outlines are represented by mesh refinements within this range.

2.8.2 Mesh organization

The mesh organization along the mainstream direction fulfills the periodic boundary conditions of the bounds and diverting range. But this computing mesh has an irregular configuration, particularly in the trailing edge.

The H-mesh, which is used for the mesh organization, is defined as follows: by straight lines parallel to the circumferential direction, intersects the lines, in profile periodicity areas parallel to the axial direction, but in the channel range, being limited by both blades parallel to the blade profile. The H-mesh is associated in Fig.(2.1).

The H-mesh does not only fulfill the periodic conditions and the diverting range, also, irregular mesh configurations are not generated. Therefore, the H-mesh fulfills in best form the necessary conditions. Since the inclination of the blade profile is different against the circumferential direction, the mesh organizations with variable distances are divided in axial direction. A strongly curved outline as a leading and trailing edge can be approximated with closer mesh organization, whereby clear damages occur.

It is also conceivable that the mesh configuration is divided in circumferential direction with different distances. However, the calculation becomes with an extremely different element volume unstably. Therefore, the mesh organizations into circumferential direction are equidistantly divided. The Fig.(2.1) shows the mesh organizations, which were divided with different distances in x-direction and equidistantly into y-direction.

2.9 Balance equations for turbulent boundary layer

In the proximity of the surface of the wet blade the drop movement is affected by the boundary layer in the profile. The computing procedure belongs to the group of the integral methods, which results from the integration of the partial differential equations of the flow over the boundary layer thickness.

2.9.1 Integral condition for the impulse

The integral condition for the impulse as the force equilibrium in x-direction, averaged over the boundary layer thickness δ

$$\frac{d}{dx} \int_0^{\delta} \rho u^2 dy = \tau_w \quad (2.47)$$

with the definitions

$$\delta_1 = \int_0^{\delta} \left(1 - \frac{u}{u_b}\right) dy \quad : \text{Displacement thickness} \quad (2.48)$$

$$\delta_2 = \int_0^{\delta} \frac{\rho}{\rho_b} \left(1 - \frac{u}{u_b}\right)^2 dy \quad : \text{Impulse loss thickness} \quad (2.49)$$

$$c_f = \frac{\tau_w}{\frac{\rho_b}{2} u_b^2} \quad : \text{Friction coefficient} \quad (2.50)$$

$$\tau_w = \left(\mu \frac{\partial u}{\partial y} \right)_{y=0}$$

$$M_\delta = \frac{u_\delta(x)}{a_\delta(x)} \quad : \text{local Mach number} \quad (2.51)$$

The local speed sound $a_\delta(x)$ is according gas dynamics laws from the velocity $u_\delta(x)$ and $M_\delta(x)$. In addition the loss of energy thickness δ_3

$$\delta_3 = \int_0^{\delta} \frac{\rho}{\rho_b} \left[1 - \left(\frac{u}{u_b} \right)^2 \right] dy \quad : \text{energy thickness} \quad (2.52)$$

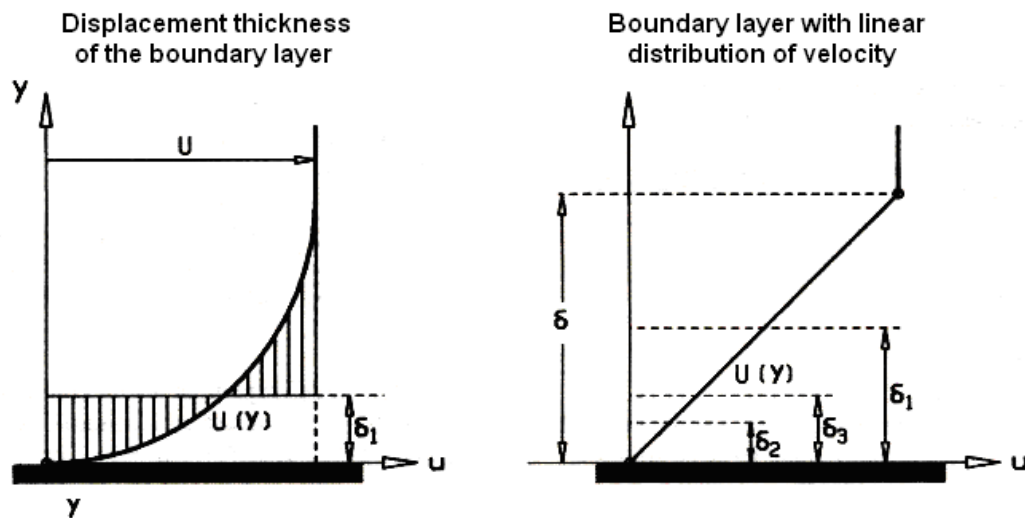


Figure 2.5: Representation of the boundary layer thicknesses.

In Fig.(2.5) is represented a boundary layer with linear velocity profile and the quantitative relation of δ_1 , δ_2 and δ_3 .

2.10 Drop movement of individual drop

In order to calculate the distribution of drops on blade profiles, first is necessary to describe the movement of drops in a zone of flow. In particular, the behavior must be considered by nebula drops in the low pressure saturated steam.

The movement of nebula drops in the low pressure section is of special importance, since only under the dominant conditions a remarkable separation of the water and vapor phase is expected with flow streams. The separation of nebula drops on blades supposes the transport of the drops toward the surface and their adherence. The transportation effects are essentially based on the effect of forces of inertia.

The beginning for the calculation of individual drop movement to the stream in turbines proceeds from the force equilibrium:

$$\sum \vec{K} = 0 \quad (2.53)$$

The sum of all forces around a drop is zero. The resulting strength is developed itself generally as follows

$$\vec{W} + \vec{T} + \vec{A} + \vec{G} + \vec{W}_M + \vec{K}_p + \vec{K}_E = 0 \quad (2.54)$$

Therein mean

\vec{W} : Drag force

\vec{T} : Force of inertia

\vec{A} : Lift force

\vec{G} : Gravity force

\vec{W}_M : Force due to additionally move along steam mass

\vec{K}_p : Field force due to a pressure gradient

\vec{K}_E : Electrostatic forces.

In case of the movement of small drops in steam flow the relationship is simplified. The lift force can be neglected only if the densities of drops and flow medium are of the same large order. The gravity force is neglected likewise, since it cannot exert noticeable influence with the dominant velocity and the short ways which can be regarded. The force \vec{W}_M remains likewise unconsidered, since the influence along the moved steam mass is negligibly small due to the large density variation. The field force due to a pressure gradient is under the given conditions, likewise lies around several orders of magnitude lower than the force, as a calculation showed. Finally, generally also the electrostatic forces can be neglected in case of the steam flow.

The Eq.(2.53) and (2.54) lead to the simple relationship

$$\vec{W} + \vec{T} = 0 \quad (2.55)$$

The force becomes

$$\vec{W} = c_w \cdot \frac{\rho}{2} \cdot w_{rel}^2 \cdot \pi \cdot r_T^2 \quad (2.56)$$

and the force of inertia is defined

$$\vec{T} = m_T \cdot \frac{d\vec{v}_T}{dt} \quad (2.57)$$

Here c_w is the coefficient of drag, ρ is the steam density, r_T the drop radius and w_{rel} the relative velocity between steam and drop in accordance with the relationship

$$\vec{w}_{rel} = \vec{w}_D - \vec{w}_T \quad (2.58)$$

The drop mass m_T is calculated with

$$m_T = \frac{4}{3} \pi \rho \cdot r_T^3 \quad (2.59)$$

From this, the general differential equation for the drop movement follows

$$m_T \frac{d\vec{v}_T}{dt} = c_w \cdot \frac{\rho}{2} \cdot \pi \cdot r_T^2 \cdot (\vec{w}_D - \vec{v}_T)^2 \quad (2.60)$$

In this work, the drops with a selected size always have a spherical shape, which is forced by the surface tension maintaining as constant. For the coefficient of drag c_w the spherical particle is presented theoretically and

experimentally determined by relations. The coefficient of drag for three ranges of Reynolds number Re_T is approximated by the following:

$$Re_T < 0.2 \quad (2.61)$$

$$c_w = \frac{24}{Re_T} + 2C$$

$$0.2 < Re_T \leq 8.0 \quad (2.62)$$

$$c_w = \frac{24}{Re_T} + 2C$$

$$Re > 8.0$$

$$c_w = \frac{216}{Re_T Re} + 2C \quad (2.63)$$

The Reynolds number is formed by the relative velocity with the drop diameter d_T and w_{rel} .

$$Re = \frac{d_T \cdot w_{rel}}{\nu} \quad (2.64)$$

ν is the kinematic viscosity of steam. The theoretical calculations show that for the movement of nebula drops $Re_T \ll 0.2$ is generally always valid.

The Eq.(2.62) and (2.63) are valid under the condition of a continuous medium. In case of extremely small body, generally no more continuum stream is presented. As a measure of the deviation, the Knudsen number K_n is consulted,

$$K_n = \frac{\lambda}{d_T} \quad (2.65)$$

the relationship of mean free path λ of the molecules refers to a characteristic length of wet flowing through the drop. Appropriately, during the drop generation the drop diameter d_T is selected.

With increasing deviation from the continuum stream, the Knudsen wet number decreases. The correction factor f_c is developed [49], the free molecule in the stream is validated and the drag coefficient in the case of a deviation from the continuum stream is corrected.

$$f_c = \frac{1}{1 + 2.5 K_n} \quad (2.66)$$

The mean free path λ in Eq.(2.70) is calculated by

$$\lambda = 15 \frac{\mu}{\rho R T} \quad (2.67)$$

where μ is the dynamic viscosity of steam, ρ is in the state of saturation, R is the gas constant and T is the absolute temperature.

For the calculation of drop courses the velocity field must be given by drops moving with the help of the Eq.(2.60). Appropriately, the Eq.(2.60) transforms the individual components of a coordinate system formulated. Since the investigations are referred to the stream on the basis of the Eq.(2.60) a set of equations for the two-dimensional drop movement in the Cartesian coordinate system is derived. With the identities

$$\begin{aligned} v_x &= \bar{x} & \dot{v}_x &= \bar{\alpha} \\ v_y &= \bar{y} & \dot{v}_y &= \bar{\beta} \end{aligned} \quad (2.68)$$

and the amount of the relative velocity

$$w = \sqrt{(v_x - \bar{x})^2 + (v_y - \bar{y})^2} \quad (2.69)$$

whereby the steam flow in the place (x, y) by the velocities w_{Dx} and w_{Dy} is given, follows the relationship of the Eq.(2.60) of the equation system:

$$\frac{dw}{dt} = \frac{dw_{Dx}}{dt} + \frac{dw_{Dy}}{dt} \quad (2.70)$$

$$\frac{dw}{dt} = \frac{dw_{Dx}}{dt} + \frac{dw_{Dy}}{dt} \quad (2.71)$$

2.11 Interpolation of flow parameters between the mesh points

The momentary position $x(i)$ and $y(i, j)$ of the drop is admitted from the Eq.(2.70) and (2.71). Index i and j refers to the x and y direction. Actually, the flow parameters of the steam flow are well-known only in the points of mesh, thereby they must be determined only by arbitrary drop positions. They are interpolated linearly from the points of neighbor, if the position of the drop does not agree with the mesh point (see Fig.(2.6)).

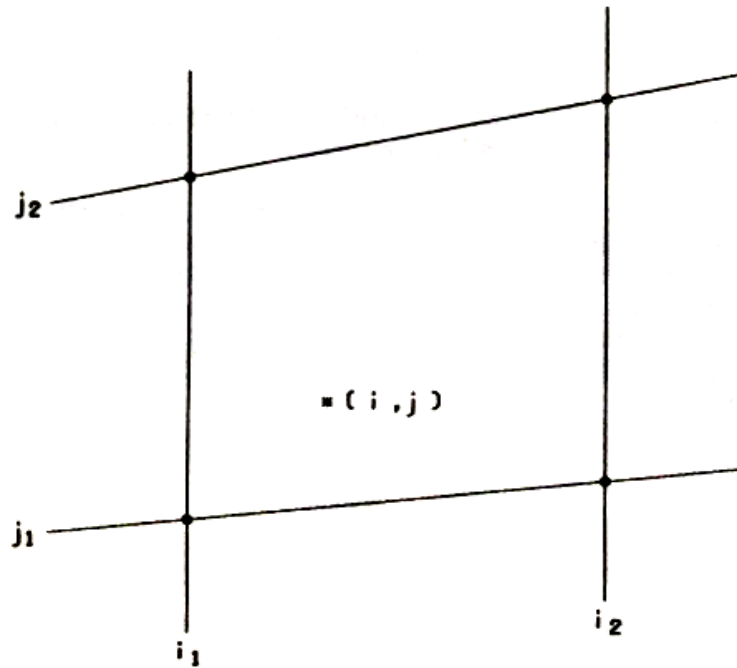


Figure 2.6: Mesh indices.

$$\begin{aligned}
 k_x &= [x(i) - x(i_1)] / [x(i_2) - x(i_1)] \\
 y(i, j_1) &= y(i_1, j_1) + k_x \cdot [y(i_2, j_1) - y(i_1, j_1)] \\
 y(i, j_2) &= y(i_1, j_2) + k_x \cdot [y(i_2, j_2) - y(i_1, j_2)] \\
 k_y &= [y(i, j) - y(i, j_1)] / [y(i, j_2) - y(i, j_1)] \\
 f(i, j_1) &= f(i_1, j_1) + k_x \cdot [f(i_2, j_1) - f(i_1, j_1)] \\
 f(i, j_2) &= f(i_1, j_2) + k_x \cdot [f(i_2, j_2) - f(i_1, j_2)] \\
 f(i, j) &= f(i, j_1) + k_y \cdot [f(i, j_2) - f(i, j_1)]
 \end{aligned} \tag{2.72}$$

Here the function f generally needs the functions σ , P , U and V .

2.12 Drop distribution in the mesh outlet plane

The deviation must show that the drop courses from the steam streamlines have an inhomogeneous distribution of the nebula drops in the stream range of the blade channel as well as behind the mesh.

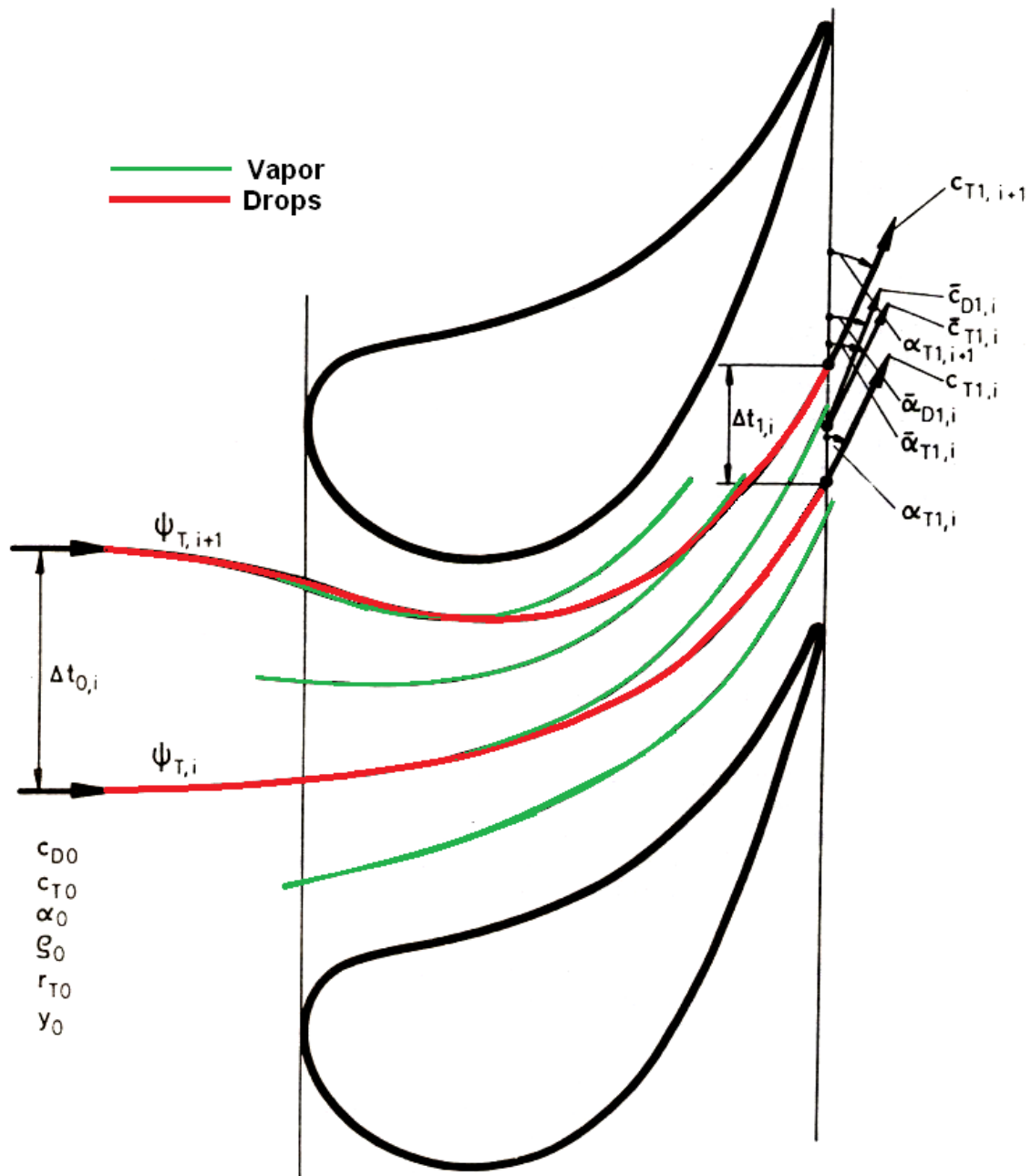


Figure 2.7: Nomenclature for the moisture distribution in the mesh outlet plane.

In Fig.(2.7) follows the drop distribution represented on the basis of a fundamental flow pattern in a blade channel. It provides that the drops before the mesh are homogeneous distributed and that the drop velocity and steam velocity are identical to c_{T0} and c_{D0} here. The stream condition continues homogeneous by p_0 and Y_0 . The drop radius is r_{T0} .

Between the two drop courses $\psi_{T,i}$ and $\psi_{T,i+1}$ in the distance $\Delta t_{0,i}$, which are identical to the steam streamlines in the mesh and two surfaces parallel to the indication level $\Delta t_{0,1}$, the water mass flow is

$$\dot{m}_{0i} = Y_0 \cdot \dot{m}_{0i} \quad (2.73)$$

whereby $\dot{m}_{0,i}$ is the total mass stream between the streamlines and Y_0 is the humidity content in the inlet. The number of drops flowing is then

$$\dot{n}_{0i} = \frac{\dot{m}_{0i}}{\frac{4}{3} \pi r_{T0}^3 \cdot \rho} \quad (2.74)$$

The water mass flow and the number of drops through the mesh for simplification are assumed as constant and permissible [48]. Then is valid

$$\dot{n}_{1,i} = \dot{n}_{0,i} \quad (2.75)$$

Behind the mesh, water and vapor phase are not uniformly mixed and then are equally accepted before the mesh. A certain part of the drops which flow between the pressure side of the blade and the outlet border come in contact with the profile, whereby the simplifying is accepted here and all these drops concentrating in a very thin layer close in the profile surface strongly and finally in a narrow volume of the trailing edge. Really, they form a water film. The remaining drops leave from the mesh with a velocity which more or less deviates to magnitude and direction from the local steam velocity. In addition, they are irregularly distributed over the division. The local moisture content behind the mesh is defined as

$$Y_i = \frac{\dot{m}_{1i}}{\dot{m}_{1i} + \dot{m}_{2i}} \quad (2.76)$$

Therein $\dot{m}_{T1,i}$ represents the quantity of water in the level 1 by the cross section of the height 1 between the courses $\psi_{T,i}$ and $\psi_{T,i+1}$. The zone of flow of steam is presented from the calculation of the transonic stream. The quantity of water between the two drop courses in the level 1 is calculated by

$$\dot{m}_B = \rho_v \frac{4}{3} \pi r^3 \cdot A \quad (2.77)$$

The middle drop course in the steam flow between the courses $\psi_{T,i}$ and $\psi_{T,i+1}$ in the level 1 is:

$$\dot{m}_{D1,i} = \rho_v \frac{4}{3} \pi r^3 \cdot A \quad (2.83)$$

Steam has a medium velocity $\bar{c}_{D1,i}$ in the level 1 in the cross section. This direction is given by $\bar{\alpha}_{D1,i}$. The term $\omega(\alpha_{D1,i} - \bar{\alpha}_{D1,i})$ of the steam quantity is referred to the drop course direction.

2.13 Particular data of stator blade in the last stage of low pressure

Mechanical components in a steam turbine may experience heavy damage by erosion when subjected to repeated impingement of liquid droplets. The flow parameters are in game into the erosion process on blades of last stage of low pressure section. Program code is in function of data base of geometry about introduced stator blade profile.

From the geometric data of the turbine blades and their flow values the knowledge of conditions that govern the low pressure section of steam turbines in the last stage to have an approximate movement of the droplets in the blade cascades and the accumulation of droplets on the stator blades, flowing through the steam by the calculation of the velocity distribution on the basis of the frictionless, two-dimensional, stationary, transonic and homogenous flow will be established.

The determination of the drop distribution in the channel of flow of stator blades provides fundamental information that it can be used to diminish and to solve the problems that arise when they form liquid films in the surface of the blades. The main detail is to know the behavior and the influence in the geometry that can have this type of damages in the blades operating normally.

The steam turbine taken as a reference in this study is from GE and gives 30 MW of power and is analyzed a stator blade in the last stage. The turbine is working in a plant that process phosphoric acid and phosphates, installed in the Industrial Complex Pajaritos in Coatzacoalcos, Veracruz, México. The low pressure section of the steam turbine has five stages. The row of stator step consists of 70 working blades with a measurement of 600 ± 0.5 mm each one; the profile of the stator blade to treat is 980BE23 and the chord is of 44 cm. The pressure that reigns in the input of stator stage is 49 kPa, and the temperature is approximately 86°C. The humidity at the inlet of the stator blade of 8% is found in the Mollier diagram in agreement with reports.

The equations presented previously are discretized to reach the development of the programming code of calculation procedure when coming out of this set of blades when the flow has certain humidity degree. The main detail is to know the behavior and the influence in the geometry that can have this type of damages that are had in the blades in normal operation.

The set of blades must be analyzed considering the amount of drops by cloudiness that exists in the same steam when it begins to become water and cause damages in the trailing edge of the blades stators as a set, appearing erosion problems, that they essentially cause damages in the edge of entrance of the crown rotor blades. Then the analysis of the influence of water in the flow, seeing this like loss of damage of the wet steam is presented.

The results will be presented in according to its influence of the characteristics of clusters conformed by certain number of molecules approximately. The condensation on the last stage of this steam turbine shows the phase change governed by homogeneous nucleation and the nonequilibrium process of condensation. It is known that condensed water vapor affects the performance of the steam turbine, and the blades of the steam turbine are occasionally damaged by erosion due to the interaction with this condensed water. The cluster of droplets is assumed to be spherical, as a one droplet, chemically inert, equal in size, with a smooth surface and the interface has zero thickness.

First, the system of finite mesh is obtained in two dimensions of the flow channel of the stator blades in a cascade of the turbine. For this, they are needed to enter the coordinates of a steam turbine blade profile (table 3.1). Then, the profile coordinates are transformed with the angle that is selecting through the suitable subroutine. The resulting profile is in the Fig.(2.8). The points that conform the stator blade are in table 2.1.

The following is to develop the set of subroutines that will allow it to obtain the coordinates of the mesh in the flow channel. Like input data in the program is necessary to provide the coordinates of the profile, as length and to select the angle to transform the coordinates.

Table 2.1: Points that conform the stator blade.

X	Y	X	Y	X	Y	X	Y
0.288	34.809	19.111	22.98	33.332	-0.597	19.208	35.164
0.577	34.276	20.144	21.904	33.379	-0.58	17.98	36.331
0.865	33.897	21.176	20.751	33.425	-0.557	16.753	37.33
1.153	33.604	22.208	19.515	33.472	-0.53	15.525	38.178
1.441	33.37	23.241	18.19	33.518	-0.497	14.297	38.886
1.73	33.181	24.273	16.765	33.565	-0.457	13.07	39.464
2.018	33.03	25.305	15.231	33.611	-0.408	11.842	39.919
2.306	32.91	26.337	13.574	33.658	-0.346	10.615	40.257
2.594	32.82	27.37	11.779	33.704	-0.261	9.387	40.48
2.594	32.82	28.402	9.826	33.751	0.112	8.159	40.591
3.627	32.525	29.434	7.689	32.91	4.202	6.932	40.588
4.659	32.194	30.467	5.338	32.07	7.638	5.704	40.471
5.691	31.826	31.499	2.728	31.229	10.65	4.476	40.235
6.724	31.42	32.531	-0.198	30.389	13.359	3.249	39.872
7.756	30.974	32.607	-0.352	29.548	15.836	2.021	39.372
8.788	30.488	32.682	-0.444	28.708	18.128	2.021	39.372
9.821	29.959	32.758	-0.509	27.867	20.267	1.797	39.258
10.853	29.387	32.833	-0.556	27.027	22.278	1.572	39.121
11.885	28.77	32.909	-0.591	26.186	24.178	1.347	38.96
12.918	28.106	32.984	-0.614	25.346	25.981	1.123	38.769
13.95	27.392	33.059	-0.627	24.118	28.372	0.898	38.541
14.982	26.626	33.135	-0.631	22.891	30.447	0.674	38.265
16.014	25.805	33.21	-0.626	21.663	32.249	0.449	37.916
17.047	24.927	33.286	-0.611	20.435	33.812	0.225	37.434
18.079	23.986					0.000	36.200

In the flow channel the mesh is adapted through an interpolation polynomial. The contours can be treated like the superior and inferior boundaries of the flow channel reason why resorting to the suitable subroutines the flow channel that forms is the one that is in the Fig.(2.9). With the obtained flow channel the characteristics are introduced in the region of mesh (the parameters of entrance for the flow can be found in tables). The values to introduce are the flow angle, the velocity, the density and the pressure of the steam to the input passage, as

well as the value of the isentropic exponent for the gas, the efficiency of the flow channel and the number of the initial iteration.

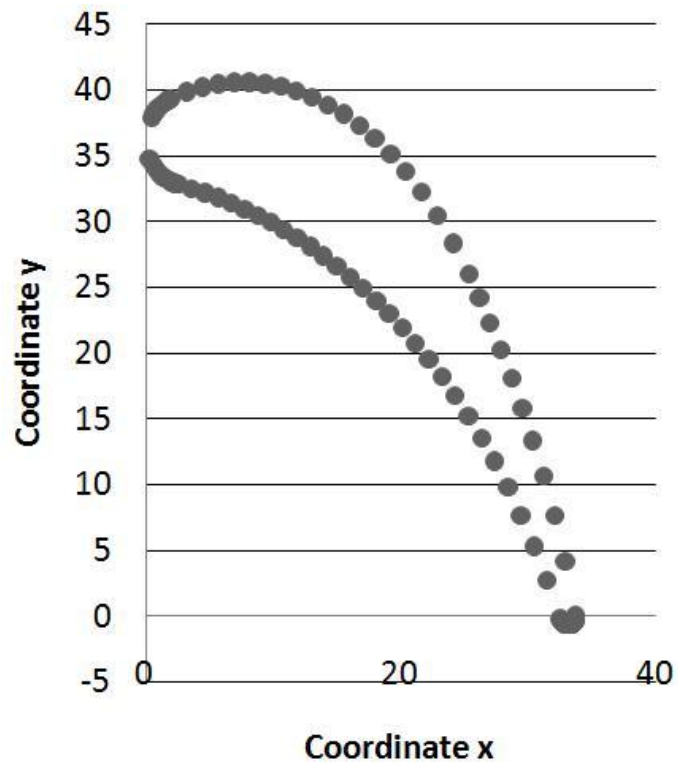


Figure 2.8: Stator blade 980BE23 of low pressure section in a steam turbine.

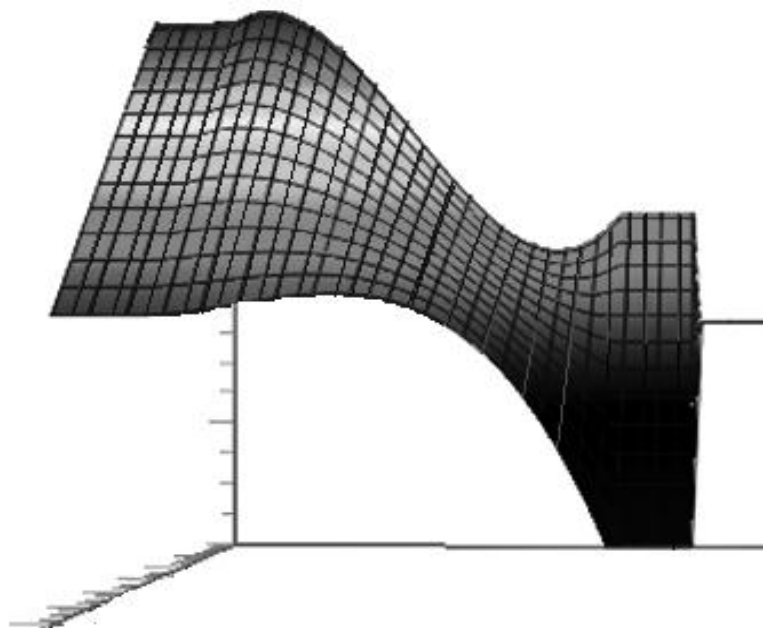


Figure 2.9: Mesh flow channel.

The units used for these magnitudes are the corresponding to SI units. Then, the calculation displays the density and momentum distribution for the potential flow in two dimensions.

The considerations of bidimensional steam flow are:

- Subsonic-transonic,
- Inviscid,
- Compressible,
- Stationary,
- Cluster as a drop is spherical, constant diameter size of drop is 25 μm ,
- Boundary layer in surface of profile.

The flow properties of wet steam on stator blade:

- Inlet temperature = 86.13 $^{\circ}\text{C}$
- Inlet pressure = 0.49 bar
- Inlet steam quality = 0.9
- Inlet stator Mach number = 0.23
- Exit stator temperature = 65 $^{\circ}\text{C}$
- Exit stator pressure = 0.2 bar
- Exit stator steam quality = 0.893
- Exit stator Mach number = 0.9

Considerations of code:

- Number of coordinates of the profile (x,y) = 98
- Number of nodes x = 90
- Number of nodes y = 12
- Interval between nodes = 0.8
- Long of the profile = 0.60 m.

Once given the geometry of the element and the organization of the mesh for the calculation, are realized the first iterations with an initial estimation of the distribution of the searched parameters of flow.

In agreement they pass the number of iterations, the initial distribution more and more comes near to the stationary solution of the zone of flow, maintaining constant the conditions of border. The number of iterations used for the calculation is in a rank from 1 to 500. After 800 iterations the result depends of the time. From 1000 steps they begin to give deviations in the mass flow which takes to errors in the calculation.

Finally, it is obtained in pressure and suction sides of the blade profile a field of pressure, velocity, impulse, boundary layer, friction coefficient, etc. in the flow channel.

2.14 Calculation and control of the transonic stream

The process of steam expansion on the rows is very complicated. The drop velocities are different of the steam velocity as much by their magnitude as by their direction; in fact, it can't give a general scheme of the movement of wet steam. The path of the droplets in the channel of the blade rows can be different as is observed. In this case, the drops in the steam flow can lose their stability and be divided.

The approach of the results of calculation to the stationary solution is effectuated several times and must be examined. The local Mach numbers of the different conditions are represented, with four flow parameters from

$$M = \frac{c}{a} = \sqrt{\frac{c_x^2 + c_y^2}{\kappa \frac{P}{\rho}}} \quad (2.84)$$

To differentiate M is the Mach number, which can be calculated from the relationship of the local pressure p to the pressure in the rest of the inflow p (see Eq.(2.10)).

Originally substantial problems results along the blade profiles in the case of the evaluation of pressure and Mach number process that can cause the inaccurate treatment of the zone of flow within the range of the blade points that are found. These difficulties are avoided with the mesh organization. With a relatively small range in the proximity of the front stagnation point obviously errors result, since for the relationship of the static pressure to the total pressure inflow. Thus, it becomes clear that with the calculation of gradients the inaccuracies increase. In similar way is expected the inaccuracy remaining in the calculation into a continuous increase of pressure in the case of an increasing compression shock.

For the quantitative examination of the calculation the representation of the total enthalpy is better. The isentropic total enthalpy shows that the arithmetic procedures in the leading of the profile have better agreement than in the trailing side.

The control of the transonic flow calculations is accomplished by the comparison in the inlet and outlet mass flows. In inlet and outlet plane as well as in the closest cross section the process of the mass stream density ρ is continued to effectuate the calculations. Before and behind the mesh the values are constant because of the balanced parallel flow. In the closest cross section of curvature a variation entails the streamlines transverse to the stream, which however runs evenly. A more exact solution can become by the refinement of the computing mesh.

2.15 Diagram of calculations for flow pattern with liquid droplets

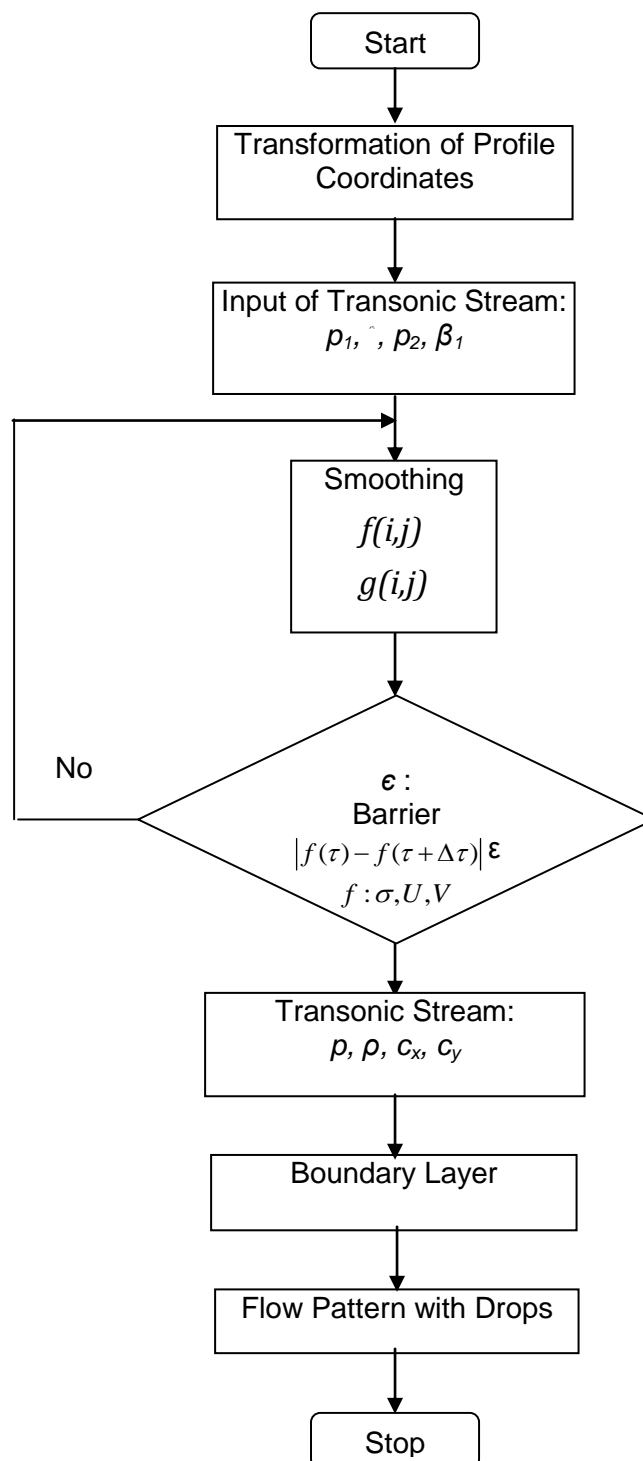


Figure 2.10: Flow chart of the methodology of calculation of flow pattern with droplets in the stator blade cascade.

The flow chart of the methodology in Fig.(2.10) consists of the lattice geometry and the mesh organization of the computational net. An estimated initial distribution of the searched flow parameters σ , P , U and V must be entered. With the progress of time, if the boundary conditions are kept constant, the distribution is approximately iterated more and more to the stationary solution of the zone of flow. If the difference of the flow functions is successively under a barrier which can be given, the approach to the stationary final state is terminated.

The solution functions σ , P , U and V of the iterated final state, must be converted in ρ , ρ , c_x and c_y . The first parameter ρ is selected in such a way that the given pressure P of the Equation (2.1) fulfills the turbine design values. The positions of drops are relevant for the calculation of the drops distribution, and are calculated with a subroutine. The approximate results of calculation for the stationary solution must be effectuated several times and examined.

CHAPTER

RESULTS ANALYSIS

3

It implies a procedure of calculation of this set of blades when the flow has certain humidity degree. The main detail is to know the behavior and the influence in the geometry that can have this type of damages that are had in the blades in normal operation. In order to understand the causes that originate the erosion on the blades of the last stages in low pressure section of steam turbines, the previous procedure is developed in a code in Fortran. In accordance with values shown by the program are generated graphics that show the behavior for the different fields of analysis. The obtained results of velocity and pressure distribution and the analysis of the boundary layer in the proximity of the exit blade surface that have flow conditions of wet steam are presented.

The set of blades are analyzed considering the cloudiness of drops that exist in the same steam when it begins to become water and cause damages in the trailing edge of stator blades as a whole, appearing erosion problems that essentially cause the damage in the inlet edge of the rotor crown of blades. The analysis of the influence of the water is had then presents in the flow, appearing damages and losses by humid steam. This measurement is interesting and from the technical point of view necessary to realize it.

3.1 Flow calculations

The lattice geometry and the mesh organization of the computation net are given. The geometry of the blade is given point by point and represented by polynomial factors. In the next table 3.1 and Fig.(3.1) is presented the coordinates of profile in order to suction and pressure side. The outline computing mesh adapted for the blade cascades was already shown in the Fig.(2.9). It covers $206 \cdot 97 = 19,982$ nodes. The computing lattice is thus finely enough, in order to calculate the expected gradients. The individual structure for the theoretical calculation of the flow with drops was compiled.

An estimated initial distribution of the searched flow parameters σ , P , U and V must be entered. With time progress the initial distribution, if the boundary conditions are kept constant, is approximately iterated more and more to the stationary solution of the zone of flow. If the difference of the flow functions is successively under a barrier which can be given, the approach to the stationary final state is terminated. Then, the velocity fields are corrected in the suction and pressure side of the blade surface with the boundary layer calculation.

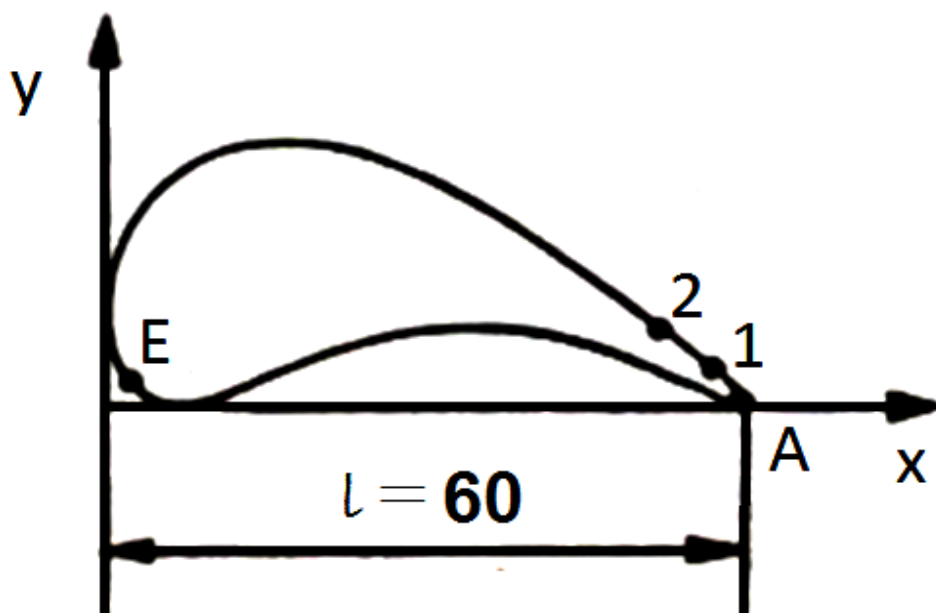


Figure 3.1: Suction and pressure side of stator blade. Dimensions are in cm.

Table 3.1: Coordinates of suction and pressure side of stator blade. Measured in cm.

Point	Suction Side				Point	Pressure Side					
	X	Y	X	Y		X	Y	X	Y		
24	19.111	22.98	49	0.288	34.809	73	19.208	35.164	97	33.332	-0.597
23	20.144	21.904	48	0.577	34.276	72	17.98	36.331	96	33.379	-0.58
22	21.176	20.751	47	0.865	33.897	71	16.753	37.33	95	33.425	-0.557
21	22.208	19.515	46	1.153	33.604	70	15.525	38.178	94	33.472	-0.53
20	23.241	18.19	45	1.441	33.37	69	14.297	38.886	93	33.518	-0.497
19	24.273	16.765	44	1.73	33.181	68	13.07	39.464	92	33.565	-0.457
18	25.305	15.231	43	2.018	33.03	67	11.842	39.919	91	33.611	-0.408
17	26.337	13.574	42	2.306	32.91	66	10.615	40.257	90	33.658	-0.346
16	27.37	11.779	41	2.594	32.82	65	9.387	40.48	89	33.704	-0.261
15	28.402	9.826	40	2.594	32.82	64	8.159	40.591	88	33.751	0.112
14	29.434	7.689	39	3.627	32.525	63	6.932	40.588	87	32.91	4.202
13	30.467	5.338	38	4.659	32.194	62	5.704	40.471	86	32.07	7.638
12	31.499	2.728	37	5.691	31.826	61	4.476	40.235	85	31.229	10.65
11	32.531	-0.198	36	6.724	31.42	60	3.249	39.872	84	30.389	13.359
10	32.607	-0.352	35	7.756	30.974	59	2.021	39.372	83	29.548	15.836
9	32.682	-0.444	34	8.788	30.488	58	2.021	39.372	82	28.708	18.128
8	32.758	-0.509	33	9.821	29.959	57	1.797	39.258	81	27.867	20.267
7	32.833	-0.556	32	10.853	29.387	56	1.572	39.121	80	27.027	22.278
6	32.909	-0.591	31	11.885	28.77	55	1.347	38.96	79	26.186	24.178
5	32.984	-0.614	30	12.918	28.106	54	1.123	38.769	78	25.346	25.981
4	33.059	-0.627	29	13.95	27.392	53	0.898	38.541	77	24.118	28.372
3	33.135	-0.631	28	14.982	26.626	52	0.674	38.265	76	22.891	30.447
2	33.21	-0.626	27	16.014	25.805	51	0.449	37.916	75	21.663	32.249
A	33.286	-0.611	26	17.047	24.927	50	0.225	37.434	74	20.435	33.812
			25	18.079	23.986	E	0.000	36.200			

In addition, the solution functions σ , P , U and V of the iterated final state, must be converted into the material sizes ρ , p , c_x and c_y . In addition, the first parameter ρ_1 is selected in such a way that the given pressure P_1 of the Eq.(2.1) fulfils the turbine design. Thus, inlet and outlet Mach number and the exit angle results from the calculation.

Each step of the calculation in the time t , with $t + \Delta t$ in each point in the mesh to examine in the Eq.(2.23), is in order to avoid the instability of the calculation. If the dimensionless σ_k becomes negative, is a time Δt selected and the calculation must be on the basis of $t = 0$ with a smaller Δt to be repeated. After everyone solutions the time of smoothing by means of the empirical function is the Eq.(2.36).

The sharp curvature of the profile outline, particularly in the trailing edges, leads to difficulties with the calculation. For the necessary adjustment of the mesh organization in these ranges a special program section was developed. Also, to proceeds into the development of the program, in the environment of the given stagnation points, physically meaningful boundary conditions are guaranteed. Since the situation of the front and rear stagnation point which can be given is held with the process of calculation, an error would have by default in the front stagnation point (resulted of the distribution of velocity and/or pressure) to be particularly corrected and a new calculation is accomplished.

Is pointed out the turbulent viscose stream in a turbine lattice like economic criteria and can be seized only with an approaching model, whose largest inadequacy represents the neglect of all friction terms. The reason for it lies in that is not yet able to treat transonic viscous flows in channels in economically justifiable way.

In the geometrically periodic bounds the result of calculation of the drop distribution fulfills likewise the periodicity condition in both edges. With iterations, the initial distribution is more and more comes near to the stationary solution of the zone of flow, maintaining constant the conditions of border. The number of iterations used for the calculation is in a rank from 1 to 500. After 800 iterations the result depends of the time. From 1000 steps they begin to give deviations in the mass flow which takes to errors in the calculation.

3.2 Mach distribution

For the mesh represented in Fig.(2.9) an example of calculation is accomplished. Are given the lattice of pressure of the measuring condition, according to the isentropic diverting Mach number M_{2is} (p_2/p_1) = 1.07 from the Eq.(2.10) and the polytropic efficiency $\eta_p = 0.98$. As resulted of the example of calculation the Mach numbers are indicated in the Fig.(3.2) and its values in the table (3.2).

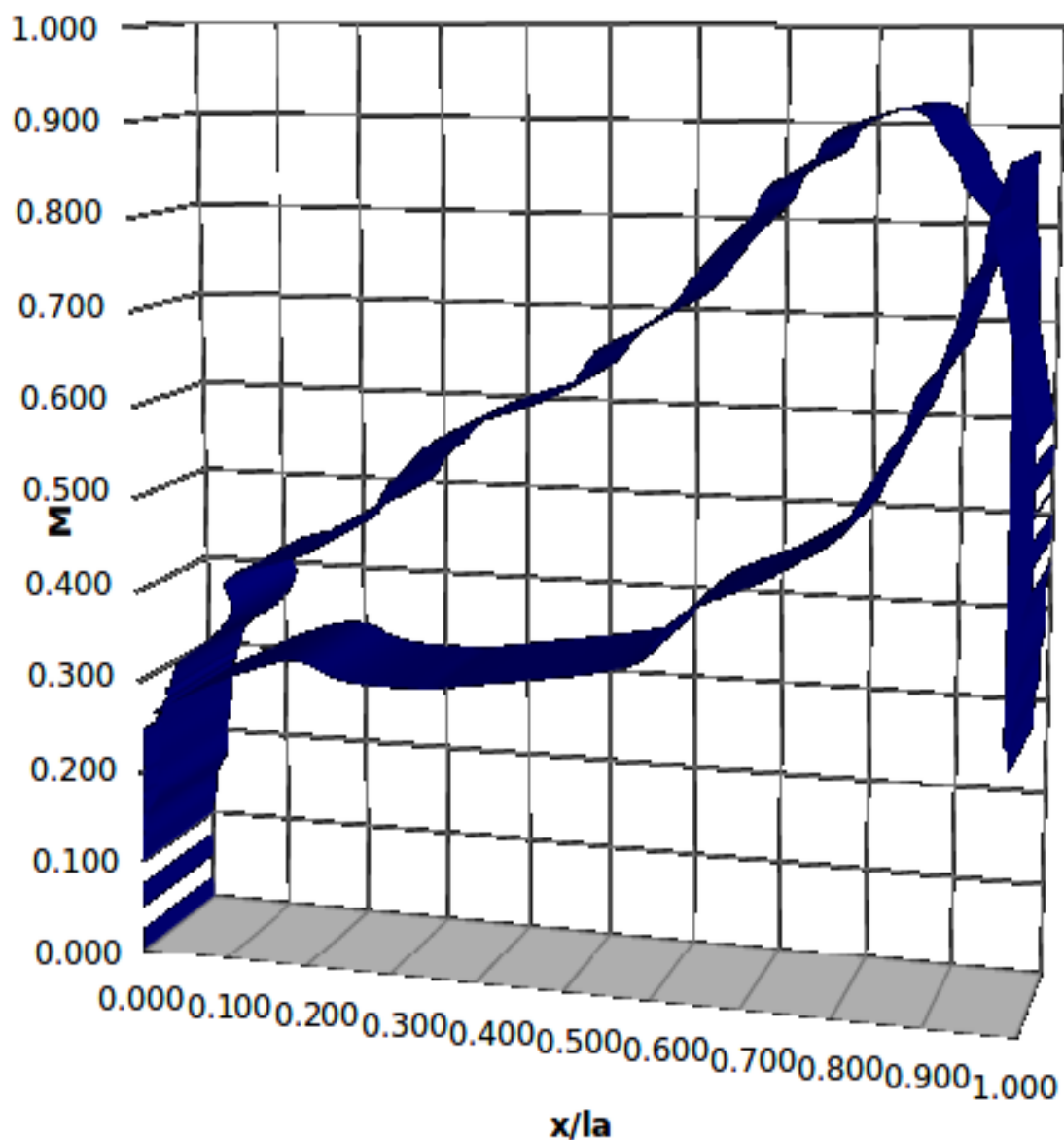


Figure 3.2: Graphic that shows the Mach values in the stator blade channel.

Table 3.2: Mach number throughout stator blade channel.

M	x/l_a	M	x/l_a	M	x/l_a	M	x/l_a
0.000	0.000	0.850	0.725	0.325	0.980	0.475	0.760
0.025	0.000	0.875	0.770	0.350	0.980	0.450	0.715
0.050	0.000	0.900	0.790	0.375	0.980	0.425	0.655
0.075	0.000	0.925	0.870	0.400	0.980	0.400	0.620
0.100	0.000	0.900	0.900	0.425	0.980	0.375	0.600
0.125	0.005	0.875	0.920	0.450	0.980	0.350	0.560
0.150	0.007	0.850	0.930	0.475	0.980	0.275	0.030
0.175	0.020	0.825	0.955	0.500	0.980	0.270	0.027
0.200	0.021	0.875	0.920	0.525	0.980	0.265	0.025
0.225	0.025	0.850	0.930	0.550	0.980	0.260	0.021
0.250	0.027	0.825	0.955	0.575	0.980	0.255	0.020
0.275	0.030	0.800	0.960	0.600	0.980	0.250	0.007
0.280	0.030	0.775	0.965	0.625	0.980	0.215	0.005
0.285	0.035	0.750	0.970	0.650	0.980	0.210	0.005
0.290	0.035	0.725	0.975	0.675	0.980	0.205	0.005
0.295	0.035	0.700	0.980	0.700	0.980	0.200	0.004
0.300	0.040	0.675	0.985	0.725	0.980	0.195	0.004
0.325	0.050	0.650	0.990	0.750	0.980	0.190	0.004
0.350	0.085	0.625	0.995	0.775	0.980	0.185	0.004
0.375	0.110	0.600	1.000	0.800	0.975	0.180	0.004
0.400	0.113	0.575	1.000	0.825	0.975	0.175	0.003
0.425	0.117	0.550	1.000	0.850	0.975	0.170	0.003
0.450	0.200	0.525	1.000	0.875	0.975	0.165	0.003
0.475	0.230	0.500	1.000	0.850	0.965	0.160	0.003
0.500	0.280	0.475	1.000	0.825	0.955	0.155	0.003
0.525	0.300	0.450	1.000	0.800	0.950	0.150	0.002
0.550	0.325	0.425	0.995	0.775	0.945	0.145	0.002
0.575	0.350	0.400	0.995	0.750	0.930	0.140	0.002
0.600	0.400	0.375	0.995	0.725	0.925	0.135	0.002
0.625	0.475	0.350	0.990	0.700	0.915	0.130	0.002
0.650	0.515	0.325	0.990	0.675	0.905	0.125	0.001
0.675	0.535	0.300	0.985	0.650	0.885	0.120	0.001
0.700	0.580	0.275	0.985	0.625	0.875	0.115	0.001
0.725	0.620	0.280	0.985	0.600	0.860	0.110	0.001
0.750	0.640	0.285	0.985	0.575	0.845	0.105	0.001
0.775	0.660	0.290	0.985	0.550	0.830	0.100	0.001
0.800	0.685	0.295	0.985	0.525	0.815		
0.825	0.710	0.300	0.980	0.500	0.800		

The estimated parameters of pressure and density fields are introduced as initial values for the iterative methods. The pressure sizes p_1 and p_2 are well-known from the given state of flow. Also is known c_1 and c_2 in each case with p_1 and p_2 from the Eq.(2.7). Thus the Fig.(3.2) shows the estimated process of the Mach fields over the axial run length x/l_a .

There is a clear difference between suction and pressure Mach number. In the graphic of the Fig.(3.2) it is shown the distribution of Mach number of the suction side in the superior region and pressure side in the inferior region.

It is observed an increase in the magnitude of Mach number in agreement with the advance of flow throughout the channel of blades, passing of a subsonic to transonic regimen in Mach 0.85, with values that decreasing in the zone of exit suction side due to effects of condensation phenomena. A small increase in pressure exists on the suction surface due to the fast condensation or presence of droplets travelling in the flow and is localized in the change of curvature of the profile.

According to this, the condensation occurs before the exit of the cascade (in the throat) and the expansion rate can vary in the passage of blades (the pressure distribution decrease and increase in fast form in the throat zone).

Also, the Mach range with the trailing edge shows the effects of change intentionally given in the rear stagnation point. Changes remarkably for these change conditions of the exit angles β_2 . This shows again that with relatively closely divided turbine lattices of the exit angle in a wider range is independent of the inflow angle. In addition, proves that the effect of the rear stagnation point affects the flow in the cascade.

3.3 Pressure distribution

The resulted of calculate of the pressure throughout the channel are indicated in the Fig.(3.3) and in the table (3.3). The pressure sizes p_1 and p_2 are well-known from the given state of flow. Also is known c_1 and c_2 in each case with p_1 and p_2 from the Eq.(2.7). Thus the Fig.(3.3) shows the estimated process of the pressure fields over the axial run length x/l_a .

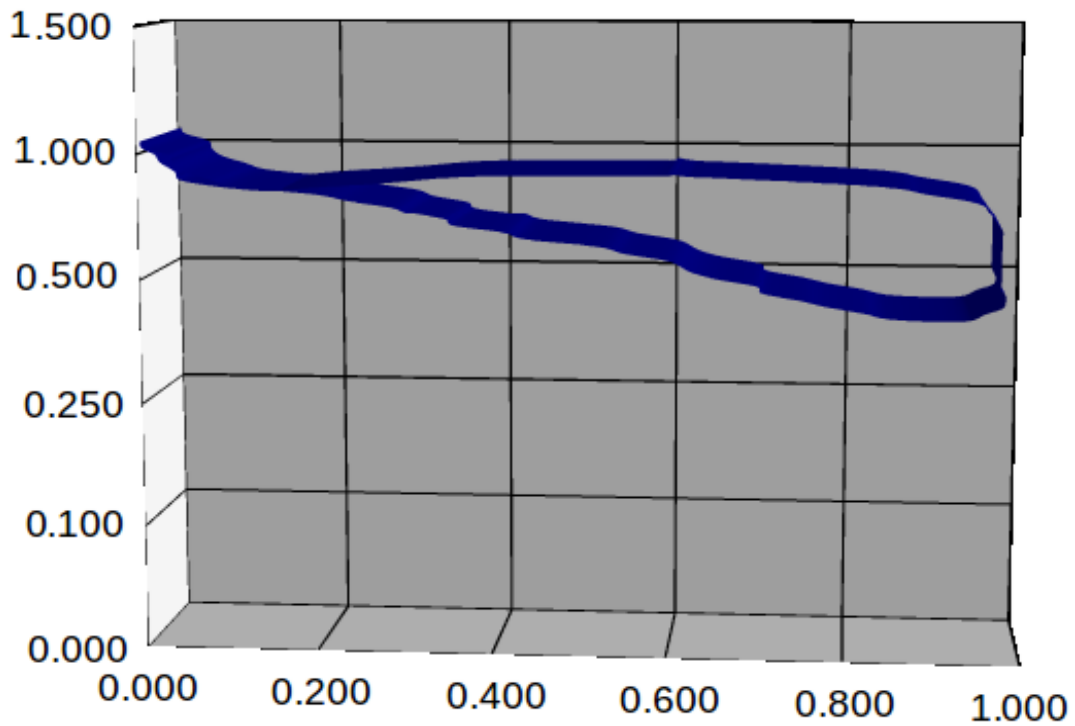


Figure 3.3: Graphic that shows the pressure values in the stator blade channel.

Table 3.3: Pressure throughout stator blade channel.

P/P_{01}	x/la	P/P_{01}	x/la	P/P_{01}	x/la
1.050	0.005	0.725	0.970	0.575	0.615
1.025	0.006	0.700	0.970	0.600	0.595
1.000	0.020	0.675	0.970	0.625	0.550
0.975	0.025	0.650	0.970	0.650	0.520
0.950	0.035	0.625	0.970	0.675	0.440
0.925	0.045	0.600	0.970	0.700	0.415
0.900	0.050	0.575	0.970	0.725	0.360
0.875	0.095	0.550	0.970	0.750	0.350
0.860	0.150	0.525	0.970	0.775	0.310
0.875	0.200	0.500	0.970	0.800	0.290
0.900	0.300	0.475	0.975	0.825	0.240
0.925	0.400	0.450	0.975	0.850	0.200
0.930	0.585	0.425	0.970	0.875	0.115
0.940	0.600	0.400	0.950	0.900	0.085
0.930	0.620	0.375	0.925	0.925	0.060
0.925	0.660	0.380	0.850	0.950	0.045
0.900	0.825	0.400	0.820	0.975	0.040
0.875	0.880	0.425	0.777	1.000	0.035
0.850	0.925	0.450	0.745	1.025	0.009
0.825	0.950	0.475	0.705	1.050	0.005
0.800	0.955	0.500	0.700		
0.775	0.960	0.525	0.660		
0.750	0.965	0.550	0.630		

In the graphic of the Fig.(3.3) it is shown the distribution of the pressure side in the superior region and suction side in the inferior region. If is compared the graphic of the Fig.(3.2) with one another Fig.(3.3), is noted that the pressure in the proximity of the front stagnation point decreasing with increasing Mach number. As was already mentioned in section 2.7, for the polytropic law the correct change of entropy does not apply with small Mach number. In addition, it was guaranteed that M_1 and β_2 increase with the constantly increase of M_2 , and that continuity condition thereby is well fulfilled.

An increase of pressure occurs near to the exit of the trailing edge of the profile. This behavior is because a phenomenon of condensation is presented near to the pressure surface locating a presence of drops that will reach the trailing edge of the blade.

Substantial problems originally resulted along the blade profiles, in the case of the evaluation process of pressure and Mach number, cause the inaccurate treatment in the zone of flow. These difficulties are avoided with the descriptive improved mesh organization.

Thus, it becomes clear that with the computation of gradients the inaccuracies increase. In similar way is expected the inaccuracy remaining in the calculation into a continuous increase of pressure in the case of an increasing compression shock.

3.4 Velocity distribution calculation

As resulted of the example of calculation the velocity distribution are indicated in the Fig.(3.4) and Fig.(3.5) and its values in the table (3.4) and (3.5). In both suction and pressure side graphics is shown an increasing value of the velocity of the flow over the surface, in according with Mach number in Fig.(3.2) and the pressure distribution in the Fig.(3.3).

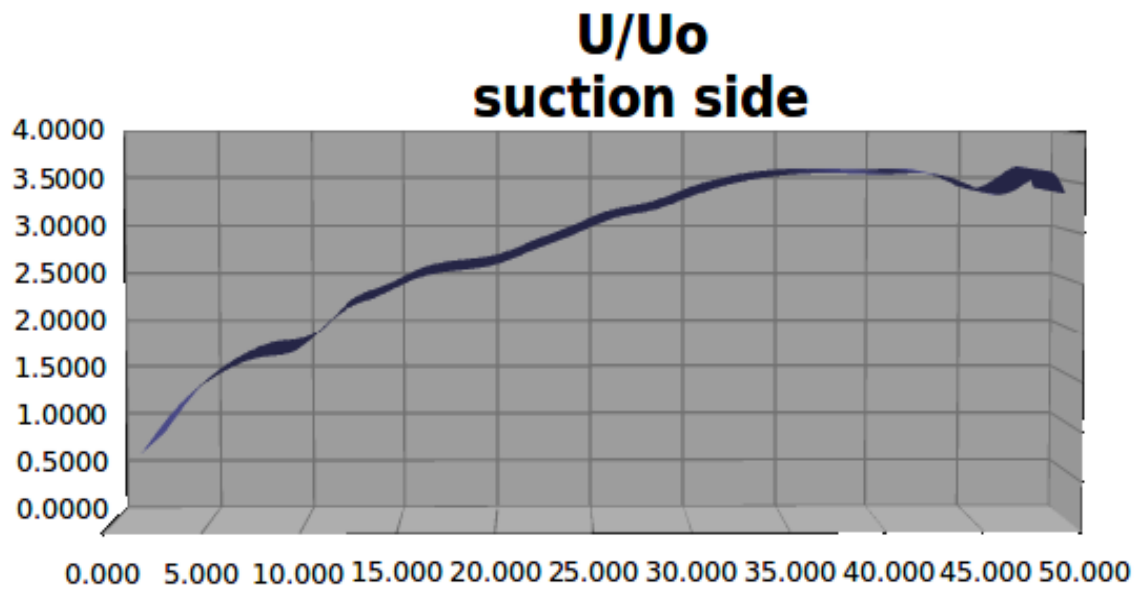


Figure 3.4: Graphic that shows the behavior of the velocity distribution on the suction side in the stator blade channel.

Table 3.4: Velocity distribution on the suction side in the stator blade channel.

x/l	U/U ₀	x/l	U/U ₀
0.000	0.000	26.000	3.160
2.000	0.800	28.000	3.240
4.000	1.300	30.000	3.380
6.000	1.600	32.000	3.500
8.000	1.760	34.000	3.570
10.000	1.850	36.000	3.600
12.000	2.200	38.000	3.600
14.000	2.380	40.000	3.590
16.000	2.560	42.000	3.600
18.000	2.640	44.000	3.500
20.000	2.700	46.000	3.400
22.000	2.850	48.000	3.620
24.000	3.000	49.000	3.400

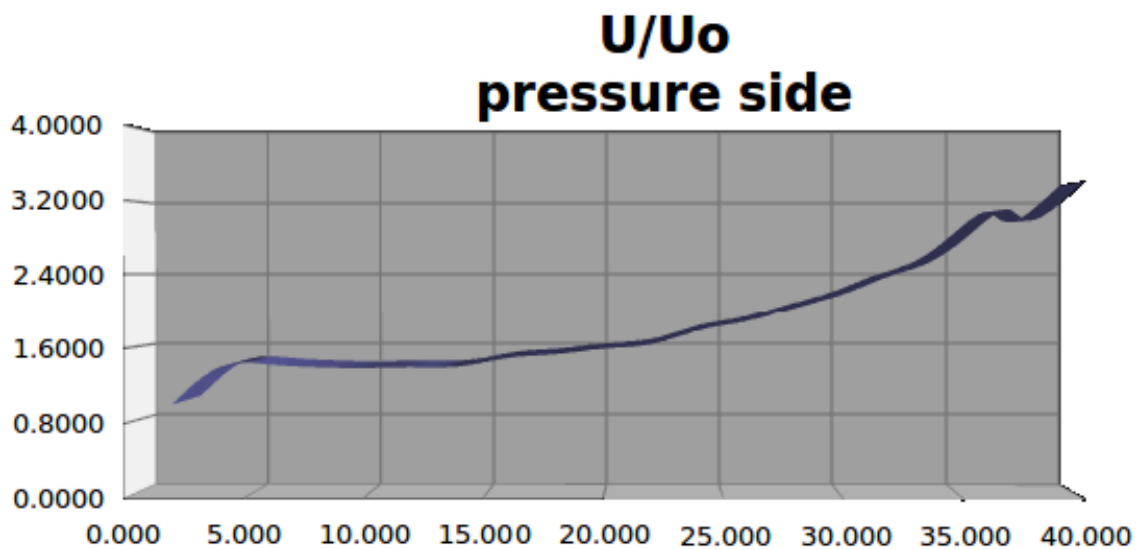


Figure 3.5: Graphic that shows the behavior of the velocity distribution on the pressure side in the stator blade channel.

Table 3.5: Velocity distribution on the pressure side in the stator blade channel.

x/l	U/U_0	x/l	U/U_0
0.000	0.000	22.000	1.650
2.000	1.000	24.000	1.800
4.000	1.400	26.000	1.900
6.000	1.430	28.000	2.050
8.000	1.400	30.000	2.400
10.000	1.390	32.000	2.600
12.000	1.400	34.000	3.000
14.000	1.410	36.000	3.080
16.000	1.500	38.000	3.000
18.000	1.540	40.000	3.400
20.000	1.600		

3.5 Enthalpy calculation

The result of quantitative examination of the calculation represent the total enthalpy throughout the channel is indicated in the Fig.(3.6), Fig.(3.7) and in the table (3.6). The comparison between calculated and isentropic total enthalpy shows that the arithmetic procedures in the leading of the profile have better agreement than in the trailing side.

The total enthalpy in the cascade is used like value of convergence because is a constant for a stationary system, which is the state looked for a certain number of iterations. Once the stationary flow is reached, the parameters do not present variation with respect to the time.

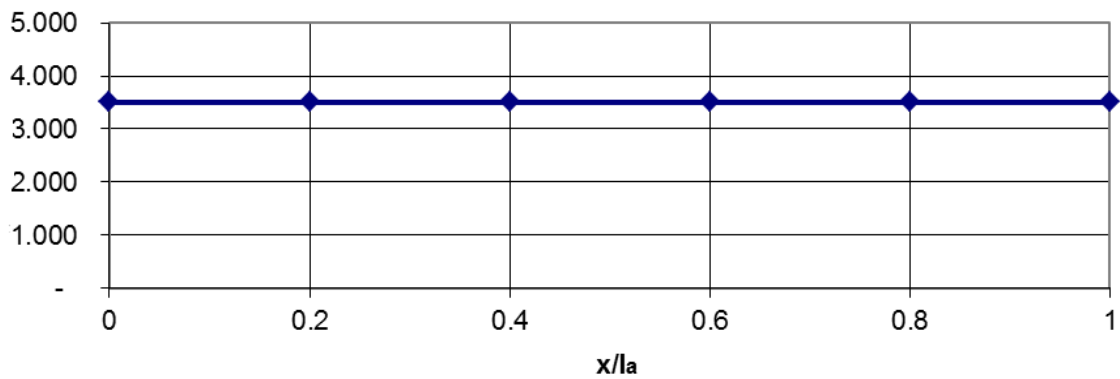


Figure 3.6: Graphic that shows the total enthalpy calculation in the suction and pressure side in the stator blade channel.

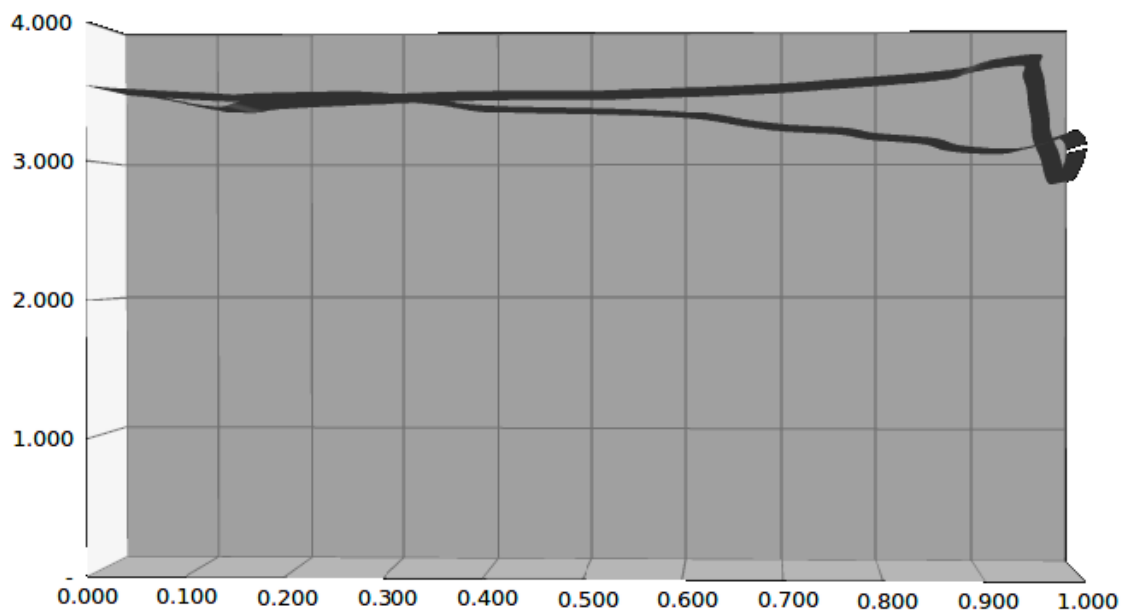


Figure 3.7: Graphic that shows the enthalpy calculation in the suction and pressure side in large x/l of the stator blade channel.

It is observed in graphic of Fig.(3.6) the total enthalpy is constant when is reached the stationary system. The graphic of Fig.(3.7) shows the pressure side in the superior part of the path of values and the suction side in the inferior part.

The lifted values of enthalpy in the pressure side indicate that formation of drops in that part of the blade is in minor grade that in the suction side. The enthalpy shows that the droplets in their pass affect this zone, interpreting this like an accumulated in the pressure side because have been depositing in this part of blade affecting the flow in local form, by the geometrical position of the blades. The values of enthalpy that are in the suction side indicate the presence of drops, since the change of phase of steam to liquid is associate to less values of enthalpy.

Table 3.6: Enthalpy throughout stator blade channel.

h/(P01/Rho1)	x/la	h/(P01/Rho1)	x/la
3.550	0.000	3.530	1.000
3.540	0.010	3.550	0.985
3.520	0.050	3.150	0.975
3.500	0.100	3.200	0.970
3.490	0.130	3.075	0.965
3.480	0.150	2.850	0.964
3.490	0.175	3.000	0.962
3.490	0.175	3.100	0.960
3.500	0.250	3.200	0.958
3.500	0.275	3.300	0.955
3.490	0.300	3.400	0.950
3.480	0.315	3.500	0.900
3.450	0.350	3.600	0.875
3.400	0.400	3.700	0.800
3.380	0.500	3.750	0.750
3.350	0.600	3.700	0.700
3.300	0.650	3.650	0.600
3.250	0.700	3.600	0.550
3.230	0.750	3.575	0.500
3.210	0.775	3.550	0.400
3.180	0.800	3.520	0.300
3.150	0.850	3.510	0.200
3.100	0.875	3.500	0.150
3.075	0.925	3.500	0.125
3.100	0.950	3.480	0.050
3.400	0.975	3.450	0.025
3.500	0.990	3.420	-

3.6 Impulse calculation

The Fig.(3.8) presents the levels of reference that help to understand the calculation of impulse throughout the blade channel and the resulted are indicated in the Fig.(3.9) and in the table (3.4). It is observed in the inlet of the blade channel 0-0 the impulse value of 2.9, and this impulse is going to incrementing due to the decrease of the pressure. In the point 1-1 the value is 7, and the exit 2-2 has this same value of 7.

In the point 1-1 is reached the value of the exit on the pressure side, but is observed that is surpassed from this point. This is due to the geometrical disposition of the channel of the pressure side on the suction side. The flow pass throughout de channel and first leave the pressure side in the throat zone, in this moment is reach de impulse value of 7. The flow follows its way increasing the impulse value.

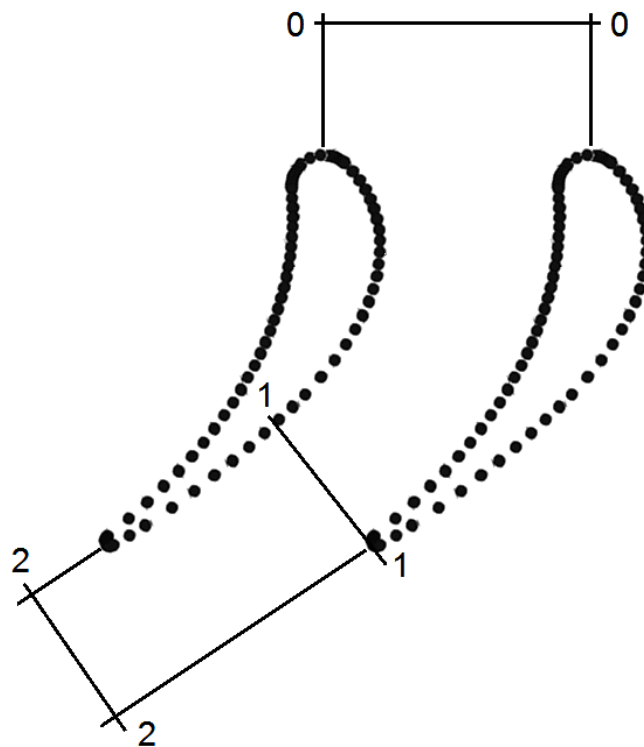


Figure 3.8: Levels of reference in the blade channel. 0-0 Inlet of flow. 1-1 Outlet of pressure side at level with suction side (throat). 2-2 Exit of blade channel.

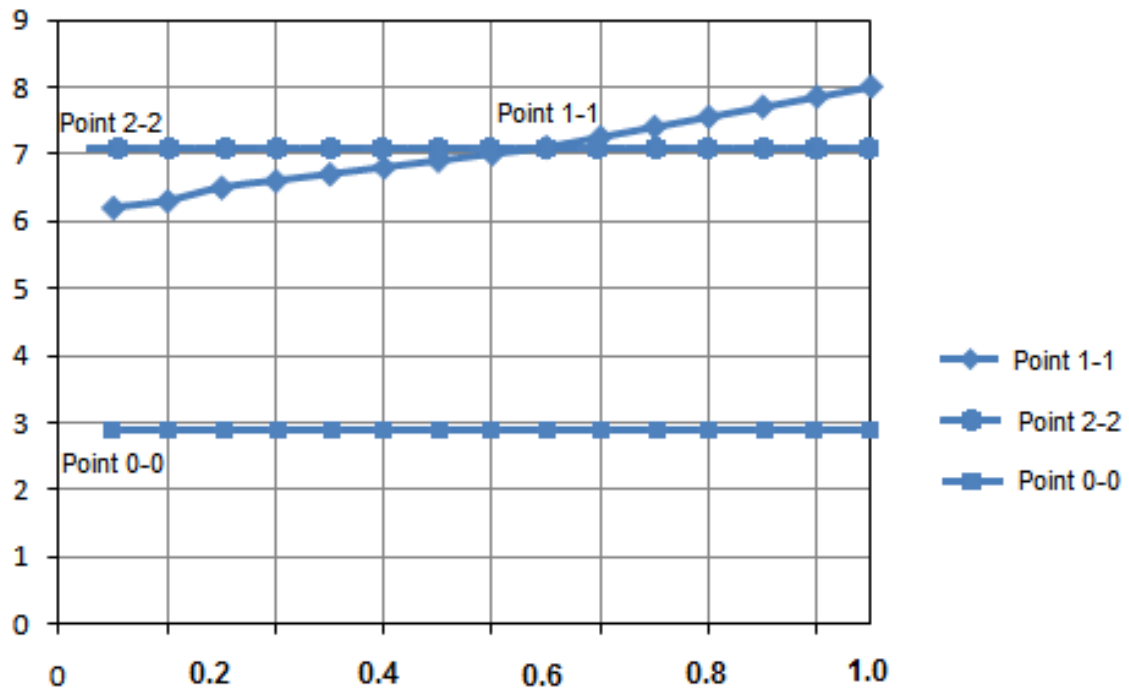


Figure 3.9: Graphic that shows the impulse calculation in the suction and pressure side in the stator blade channel.

Table 3.7: Impulse values throughout stator blade channel.

c*Rho ₀₁ (kg/s·m ²)	x/la
2.9	0.0
6.2	0.175
6.5	0.200
6.6	0.275
6.7	0.400
6.8	0.475
6.9	0.500
7	0.600
7.1	0.675
7.25	0.750
7.4	0.775
7.55	0.800
7.7	0.875
7.85	0.95
8	1.00

In relation with Fig.(3.7) is noted the values of enthalpy predominates on the pressure side, due to velocity of the flow first leaves this part of the blade and later it makes with the suction side.

The control of the transonic flow calculations was accomplished also by the comparison in the inlet and outlet mass flows. The difference in the comparison of inlet and outlet mass flows was accomplished. In inlet and outlet plane as well as in the closest cross section the process of the mass stream density $\rho \cdot c$ is continued to effectuate the calculations.

Before and behind the mesh the values are constant because of the balanced parallel flow. In the closest cross section of curvature a variation entails the streamlines transverse to the stream, which however runs evenly. A more exact solution can become by the refinement of the computing mesh.

3.7 Displacement thickness calculation

In the proximity of the blade surface the drop movement is affected by the velocity profile of the boundary layer and for the impulse as the force of equilibrium in x-direction averaged over the boundary layer thickness δ , overcome the difficulty in the fact that the fluid velocity in the boundary layer approaches asymptotically to the free stream value as distance from the wall increases at any given location. The effect on the free flow is then equivalent with the displacing of the surface into the stream with no boundary layer present.

After employing the boundary layer equations to calculate the displacement thickness along the wall, a virtual wall is created by displacing the wall outward by the displacement thickness. A new inviscid solution is computed using this virtual wall. This yields slightly different free-stream conditions than the initial

calculation. A balance of mass is calculated. The boundary layer solution is then recalculated, using the new free-stream conditions, for the real wall. The process is repeated moving with each iteration until the mass balance is equal to a certain value and the displacement thickness stops.

The resulted of calculate of the displacement thickness of the boundary layer throughout the surfaces of blade channel are indicated in the Fig.(3.10), Fig.(3.11) and in the tables (3.8) and (3.9). Considering the results of boundary layer thickness, it is shown that they are thin on the pressure side and up to approximately at 37% of length of the axial chord of the suction side.

It is observed the increment in the thickness boundary layer conform the flow passes throughout the suction side. Beyond this point there is some growth. There is a variation in the 90% of the curve of thickness of boundary layer on the length of the suction in the graphic of Fig.(3.10), to the 46 cm of length. This inflection shows a possible presence of flow with droplets and transition to turbulence. They are agree with the graphic of behavior of enthalpy at trailing edge shown in Fig.(3.7). length indicate the presence of drops droplets and transition to turbulence.

In the pressure side is shown a variation in loss of thickness of the boundary layer at 45% (18 cm) of length of the blade. This is because the throat causes an effect of acceleration on the flow due to geometrical disposition of the blades, incrementing the impulse of the flow and decreasing the thickness of the boundary layer. The pressure side distribution for this calculation is given in Fig.(3.3) .It is observed that in the pressure side results in thin boundary layers as shown in the graphic of Fig.(3.11).

The changes in the pressure distribution are the cause of growth in the boundary layer shown by the Fig.(3.10) and Fig.(3.11). The inflection at 82% (33 cm) of the length indicate the presence of drops and transition to turbulence.

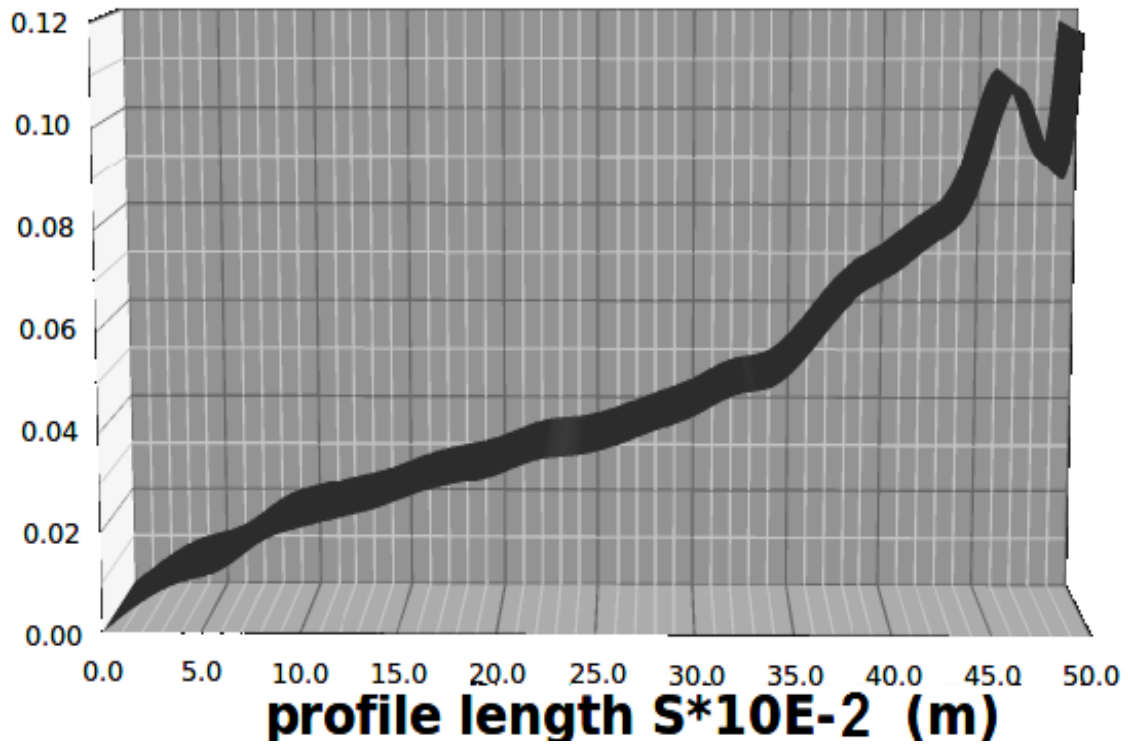


Figure 3.10: Graphic that shows the behavior of boundary layer thickness on the suction side in the stator blade channel.

Table 3.8: Boundary layer thickness values throughout suction side stator blade channel.

$\delta \times 10^{-3}$ (m)	$S \times 10^{-2}$ (m)	$\delta \times 10^{-3}$ (m)	$S \times 10^{-2}$ (m)
0.0000	0.000	0.0380	26.000
0.0060	2.000	0.0410	28.000
0.0100	4.000	0.0440	30.000
0.0125	6.000	0.0480	32.000
0.0180	8.000	0.0500	34.000
0.0210	10.000	0.0580	36.000
0.0230	12.000	0.0670	38.000
0.0250	14.000	0.0720	40.000
0.0280	16.000	0.0780	42.000
0.0300	18.000	0.0880	44.000
0.0320	20.000	0.1080	46.000
0.0350	22.000	0.0900	48.000
0.0360	24.000	0.1180	49.000

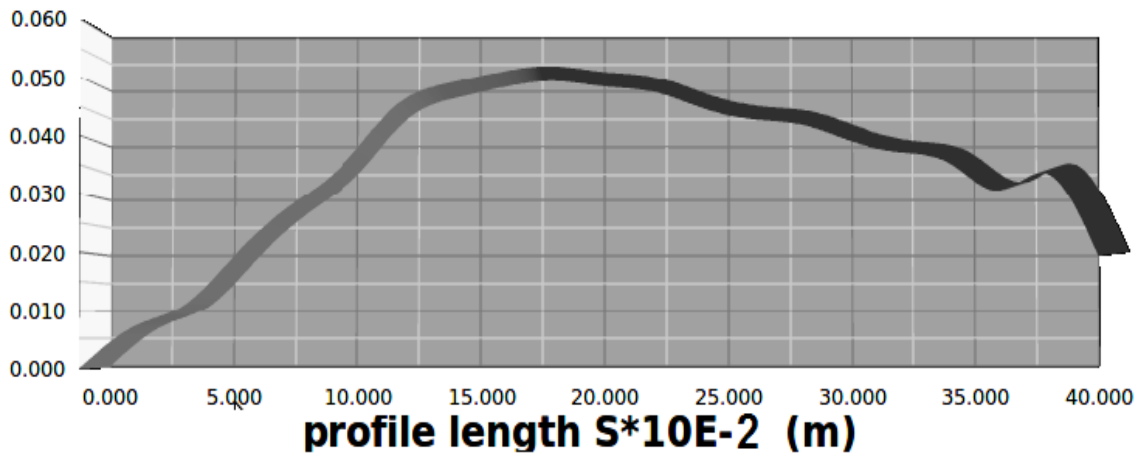


Figure 3.11: Graphic that shows the behavior of boundary layer thickness on the pressure side in the stator blade channel.

Table 3.9: Boundary layer thickness values throughout pressure side stator blade channel.

$\delta \times 10^{-3}$ (m)	$S \times 10^{-2}$ (m)	$\delta \times 10^{-3}$ (m)	$S \times 10^{-2}$ (m)
0.0000	0.000	0.0500	22.000
0.0070	2.000	0.0470	24.000
0.0110	4.000	0.0450	26.000
0.0200	6.000	0.0440	28.000
0.0280	8.000	0.0410	30.000
0.0350	10.000	0.0390	32.000
0.0450	12.000	0.0370	34.000
0.0490	14.000	0.0320	36.000
0.0510	16.000	0.0350	38.000
0.0520	18.000	0.0200	40.000
0.0510	20.000		

The boundary layer behavior in the remaining solutions is very similar. In both cases the boundary layer flow is laminar on the pressure surface and for approximately 50% of the axial chord on the suction surface and indicate the presence of droplets and transition to turbulence provoked by the pressure on the suction surface and impulse of the flow in the throat.

With help of the displacement thickness δ_1 the drop courses in the wall proximity are affected, as for these calculations the delimitations of the blade channel around δ_1 are in pressure in each case and the frictionless velocity field is supposed. In this case the boundary layer displacement thickness has been very small, the boundary layers have remained attached and the main flow has been little affected by the presence of the boundary layer.

3.8 Calculation of energy thickness

The resulted of calculate of the loss of energy thickness of the boundary layer throughout the surfaces of blade channel are indicated in the Fig.(3.12), Fig.(3.13) and in the tables (3.10) and (3.11). The graphics show the lower kinetic energy in the boundary layer relative to the inviscid outer. This can be regarded as a defect produced by the loss in kinetic energy attributable to the boundary layer.

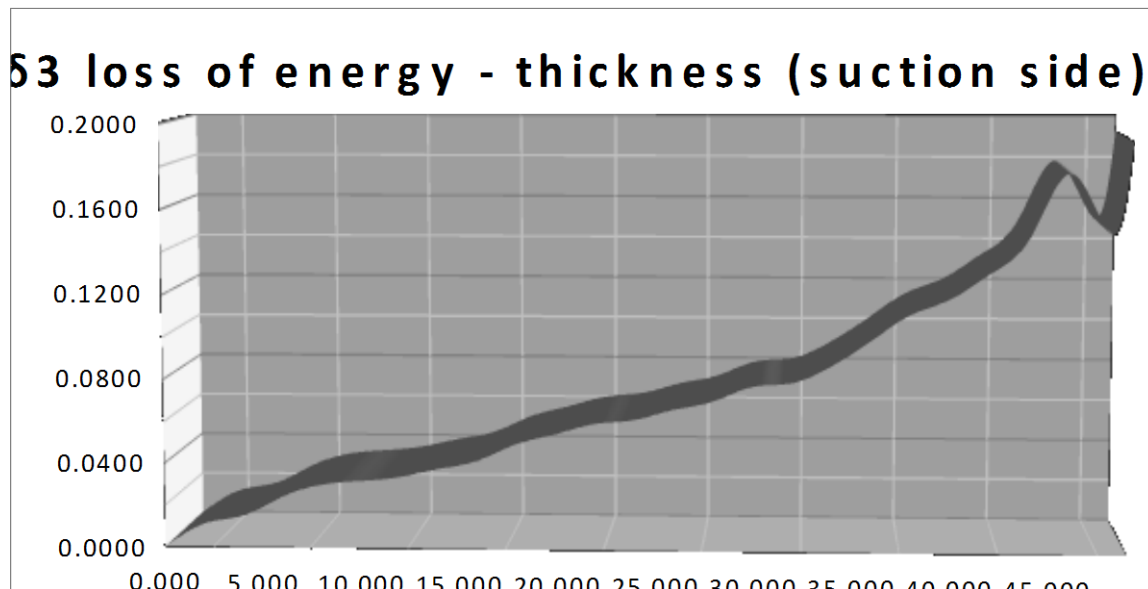


Figure 3.12: Graphic that shows the behavior of loss of energy thickness on the suction side in the stator blade channel.

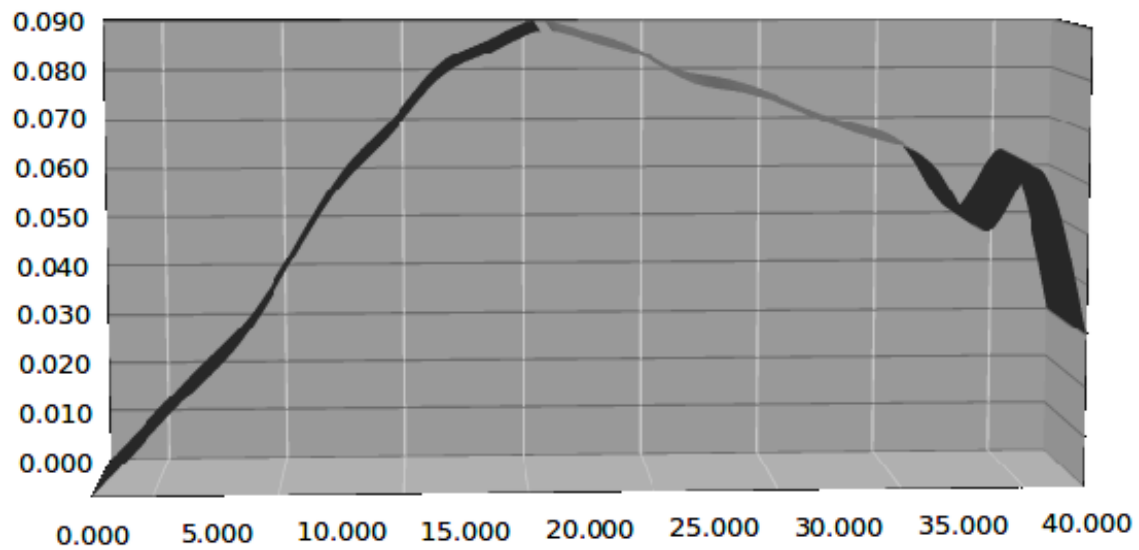


Figure 3.13: Graphic that shows the behavior of loss of energy thickness on the pressure side in the stator blade channel.

It is observed by the graphics the development of the boundary layer over surface of blades. In the suction side is seen a greater growth of the boundary layer than in the pressure side due values of pressure and Mach that operate in the channel. The low level of energy presented in the suction side in the 90% of the length of the blade indicate the presence of transition due to local velocities on the surface lower than the freestream velocity and the skin friction is decreased.

Table 3.10: Loss energy thickness values throughout suction side stator blade.

$S \times 10^{-2}$ (m)	$\delta_3 \times 10^{-3}$ (m)	$S \times 10^{-2}$ (m)	$\delta_3 \times 10^{-3}$ (m)
0.000	0.000	26.000	0.067
2.000	0.011	28.000	0.071
4.000	0.015	30.000	0.078
6.000	0.024	32.000	0.800
8.000	0.030	34.000	0.088
10.000	0.032	36.000	0.100
12.000	0.034	38.000	0.112
14.000	0.038	40.000	0.120
16.000	0.042	42.000	0.132
18.000	0.050	44.000	0.150
20.000	0.055	46.000	0.178
22.000	0.060	48.000	0.150
24.000	0.062	49.000	0.193

Table 3.11: Loss energy thickness value throughout pressure side stator blade.

$S \times 10^{-2}$ (m)	$\delta_3 \times 10^{-3}$ (m)	$S \times 10^{-2}$ (m)	$\delta_3 \times 10^{-3}$ (m)
0.000	0.000	22.000	0.085
2.000	0.010	24.000	0.080
4.000	0.020	26.000	0.078
6.000	0.030	28.000	0.075
8.000	0.045	30.000	0.071
10.000	0.060	32.000	0.868
12.000	0.070	34.000	0.062
14.000	0.081	36.000	0.051
16.000	0.086	38.000	0.063
18.000	0.090	40.000	0.030
20.000	0.088		

The transition to turbulence is provoked by the pressure on the suction surface and impulse of the flow in the throat. This inflection shows a possible presence of flow with droplets and transition to turbulence. They are agree with the graphic of behavior of enthalpy at trailing edge shown in Fig.(3.7).

The pressure side presents lowers levels of thickness of boundary layer with an inflection localized in the 82% (33 cm) of the length. The lower levels indicate pass to transition zone by a variation in loss of thickness of the boundary layer at 45% (18 cm) of length of the blade. This is because the throat causes an effect of acceleration on the flow due to geometrical disposition of the blades, incrementing the impulse of the flow and decreasing the thickness of the boundary layer .It is observed that in the pressure side results in thin boundary layers as shown in the graphic of Fig.(3.11).

3.9 Calculation of friction coefficient

The resulted of calculate the friction coefficient of the boundary layer throughout the surfaces of blade channel are indicated in the Fig.(3.14), Fig.(3.15) and in the tables (3.12) and (3.13). The friction coefficient is caused by the viscosity in the boundary layer. In the suction surface the initial values of the coefficient are higher because the development of the boundary layer

friction coefficient C_f suction side

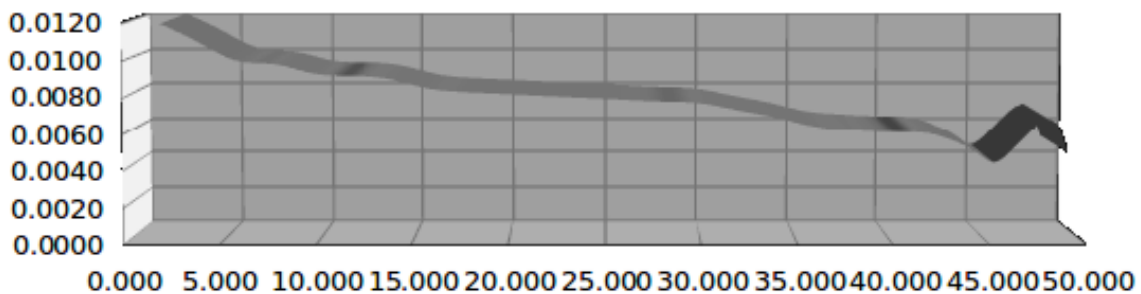


Figure 3.14: Graphic that shows the behavior of friction coefficient on the suction side in the stator blade channel.

Table 3.12: Friction coefficient values throughout suction side stator blade channel.

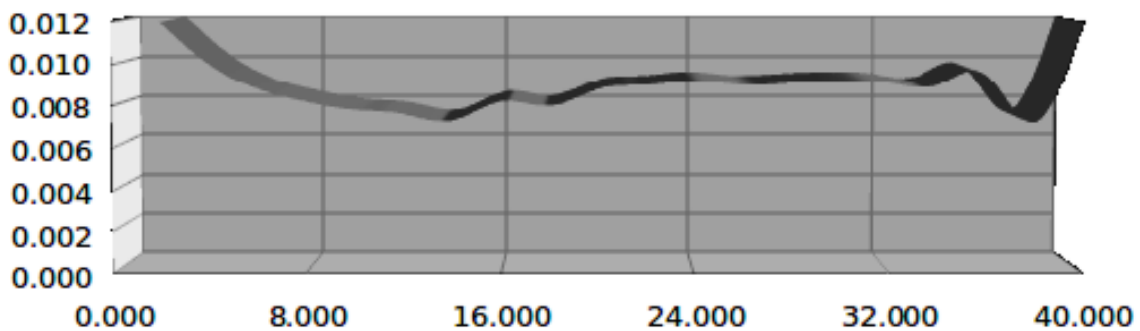
$S \times 10^{-2}$ (m)	$C_f \times 10^{-3}$ (m)	$S \times 10^{-2}$ (m)	$C_f \times 10^{-3}$ (m)
0.000	0.0000	26.000	0.0079
2.000	0.0120	28.000	0.0078
4.000	0.0110	30.000	0.0077
6.000	0.0100	32.000	0.0073
8.000	0.0098	34.000	0.0065
10.000	0.0093	36.000	0.0062
12.000	0.0092	38.000	0.0061
14.000	0.0090	40.000	0.0060
16.000	0.0085	42.000	0.0052
18.000	0.0083	44.000	0.0045
20.000	0.0082	46.000	0.0050
22.000	0.0081	48.000	0.0068
24.000	0.0080	49.000	0.0050

begins and it is observed in the Fig.(3.14) that the coefficient is decreased in the suction side due to laminar region by it crosses the flow, but in the 82% (33 cm) of the length surface exist a deflection, caused by the Mach number and the character of the boundary layer.

In the pressure surface the initial values of the coefficient are higher because the development of the boundary layer begins. The pressure side presents an inflection localized in the 82% (33 cm) of the length that indicates the pass to transition zone by a variation in thickness of the boundary layer at 45% (18 cm)

of length of the blade. This is because the throat causes an effect of acceleration on the flow due to geometrical disposition of the blades, incrementing the friction of the flow against the surface. As the velocity increases the boundary layer breaks away. The friction becomes increasingly due to the pressure built up at the front. It is observed that in the pressure side results in thin boundary layers as shown in the graphic of Fig.(3.11).

friction coefficient C_f pressure side



3.15: Graphic that shows the behavior of friction coefficient on the pressure side in the stator blade channel.

Table 3.13: Friction coefficient values throughout pressure side stator blade channel.

$S \times 10^{-2}$ (m)	$C_f \times 10^{-3}$ (m)	$S \times 10^{-2}$ (m)	$C_f \times 10^{-3}$ (m)
0.000	0.000	22.000	0.009
2.000	0.010	24.000	0.009
4.000	0.009	26.000	0.009
6.000	0.008	28.000	0.009
8.000	0.008	30.000	0.009
10.000	0.008	32.000	0.009
12.000	0.007	34.000	0.009
14.000	0.008	36.000	0.010
16.000	0.008	38.000	0.007
18.000	0.009	40.000	0.012
20.000	0.009		

3.10 Presence of droplets in the flow

According to the displayed results, in the trailing edge of the stator blades, exists a presence of drops, that in according to technical literature [50], this presence can be interpreted as a concentration layer of liquid on the surface of drops next to pressure forms near, and they are possible to be formed in the suction side, which brings about alterations in the development of the boundary layer.

The Fig.(3.7), (3.11), (3.13) and (3.15) indicates that local presence of the drops exists whose tendency is to be accumulated in the trailing edge of the pressure side of the stator blade, this phenomenon is known like accumulation of primary drops. The boundary layer effects also show that near of the pressure surface, the water presence in liquid form occurs on the section next to trailing edge, being a common characteristic the appearance of the inflection, subsequent to the change of curvature of the suction surface, as is shown in Fig.(3.8). This is because partially in the profiles the channel converges until the throat, where the flow is controlled by the pressure and suction side, but after the throat is controlled only by the suction side and the flow comes near to the following blade.

Therefore, a sudden change in the rate of expansion after the throat and great influence of the surface of suction in this region exists. A great percentage of humidity begins to give in the outlet of the throat of the channel; generally this occurs in the change of radio of curvature of the suction side of the profile.

The rate of expansion varies in flows over turbine blading. It is low in the entrance region and high in the vicinity of the throat. As a consequence, the zone of rapid condensation occurs downstream of the throat [51]. In the case of the present profile the calculations associated with the presence of drops in the flow is sufficient to provoke boundary layer transition.

The increase in the amount of humidity is translated in losses that will become evident after certain running hours from the turbine and they will be reflected in his operation. To understand the phenomenon of erosion like a problem that is derived from the humidity that exists in the flow in channels and that is accumulated in the stator blade, it allows improving the efficiency of the steam turbines until in a 8% [52]. The continuous process of accumulation of drops in the blade stator causes that the film that is formed breaks and the greatest drops will affect the leading edge of the rotor blade following by the suction side.

3.11 Comparison with other works

A measured surface in subsonic treatment is carried by Bakhtar, Mahpeykar, Mashmouhy and Jadayel [51,53] in a stator cascade of turbine in an experimental arrangement in the University of Birmingham. Many studies into the performance of the wet stages of turbines have been undertaken. However, because of the three-dimensional and complex nature of these flows, measurements in turbines do not offer a satisfactory means of investigating the influence of individual factors contributing to wetness losses. It can be seen that the agreement with results here displayed.

The work of Bakhtar, Mahpeykar, Mashmouhy and Jadayel shows an overexpansion on the suction surface on the vicinity of the throat which is well predicted in experimental and theoretical solution. In the case of flow with drops, with the flow subsonic the effect of rapid condensation on the flow has been masked by the overexpansion.

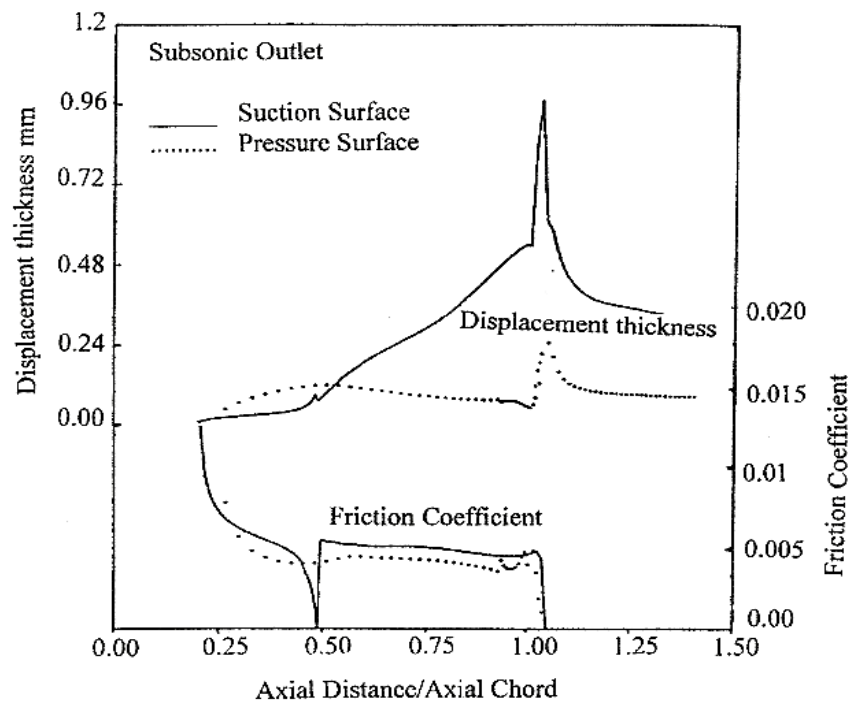


Figure 3.16: Graphic that shows the boundary layer parameters – subsonic outlet⁵².

The position of the rapid condensation zone is similar to higher outlet Mach number, but as would be expected the outlet wetness fractions are lower in according to that work. As already indicated in previous chapter 2, to describe the behavior of two-phase flows the equations about droplet behavior are combined with the standard gas dynamic field conservation equations which in the treatment were used in their inviscid form. Here, the deal with the viscous effects was assumed to be concentrated in boundary layers and a boundary layer routine is included in the treatment.

The resulting variations in displacement thickness and surface friction coefficients in the test with subsonic outlets are given in Fig.(3.16). The boundary layer characteristics compared with fig.(3.10) and Fig.(3.11) and Fig.(3.14) and Fig.(3.15) are very similar. Here is given the variations of the boundary layer as a function of the fractional axial chord, while the lower curves give the corresponding surface friction coefficients. The full line represents the results for the suction surface, while de dotted lines give the data for the pressure surface.

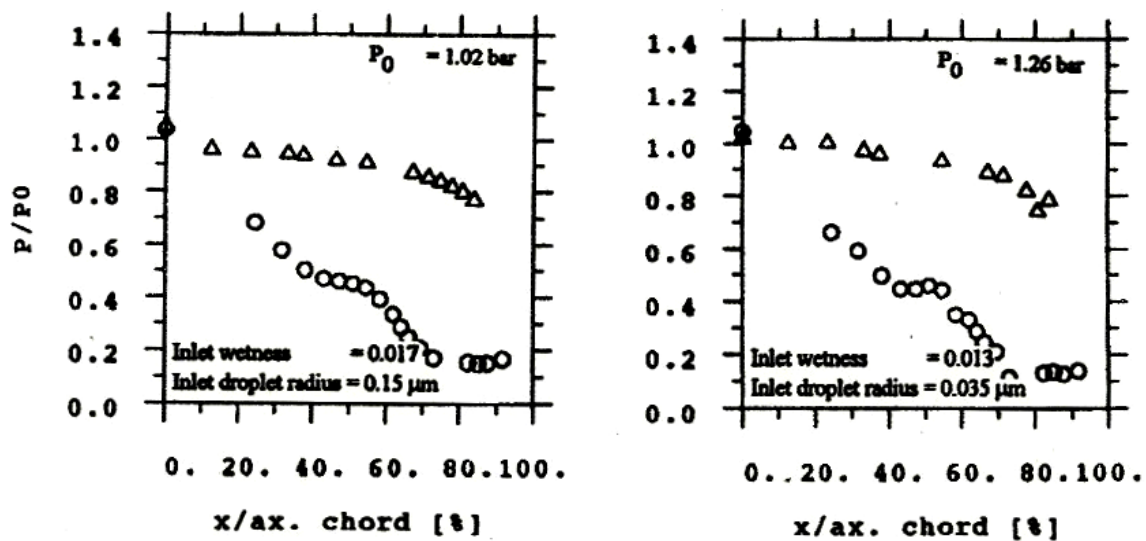


Figure 3.17: Graphic that shows the surface pressure distributions – subsonic treatment⁵³.

Considering the results for the boundary layer thicknesses, it will be seen that they are extremely thin on the pressure surface and up to approximately 50 per cent of the axial chord on the suction surface. Beyond this point there is some growth.

It will be seen that the pressure falls off steadily on the pressure surface, resulting in thin boundary layers as shown by the dotted line in Fig.(3.17). In contrast with this work, here there is a rapid pressure drop until 0.4 of the axial chord on the suction surface, beyond which there is first an inflection followed by a pressure drop and then pressure rise. The changes in the pressure distribution are the cause of growth in the boundary layer shown by the full line in Fig.(3.16).

The corresponding surface friction coefficient shows a drop at approximately 50 percent of the axial chord and then again at about 60 percent, in contrast with the friction coefficient obtained here that shows an inflection at 83% of the axial chord. However, it is observed that the coefficient, although becoming small, remains finite, indicating that the pressure changes have not been sufficient to cause boundary layer transition.

The boundary layer behavior in the remaining solutions is very similar. In this work compared with Bakhtar and Mahpeykar [P3] the boundary layer flow is laminar on the pressure surface and for approximately 70 per cent of the axial chord on the suction surface. At this point appears the transition provoked by the pressure on the suction side. The friction coefficient is low and the boundary layer is transitional for the 83% of the surface of suction and pressure side

The speed of sound in two-phase mixtures is not explicit and depends on the local conditions, like was indicated in previous chapter 2. For this reason, the overall pressure ratio was used as a more readily quantifiable measure of the inlet and outlet Mach number. Thus, to investigate the influence of droplets in the flow on the performance of the profile for a series of constant overall pressure ratios the calculations were carried out with the stagnation pressure. For the determination of the stagnation points in the time step procedure does not exist accurate solution. Depending of the blade profile, the direction of flow must be accepted in the stagnation points as in Fig.(2.2). Thus, is defined the direction of flow and the neighbor point, in order to complete the physical conditions in the blade profile. During the calculation method the accepted stagnation points remain unchanged, because their positions do not result from the calculation.

The velocity components directly on the stagnation point follow the impulse equations (2.21) and (2.22). The determination of the velocity direction at the points of neighbor is described as a function of the blade profile in the direction of flow in the chapter 2. If the resulted with the accepted stagnation points are not real, this acceptance must improve and the calculations must be repeated.

Conclusions

The available information to contribute in the knowledge of the understanding of the drops distribution in the outlet stator blade mesh is analyzed. For an appropriate mesh interpretation of the grade of saturated steam is essential the knowledge of the influence of the mesh geometry as well as the steam condition on the deposits of water to the stator blades profiles. The saturated steam stream in turbine stages connects the additional flow losses as well as the endangerment of the flow on the blade by drop impact erosion. Both features result of the expansion, which partially in the stator blade surface is deposited as finely fog-drop and finally a water film is formed becoming more largely secondary drop from the trailing edge.

A computational program for generating a bidimensional stator blade mesh for the calculation of the stationary, frictionless, transonic wet steam flow in a turbine cascade according to the time in the method of finite element is presented. The procedure contains a program section, which avoids different difficulties in the strongly curved profile of the leading and trailing edge by a developed computational mesh refinement. The mesh organization along the mainstream direction fulfills the periodic boundary conditions and due to the irregular configuration of the trailing edge an H-mesh configuration is used.

The procedure includes adaptive mechanisms to improve flow resolution in the mesh interior and smoothness. The smoothing absorbs practically the ripples of the solution functions resulted from computing inaccuracies in this case a polynomial of two degrees is used. This polynomial makes the computing time short and prevents the truncation error. For the smoothing of the two dimensional computation surface the procedure must be accomplished in both directions x, y .

From Gyarmathy [48], Bakhtar, Mahpeykar, Mashmouhy and Jadayel [51,53] it has been shown that the large secondary drops in the saturated steam stream is essentially responsible by the negative consequences. Thus, he asked himself by the places of accumulation of the fine primary drops against the stator blade surfaces with possibilities of influence. For this answer first an engineer computer model of large efficiency is indispensable, which controls also the material as the transonic flow conditions in the final stages of steam turbines. Thus, the systematic investigations of influence of the blade shape on the drops stream also accomplished the water separation by exhaust.

For an appropriate mesh interpretation of the grade of saturated steam is essential the knowledge of the influence of the mesh geometry as well as the steam condition on the deposits of water to the stator blades profiles. The saturated steam stream in turbine stages connects the additional flow losses as well as the endangerment of the flow on the blade by drop impact erosion. Both features result of the expansion, which partially in the stator blade surface is deposited as finely fog-drop and finally a water film is formed becoming more largely secondary drop from the trailing edge.

On the basis of the conservation laws for mass, impulse and total enthalpy is compile the calculation of the stationary, frictionless, two-dimensional, transonic flow in the turbine cascade according to the time in the method of the finite element. The velocity distribution determined by the calculation procedure for the frictionless stream finds the inlet into the calculation of the boundary layer on the blade surfaces and drops in the field.

With the help of program fortran a developed computational program of calculations is accomplished, whose results are communicated to the pressure and Mach number distribution, direction of flow and streamlines in the field and the drops distribution in the outlet of the stator blade mesh.

The procedure contains a program section, which avoids difficulties in the strongly curved profile of the leading and trailing edge by a developed computational mesh construction. For this treatment first are admitted firmly the stagnation points by a special method that keeps the conditions of the field physically correct.

The stability of the calculation can be achieved by the smoothing procedure structure in the sequence of the program, and also without the energy from other causes that dissipate generally in the zone of flow. Several inspection procedures for the results of computation are developed by the numeric approximation of time step procedures and never exclude the substantial errors, being present the unfavorable circumstances with security.

Here is introduced the proceeding for a stator blade mesh by systematic deformations for transonic flow conditions, with respect to smaller drops of water, that the flow losses and erosion damages resulting from the stream of saturated steam are reduced to a minimum.

The viscous effects can be treated by a boundary layer calculation in conjunction with an inviscid field solver. In this case the boundary layer displacement thickness and the loss of energy thickness have been very small, the boundary layers have remained attached and the main flow field has been little affected by the presence of the boundary layer.

Bibliography

- [1] Katz Joseph L.; "*Homogeneous Nucleation Theory and Experiment: A Survey*"; Pure and Appl. Chem., Vol. 64, No. 11, pp. 1661-1666; 1992.

- [2] Trudu Dornbierer Federica; Ph.D. Thesis: Computer Simulation Study of Homogeneous Nucleation in a Lenard-Jones Fluid; Swiss Federal Institute of Technology Zurich; 2006.

- [3] Tanaka Shu, Hirano Masaki, Miyashita; "*Quantum Annealing for Searching the Ground State of Entropic Slowing Down System*"; Journal of Magnetism and Magnetic Material; 2006.

- [4] Moody Michael P., Attard Phil; "*Homogeneous Nucleation of Droplets from a Supersaturated Vapor Phase*"; J. Chem. Phys., Vol. 117, Num. 14; pp. 6705-6714; 2002.

- [5] El Souadi Mohamed; Ph.D. Thesis: Estudio de los Mecanismos de Cristalización Primaria y Eutéctica de Aleaciones del Sistema Sb_2Se_3 - $GeSe_2$; Universitat Autònoma de Barcelona; 1998.

- [6] Ford Ian J.; "*Statistical Mechanics of Nucleation: A Review*"; Proc. Instn. Mech. Engrs. Vol. 218, Part C: J. Mechanical Engineering Science; 2004.

- [7] Merikanto Joonas; "Monte Carlo Simulations of Molecular Clusters in Nucleation"; Report Series in Aerosol Science, No. 88; 2007.

- [8] Wedekind Jan; Nano-droplets at Birth: Computer Experiments on Gas Phase Nucleation; Cuvillier Verlag, Göttingen, ISBN 10: 3-86727-084-8; 2006.

- [9] Jackson Kenneth A.; "Kinetic Processes. Crystal Growth, Diffusion, and Phase Transitions in Materials"; Wiley-VCH; 2004.
- [10] Gibbs Josiah Willard; The Collected Works. Thermodynamics Vol. I; Logmans, Green and Co.; 1928.
- [11] Domin Lee Thomas; Doctor of Philosophy Thesis: Surface Characterization by Heterogeneous Nucleation From the Vapor; Harvard University, Cambridge, Massachusetts; 1998.
- [12] Kaschiev Dimo; Nucleation. Basic Theory and Applications; Butterworth-Heinemann Publications; 2000.
- [13] Wang C. X.; Yang G. W.; "Thermodynamics of Metastable Phase Nucleation at the Nanoscale"; Material Science and Engineering R 49; 2005.
- [14] Schmelzer Jörn W. P.; Nucleation Theory and Application; Wiley-SCH; pp. 40; 2005.
- [15] Ford Ian J., Vehkamäki Hanna; "Critical Cluster Size and Droplet Nucleation Rate from Growth and Decay Simulations of Lennard-Jones Clusters"; Journal of Chemical Physics, Vol. 112, Num. 9; 2000.
- [16] Ford I. J.; "*Thermodynamic Properties of Critical Clusters from Measurements of Vapour-Liquid Homogeneous Nucleation Rates*"; J. Chem. Phys.; pp. 8324-8332; 1996.
- [17] Clift R., Grace J. R., Weber E.; *Bubbles, Drops and Particles*; Academic Press, 1978.

- [18] Bellan J.; “*Dynamics and Thermodynamics of Dense and Dilute Clusters of Drops*”; NASA Jet Propulsion Laboratory; 1994.
- [19] Katz Joseph L., Fisk Jeffery A., Rudek Markus M.; “*Nucleation of Single Component Supersaturated Vapors*”; Nucleation and Atmospheric Aerosols 1996, Proceedings of The Fourteenth International Conference on Nucleation and Atmospheric Aerosols; Pergamon; pp. 1-10; 1996.
- [20] Wegner Peter P., Parlange Jean-Yves; “*Condensation by Homogeneous Nucleation in the Vapor Phase*”; Naturwissenschaften; Springer Berlin / Heilderberg; Vol. 57, Num. 11; pp. 525-533; 1970.
- [21] Ashgriz, N., and Poo, J.Y., “*Coalescence and Separation in Binary Collisions of Liquid Drops*”; Journal of Fluid Mechanics, Vol. 221, pp. 183-204; 1990.
- [22] Arstila Hanna; “*Kinetic Effect of Cluster-Cluster Processes on Homogeneous Nucleation Rates in One-and Two-Component Systems*”; J. Chem. Phys. 107 (8); pp. 3196-3203; 1997.
- [23] Christen W., Even U.; “*Collision-Induced Fragmentation and Neutralization of Methanol Cluster Cations*”; The European Physical Journal, D16, 87-90; 2001.
- [24] Mizan Tahmid I., Savage Phillip E. , Ziff Robert M.; “*A Comparison of Rigid and Flexible Water Models in Collisions of Monomers and Small Clusters*”; Journal of Computational Chemistry, Vol. 17, Issue 15, pp. 1757 – 1770; 1998.
- [25] Kalweit Marco, Drikakis Dimitris; “*Collision Dynamics of Nanoscale Lennard-Jones Clusters*”; Physical Review, B74, pp. 235415(1-16); 2006.

- [26] Troyanovski B. M., Filippov G. A., Bulkin A. E.; Turbinas de Vapor y de Gas de las Centrales Nucleoeléctricas; Editorial Mir Moscú, 1987.
- [27] Michaelides E. E.; Particles, Bubbles and Drops, Their Motion, Heat and Mass Transfer; World Scientific Publishing; 2006.
- [28] Renardy Y., Popinet S., Duchemin L., Renardy M., Zaleski S., Josserand C., Drumright-Clarke M. A., Richard D., Clanet C., Quéré D.; “*Pyramidal and Toroidal Water Drops After Impact on a Solid Surface*”; J. Fluid Mech., Vol. 484, pp. 69-83; 2003.
- [29] Manzello Samuel L., Yang Jiann C.; “*On the Collision Dynamics of Water Droplet Containing an Additive on a Heated Solid Surface*”; Proceedings of The Royal Society. Mathematical, Physical and Engineering Sciences, Vol. 458, Num. 2026, pp.2417-2444; 1996.
- [30] Wierzba A.; “*Deformation and Breakup of Liquid Drops in a Gas Stream at Nearly Critical Weber Numbers*”; Experiment in Fluids; Springer-Verlag, Num. 9, pp. 59-64; 1990.
- [31] Parra Santos Maria Teresa; Ph.D. Thesis: Simulación de la Interacción de una Llama Premezclada; Universidad de Valladolid; 1999.
- [32] Knezevic Kristian Haller; Ph.D. Thesis: High-Velocity Impact of a Liquid Droplet on a Rigid Surface: The Effect of Liquid Compressibility”; Swiss Federal Institute of Technology Zurich; 2002.
- [33] Field J. E.; “The physics of liquid impact, shock wave interactions with cavities, and the implications to shock wave lithotripsy”; Phys. Med. Biol., Vol. 36, Num. 11, pp. 1475- 1484; 1991.

- [34] Schegláiev A. V.; Turbinas de Vapor. La Teoría del Proceso Térmico y las Construcciones de Turbinas. Parte I.; Edit, Mir Moscú; 1985.
- [35] Liu Huimin; Science and Engineering of Droplets: Fundamentals and Applications; Noyes Publications; 2000.
- [36] Jonas Otakar; "Condensation in Steam Turbines – New Theory and Data"; International Joint Power Generation Conference; Baltimore; August 23-26; 1998.
- [37] Bellows James C.; "Chemistry in the Moisture Transition Region of the Steam Turbine"; J. of Solution Chem.; Vol. 32, Num. 10; 14th International Conference on the Properties of Water and Steam; Springer Netherlands; Kyoto; 2003.
- [38] Jonas Otakar, Mancini Joyce M., "Steam Turbine Problems and Their Field Monitoring"; Materials Performance; 2001.
- [39] Bakhtar F., Heaton A. V.; "Effects of Wake Chopping on Droplet Sizes in Steam Turbines"; Journal of Mechanical Engineering Science; Vol. 219 Part C; pp. 1357-1367; 2005.
- [40] Bakhtar F., White A. J., Mashmouhy H.; "Theoretical Treatments of Two-Dimensional Two-Phase Flows of Steam and Comparison With Cascade Measurements"; Journal of Mechanical Engineering Science; Vol. 219 Part C; pp. 1335-1355; 2005.
- [41] Schnerr G. H.; "Unsteadiness in Condensing Flow: Dynamics of Internal Flows With Phase Transition and Application to Turbomachinery"; Journal of Mechanical Engineering Science; Vol. 219, Part C; pp. 1369-1410; 2005.

- [42] Gerber A. G., Mousavi A.; "Representing Polydispersed Droplet Behavior in Nucleating Steam Flow"; Journal of Fluids Engineering, Vol. 129, pp. 1404-1414, November 2007.
- [43] Avallone Eugene A., Baumeister III Theodore; "Mark's Standard Handbook for Mechanical Engineers"; McGraw Hill, Tenth Edition; 1996.
- [44] Petr V., Kolovratnik M.; "Modelling of the Droplet Size Distribution in a Low-Pressure Steam Turbine"; Proc. Instn. Mech. Engrs.; Vol. 214 Part. A; pp. 145-152; 2000.
- [45] Bakhtar F., Young J. B., Whit A. J., Simpson D. A.; "Classical Nucleation Theory and its Application to Condensing Steam Flow Calculations"; Journal of Mechanical Engineering Science; Vol. 219 Part C; pp. 1315-1333; 2005.
- [46] Westra Remko Willem; Thesis: "Inverse-Design and Optimization Methods for Centrifugal Pumps Impellers"; University of Twente; The Netherlands; 2008.
- [47] Veuillot J. P., Viviand H.; "Pseudo-Unsteady Method for the Computation of Transonic Potential Flows"; American Institute of Aeronautics and Astronautics Journal; pp. 691-692; 1979.
- [48] Gyarmathy G.; "Two Phase Steam Flow in Turbines and Separators, Theory, Instrumentation, Engineering. Condensing in Flowing Steam"; Mcgraw-Hill Company; 1976.
- [49] Schaaf S. A., Chambre' P. L.; "Flow of Rarefied Gases"; Princeton University Press; 1961.

- [50] White J. A.; "Theoretical Treatments of Two-Dimensional Two-Phase Flows of Steam and Comparison with Cascade Measurements"; Mechanical Engineering Science. Vol. 219 part. A; pp.1351; 2005.
- [51] Bakhtar F., Mashmoushy H., Jadayel O. C.; "On the Performance of a Cascade of Turbine Rotor Tip Section Blading in Wet Steam. Part 2: Surface Pressure Distributions"; Proceedings of the Institute of Mechanical Engineers; Vol. 211, Part C; pp. 531-540; 1997.
- [52] Otakar Jonas; "Condensation in Steam Turbine, New Theory and Data"; Editorial Jonas , Inc. pp.7; 1998.
- [53] Bakhtar F., Mahpeykar M. R.; "On the Performance of a Cascade of Turbine Rotor Tip Section Blading in Wet Steam. Part 3: Theoretical Treatment"; Proceedings of the Institute of Mechanical Engineers; Vol. 211, Part C; pp. 195-209; 1997.

Annex

Computational Program: Stator Drop

```
! PROGRAM STATOR DROP
!
! PL   : PROFIL LENGTH
! T    : INTERVAL OF PROFIL GRID
! TTOL : T/PL
! BETAS : STAPLE ANGLE (RAD)
! DS   : MAXIMAL PROFIL SURFACE LENGTH OF UNIT MESH
! DSTOL : DS/PL
! DTAN : MAXIMAL GRADIENT OF PROFIL SURFACE (RAD)
! NPROF : NUMBER OF ORIGINAL PROFIL COORDINATES
! XPROF : BITANGENTIAL X-AXIAL COORDINATE OF PROFIL
! YPROF : " Y-AXIAL "
! NX1   : NUMBER OF X-AXIAL FOREWARD PROFIL END
! NX2   : " Y-AXIAL AFTERWARD "
! NX    : NUMBER OF X-AXIAL MESH COORDINATES
! NY    : " Y-AXIAL "
! X     : X-AXIAL MESH COORDINATE
! Y     : Y-AXIAL
! INPUT : PL,TTOL,BETAS,DSTOL,DTAN,NPROF,XPROF,YPROF
! OUTPUT : NX1,NX2,NX,NY,X,Y
! RP    : RADIUS OF PARTICLE (M)
! RHOW  : DENSITY OF PARTICLE (KG/M**3)
! ETADYN : DYNAMIC VISCOSITY (KG/M SEC)
! DT    : TIME SEGMENT (SEC)
! NX1   : NUMBER OF X-AXIAL FOREWARD PROFIL END
! NX2   : " Y-AXIAL AFTERWARD "
! NX01  : NUMBER OF X-AXIAL FOREWARD STAGNATION POINT
! NY01  : " Y-AXIAL "
! NX02  : NUMBER OF X-AXIAL AFTERWARD STAGNATION POINT
! NY02  : " Y-AXIAL "
! NX    : NUMBER OF X-AXIAL MESH COORDINATES
! NY    : " Y-AXIAL "
! X     : X-AXIAL MESH COORDINATE
! Y     : Y-AXIAL
! XIN   : X-AXIAL COORDINATE OF INLET STEAM
! YIN   : Y-AXIAL "
! FIN   : EACH FLOW QUANTITY OF STEAM AT INLET
! XOUT  : X-AXIAL COORDINATE OF OUTLET STEAM
! YOUT  : Y-AXIAL "
! RHO   : DENSITY OF STEAM
! PRES  : PRESSURE
! CX    : X-AXIAL VELOCITY COMPONENT OF STEAM
```

```

! CY : Y-AXIAL "
! NWAY : " STREAM LINE
! XDOT : X-AXIAL COORDINATE OF PARTICLE MOVEMENT
! YDOT : Y-AXIAL "
! RHODOT : DENSITY OF PARTICLE (KG/M**3)
! PDOT : PRESSURE " (N/M**2)
! CXDOT : X-AXIAL VELOCITY COMPONENT OF PARTICLE (M/SEC)
! CYDOT : Y-AXIAL "

```

```

PROGRAM STATORDROP
IMPLICIT NONE

```

```

REAL,DIMENSION (100):: X,XPROF,YPROF
REAL,DIMENSION (100,100) :: Y
REAL :: TTOL,BETAS,DSTOL,DTAN,PL
INTEGER :: I,J,NX1,NX2,NX,NY,NPROF
READ(5,1000) NPROF,PL,TTOL,BETAS,DSTOL,DTAN

```

```

DO 10 I=1,NPROF
10 READ(5,1100) XPROF(I),YPROF(I)

```

```

CALL
GRID(PL,TTOL,BETAS,DSTOL,DTAN,NPROF,XPROF,YPROF,NX1,NX2,
NX,NY,X,Y)

```

```

WRITE(10) TTOL,BETAS,NX,NY,NX1,NX2
1000 FORMAT(I10,6F10.0)
1100 FORMAT(2F10.0)
END

```

```

SUBROUTINE

```

```

GRID(PL,TTOL,BETAS,DSTOL,DTAN,NPROF,XPROF,YPROF,NX1,NX2,&
&NX,NY,X,Y)

```

```

IMPLICIT NONE

```

```

REAL :: TTOL,BETAS,DSTOL,DTAN,DTAL,PL
INTEGER :: NPROF,NSUCT,NPRES,NA,NX1,NX2,NX,NY,N1,N2,N
REAL,DIMENSION (100):: X
REAL,DIMENSION (NPROF) :: XPROF,YPROF
REAL,DIMENSION (100,100) :: Y
TTOL= 0.90000
DTAN= 0.7265
DSTOL= 0.0066889

```

```

! THE MESH COORDINATES OF PROFIL CASCADE
DO 10 I=NX1,NX2
X(I)=XA(I-NX1+1)

```

```

      YS(I)=YAS(I-NX1+1)
      YP(I)=YAP(I-NX1+1)
10 CONTINUE

```

! THE MESH COORDINATES OF UPSTREAM

```

      DO 20 I=1,NX1
        X(NX1-I+1)=XUP(I)
        YS(NX1-I+1)=YUPS(I)
        YP(NX1-I+1)=YUPP(I)
20 CONTINUE

```

! THE MESH COORDINATES OF DOWNSTREAM

```

      DO 30 I=NX2,NX
        X(I)=XDN(I-NX2+1)
        YS(I)=YDNS(I-NX2+1)
        YP(I)=YDNP(I-NX2+1)
30 CONTINUE

```

! THE WHOLE MESH COORDINATES

```

      DO 40 I=1,NX
        DY=(YP(I)-YS(I))/(NY-1)
      DO 40 J=1,NY
        40 Y(I,J)=YS(I)+(J-1)*DY

```

RETURN

END

! THE EQUIDISTANT INTERPOLATION OF TURBINE CASCADE

```

      NXINT=48
      DXINT=(X2-X1)/(NXINT-1)
      DO 10 I=1,NXINT-1
        10 XINT(I)=X1+(I-1)*DXINT
      XINT(NXINT)=X2

```

```

      CALL DIFF(NSUCT,XTS,YTS,FPS1,0)
      CALL INTERP(NSUCT,XTS,YTS,FPS1,NXINT,XINT,YINTS,FPS2)
      CALL DIFF(NPRES,XTP,YTP,FPP1,0)
      CALL INTERP(NPRES,XTP,YTP,FPP1,NXINT,XINT,YINTP,FPP2)

```

! THE TRANSFORMED PROFIL COORDINATES WITH ANGLE(BETAS)

```

      DBETAS=PI/2.-BETAS
      CALL TRANS(DBETAS,NPROF,T1,T2,XPROF,YPROF,XT,YT)

```

SUBROUTINE INTERP(N1,X1,F1,FP1,N2,X2,F2,FP2)

IMPLICIT NONE

```

! CUBIC INTERPOLATION
  REAL :: DXX,DXX2,DXX3,FPP1,FPPP1,DX,DF,DX2,DF1,DX3,FPP
  INTEGER :: N1,N2,JJ,JT,JTT,I,J,J1
  REAL,DIMENSION (N1) :: X1,F1,FP1
  REAL,DIMENSION (N2):: X2,F2,FP2
  DO 50 I=1,N2
    DO 10 J=JT,N1
      JTT = J
      IF (X1(J).GE.X2(I)) GOTO 20
    10 CONTINUE
    20  JT = JTT
      J = JT
      IF (X1(J).EQ.X2(I)) GOTO 40
      IF (J.EQ.JJ) GOTO 30
      JJ=J
      J1=J-1
      DX=X1(J)-X1(J1)
      DF=F1(J)-F1(J1)
      DX2=DX*DX
      DX3=DX2*DX
      DF1=FP1(J)-FP1(J1)
      FPP=FP1(J)+FP1(J1)
      FPPP1=(2.*DF-DX*FPP)/(-DX3/6.)
      FPP1=DF1/DX-DX*FPPP1/2.
    30 DXX=X2(I)-X1(J1)
      DXX2=DXX*DXX/2.
      DXX3=DXX2*DXX/3.
      F2(I)=F1(J1)+DXX*FP1(J1)+DXX2*FPP1+DXX3*FPPP1
      FP2(I)=FP1(J1)+DXX*FPP1+DXX2*FPPP1
      GOTO 50
    40 F2(I)=F1(J)
      FP2(I)=FP1(J)
      JJ=0
    50 CONTINUE
      RETURN
  END

```

SUBROUTINE TRANS(PHI,N,T1,T2,X0,Y0,X,Y)
 IMPLICIT NONE

```

  REAL,DIMENSION (2,2):: D
  REAL,DIMENSION (33,2) :: T1,T2
  REAL,DIMENSION (33) :: X0,Y0,X,Y
  INTEGER :: N,I,J,K
  REAL :: PHI

```


! THE TRANSFORMATION OF PROFIL COORDINATES

```
D(1,1)=COS(PHI)
D(1,2)=SIN(PHI)
D(2,1)=-SIN(PHI)
D(2,2)=COS(PHI)
```

```
DO 10 I=1,N
  T1(I,1)=X0(I)
  T1(I,2)=Y0(I)
10 CONTINUE
DO 30 I=1,N
  DO 20 J=1,2
    T2(I,J)=0
    DO 20 K=1,2
      T2(I,J)=T2(I,J)+D(J,K)*T1(I,K)
    20 CONTINUE
  X(I)=T2(I,1)
  Y(I)=T2(I,2)
30 CONTINUE
RETURN
END
```

SUBROUTINE ENT(C1,P1,RHO1,PN,NX,NY,RHO,PRES,CX,CY,SIGMA,&
&U,V,VARI,NITER,NITER1,NITER2)

! THE TOTAL ENTHALPIE IN TURBINE CASCADE

```
DO 40 I=1,NX
DO 40 J=1,NY
  C=SQRT(CX(I,J)**2+CY(I,J)**2)
  H=PN/(PN-1.)*PRES(I,J)/RHO(I,J)+0.5*C**2
  HREL(I,J)=H/(P01/RHO01)
40 CONTINUE
```

```
RETURN
END
```

SUBROUTINE IMPULS(AL,C1,A1,AM1,RHO1,ETAP,DTAU,NX1,NX2,&
&NX,NY,STAU,PTAU,UTAU,VTAU)

IMPLICIT NONE

REAL :: DTAU,ETAP,RHO1,AM1,A1,C1,AL,S1N,S1,S2,S3,S4,S5,S6

REAL :: DP,RHOM,DPRES,DF,PHI,S,DN,DV,F11,F12,&
&F21,F22,F31,F32,F41,F42,F51,F52,F61,F62

INTEGER :: NX,NY,IX1,IX2,II,JJ,NX1,NX2,I,J,R,STATUS

REAL,DIMENSION (NX,NY) :: STAU,PTAU,UTAU,VTAU

REAL,DIMENSION (100,100) :: SIGMA,P,U,V,UP,VP,SIGMAP

COMMON/MASS1/ SIGMAP,UP,VP

! THE CHARACTERS REDESIGNATION FOR PERIODIC REGION

```

DO 10 I=1,NX
  DO 10 J=1,NY
    SIGMA(I+1,J+1)=STAU(I,J)
    P(I+1,J+1)=PTAU(I,J)
    U(I+1,J+1)=UTAU(I,J)
    V(I+1,J+1)=VTAU(I,J)
  10 CONTINUE

```

```

DO 20 J=1,NY
  SIGMA(1,J+1)=SIGMA(2,J+1)
  P(1,J+1)=P(2,J+1)
  U(1,J+1)=U(2,J+1)
  V(1,J+1)=V(2,J+2)
  SIGMA(NX+2,J+1)=SIGMA(NX+1,J+1)
  P(NX+2,J+1)=P(NX+1,J+1)
  U(NX+2,J+1)=U(NX+1,J+1)
  V(NX+2,J+1)=V(NX+1,J+1)
20 CONTINUE

```

! THE INLET CONDITION OF X- AND Y-VELOCITY

```

IF (NX1.EQ.NX01) THEN
  W(NX1,1)=SQRT(U(NX1,1)**2+V(NX1,1)**2)
  U(NX1,1)=W(NX1,1)*COS(THETA(NX1,1))
  V(NX1,1)=W(NX1,1)*SIN(THETA(NX1,1))
  W(NX1,NY)=SQRT(U(NX1,NY)**2+V(NX1,NY)**2)
  U(NX1,NY)=W(NX1,NY)*COS(THETA(NX1,NY))
  V(NX1,NY)=W(NX1,NY)*SIN(THETA(NX1,NY))
END IF

```

! THE VELOCITIES AT PROFILE SURFACE

```

DO 50 I=NX1,NX2
  DO 50 J=1,NY,NY-1
    U(I,J)=W(I,J)*COS(THETA(I,J))
    V(I,J)=W(I,J)*SIN(THETA(I,J))
  50 CONTINUE
RETURN
END

```

```

SUBROUTINE FLOW1(C1,AM1,P1,P2,RHO1,PN,NX01,NX02,NX,NY,X,&
&RHO,CX,CY,SIGMA,U,V,NITER1)
  IMPLICIT NONE
  REAL,DIMENSION (20) ::
  XCAL,YCAL,DYCAL,YOCAL,XIN,YIN,DIN,FIN

```

```

REAL,DIMENSION (75) :: X
REAL,DIMENSION (75,48) :: Y,RHO,PRES,CX,CY
REAL,DIMENSION (2,20) :: NDOT,XOUT,YOUT,DOUT,FOUT,SFOUT
REAL,DIMENSION (2,20,1000) :: XDOT,YDOT,RHODOT,PDOT,&
&CXDOT,CYDOT
INTEGER :: NX1,NX2,NX,NY,NX01,NY01,NWAY,NRHO,TTOL,&
&BETAS,I,J,NX02,NY02,NFLOW,NCAL
REAL :: T,PROFL,XMES,RP,RHOW,RHOG,RX,FCW,DT,

```

! THE INPUT DATAS FOR STREAM LINE

```

READ (5,1000) NRHO,NWAY
READ (5,1100) RP,RHOW,ETADYN,RX,FCW,DT,YO
NWAY=20
RHOW=994.8
ETADYN=0.00000001
DT=0.00000001
NRHO=2

```

! THE GAS CONSTANT FOR IDEAL GAS

```

! KAPPA=1.4
! ETAP=1.0
AKAPPA=1.4
ETAP=1.0
PN=AKAPPA/(AKAPPA-ETAP*(AKAPPA-1.))
C1=SQRT(CXDOT(1,1,1)**2+CYDOT(1,1,1)**2)
RHO1=RHODOT(1,1,1)
P1=PDOT(1,1,1)
A1=SQRT(PN*P1/RHO1)
AM1=C1/A1
P0=P1*(1.+(PN-1.)/2.*AM1**2)**(PN/(PN-1.))
RHO0=RHO1*(P0/P1)**(1./PN)
CA=SQRT(2.*PN/(PN+1.)*P0/RHO0)

```

RETURN

2010 FORMAT(1H1,9X,'THE COORDINATES AND VELOCITIES OF GAS FLOW
LINES', &

&

10X,'=====',//,&

& 3X,'NWAY',1X,'NDOT',6X,'X/LA',6X,'Y/LA',9X,'MX*', &

& 7X,'MY*',7X,'M*')&

2020 FORMAT(1H1,8X,'THE COORDINATES AND VELOCITIES OF DROP
FLOW LINES',&

&

9X,'=====',//, &

& 3X,'NWAY',1X,'NDOT',6X,'X/LA',6X,'Y/LA',9X,'MX*',&

```
& 7X,'MY*',7X,'M*')
2030
FORMAT(1H1,2X,'NWAY',1X,'NDOT',6X,'X/LA',6X,'Y/LA',9X,'MX*',7X,'MY*',7X,'
M*')
2110 FORMAT(1H ,2I5,2X,2F10.4,2X,3F10.4)
2120 FORMAT(1H ,5X,I5,2X,2F10.4,2X,3F10.4)
2130 FORMAT(1H )
2210 FORMAT(1H1,///44X,'THE GAS FLOW QUANTITY TROUGH TURBINE
CASCADE',&
& //,14X,'NFLOW',6X,'X/T'2X,'DIN(KG/SM**2)',1X,'FIN(KG/S)', &
& 6X,'S/A',2X,'DMID(KG/SM*2)',1X,'FMID(KG/S)',&
& 6X,'S/A',2X,'DOUT(KG/SM*2)',1X,'FOUT(KG/S)')
2220 FORMAT(1H
,11X,I5,2X,F10.4,1X,F10.4,1X,F10.4,3X,F10.4,1X,F10.4,2X,F10.4,3X,F10.4,1X,F10.4
,2X,F10.4)
2230 FORMAT(1H ./,15X,'FSUM',22X,F10.4,26X,F10.4,26X,F10.4)
2310 FORMAT(1H ,///,12X,'BOUNDARY LAYER)
RETURN
END
```

Papers generated

HEFAT2008
6th International Conference on Heat Transfer, Fluid Mechanics and Thermodynamics
30 June to 2 July 2008
Pretoria, South Africa
Paper number: RM1

EROSION STUDY OF A ROTOR BLADE FROM A STEAM TURBINE

Rueda MF; Toledo VM; Jarquin G; Polupan G; Sánchez SF.
Laboratorio de Ingeniería Térmica e Hidráulica Aplicada
Sección de Estudios de Posgrado e Investigación
Escuela Superior de Ingeniería Mecánica y Eléctrica
INSTITUTO POLITÉCNICO NACIONAL
Edificio 5 3er. piso. Av. IPN s/n, Colonia Lindavista, 07738, México D.F.
Tel. 57296000 ext. 54754
mtv49@yahoo.com,

ABSTRACT

In this theoretical study an analysis of the mechanical erosion influence on working blades in the last stage of the pressure low section of a steam turbine with electric generation of 300 MW installed in a thermoelectrical plant is presented. First, it is described the formation of humidity and is given an analyses of nucleation theory like introduction to the problems of erosion in the working blades of steam turbines. With information of the turbine in conditions of operation and design for the 5th stage, is showed a calculation of the different physical, structural and of regime parameters (impact pressure, modal dimensions drops, impact frequency, etc.) that appear in the working blades erosion of this turbine. The model used in this work is only spherical nucleation on a flat surface and a spherically convex surface are considered, the model of drop also is spherically and it's not considered water chemistry issues. The solutions of these erosive influence equations here presented are obtained for different sections of a rotor blade: base, middle zone and peripheral zone. With the solved variables, it is obtained a table of resulted that compare the operation and design conditions and are elaborated graphics that allow correlations of values in function of drops dimension and different velocities calculated, obtaining information that shows the mass lost of the blade during the time operation work. The calculation realized gives an idea of the damage on working blades due to the presence of droplets into the flow.

Keywords: erosion, steam turbine, rotor blades, nucleation



**XI CONGRESO Y EXPOSICIÓN
LATINOAMERICANA DE
TURBOMAQUINARIA**
Veracruz, Ver. México

**XI CONGRESO Y EXPOSICIÓN
LATINOAMERICANA DE
TURBOMAQUINARIA**
14-17 Octubre 2008

DETERMINATION OF THE COMPRESSIBLE FLOW THROUGH A PLANE BLADE CASCADE OF TURBO-MACHINES

To G. Polupan for his onomastic.

AUTOR

Miguel Toledo-Velázquez
Profesor Investigador Miembro
SNI, AMC.
Laboratorio de Ingeniería
Térmica e Hidráulica Aplicada
Sección de Estudios de
Posgrado e Investigación
Escuela Superior de Ingeniería
Mecánica y Eléctrica.
INSTITUTO POLITÉCNICO
NACIONAL
Edificio 5 3er. piso. Av. IPN
s/n, Colonia Lindavista, 07738,
México D.F.
Tel. 57296000 ext. 54754
mtv49@yahoo.com

COAUTOR

Guilibaldo Tolentino-Eslava
Profesor Investigador.
Laboratorio de Ingeniería
Térmica e Hidráulica Aplicada
Sección de Estudios de
Posgrado e Investigación
Escuela Superior de Ingeniería
Mecánica y Eléctrica.
INSTITUTO POLITÉCNICO
NACIONAL

COAUTOR

René Tolentino-Eslava
Profesor Investigador.
Laboratorio de Ingeniería
Térmica e Hidráulica Aplicada
Sección de Estudios de
Posgrado e Investigación
Escuela Superior de Ingeniería
Mecánica y Eléctrica.
INSTITUTO POLITÉCNICO
NACIONAL

COAUTOR

Fernando Rueda-Martínez
Estudiante de Doctorado en
Ingeniería Mecánica.
Laboratorio de Ingeniería
Térmica e Hidráulica Aplicada
Sección de Estudios de
Posgrado e Investigación
Escuela Superior de Ingeniería
Mecánica y Eléctrica.
INSTITUTO POLITÉCNICO
NACIONAL

COAUTOR

Aldo G. Ortiz-Andrade
Estudiante de Maestría en
Ingeniería Mecánica
Laboratorio de Ingeniería
Térmica e Hidráulica Aplicada
Sección de Estudios de
Posgrado e Investigación
Escuela Superior de Ingeniería
Mecánica y Eléctrica.
INSTITUTO POLITÉCNICO
NACIONAL

ABSTRACT

The main flow problems associated with the design of turbo-machines are connected with the cascade and spatial flows. As is known, the two problems are usually dealt with separately in the theory of axial turbo-machines, the first as a plane problem, and the second as a rotationally symmetrical one. It is then assumed that the two solutions can be superposed on one another with sufficient accuracy. A similar assumption was recently made for radial machines as well, i.e. the rotationally symmetrical flow is determined through the blading, which strictly speaking represents an infinite number of blades. For evaluating the effects of a finite number of blades the rotationally symmetrical flow areas are considered given and the frictionless flow around the blades is calculated. The second step takes into account the influence of friction in the thin layer along the wall, where this resistance to motion is regarded as being concentrated (the boundary-layer effect).

Until now the flow areas of the rotationally symmetrical meridian flow were approximately represented by conical or cylindrical sections. By conformal mapping the flow around the blade profiles could be reduced to a two-dimensional problem. In contrast to previous treatments, the frictionless, compressible subsonic flow is calculated in any rotationally symmetrical reference plane through the spatial cascade in accordance with the method of singularities. According to this theory all the cascades which are of importance from an engineering aspect (conical, axial, radial and straight) can be dealt with by one and the same mathematical process. In this article the process is applied to the particularly simple example of the straight, plane blade cascade.

Keywords: blade, cascade, streamline, compressible flow.

1. NOTATION AND DEFINITIONS

F_a	Region containing sources and sinks.
L	Developed length of the profile edge.
$Ma=c/c$	Local Mach number.
O'	Origin of the complex coordinates ζ and z . ¹
$P = P(Z)$	Point in the flow area.
$Q = dF_q$	Law of conservation of mass per unit of length.

5o CONGRESO INTERNACIONAL DE
INGENIERÍA ELECTROMECÁNICA Y DE SISTEMAS
MEC100
México, D.F. 10-14 de Noviembre 2008

Artículo aceptado por refereo

Review of nucleation phenomena in steam turbines

To G. Polupan for his 60th onomastic

Rueda Martínez F.¹; Toledo Velázquez M.¹; Sánchez Silva F.¹;
Polupan G.¹; Rueda Martínez A. A.¹; Jarquín López G.²

¹Thermal Engineering and Applied Hydraulics Laboratory
SEPI-ESIME-IPN Unidad Profesional "Adolfo Lopez Mateos"
Av. IPN s/n, Col. Lindavista, 07738, Mexico, D.F.
Tel.: 57296000 ext. 54783 / Fax 57296000 ext. 54754 E-mail: mtv49@yahoo.com

²ESIME-IPN Unidad Profesional "Culhuacan"
Av. Santa Ana # 1000, Col. Culhuacan, Del. Coyoacan, México, D.F.
Tel.: 57296000 ext. 77000

Abstract --- The nucleation theory, like introduction to the problems of erosion in the working blades of steam turbines, is presented. From basic ideas of homogeneous and heterogeneous spherical nucleation model, the low pressure section of a turbine installed in a steam-electrical power plant is treated from the point of view of the erosion that appears on blades due to the droplets in the steam.

Keywords: nucleation, steam turbine, droplet, cluster, erosion.

I. INTRODUCTION

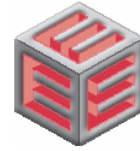
The nucleation is the energy necessary to form a stable germ, also named thermodynamic barrier of germination [1]. To microscopic level, phase fluctuations occur as random events due to the thermal vibration of atoms (collisions). In terms of classical nucleation theory, the spontaneous fluctuations lead to the formation of small embryonic droplet that can grow beyond some critical radius; it being possible overcome this barrier and sustain spontaneous growth; that is, it can only survive and grow if there is a reduction in free energy. However, if the energy barrier to spontaneous growth is large and the droplet cannot achieve critical size, it remains unstable and will in all possibility evaporate. As a result of this energy barrier, the system can exist in a metastable state with unfavorably high supersaturation levels being maintained in the gas phase [2].

A practical difficulty where the existence of formation of water droplets creates problems is the behavior of steam in turbines. The temperature and pressure gradients are such that these droplets might nucleate with undesirable effects on the performance of the machine, including the erosion of the turbine blades due to the repeated impact on them. On the other hand the steam must be expanded as much as possible to extract the most work from it [3]. In the case of condensed phases, the principal idea is that there exists a bottleneck in the transformation, which is passed through only by fragments, or molecular clusters, of the new phase. The cluster is a grouping of individual units interrelated mutually in all the senses: verticals, horizontals, etc., that establish a functional interdependence for the development of its processes. The bottleneck is narrowest when the clusters reach a so-called critical size, and therefore the properties of these critical clusters are central to the theory of nucleation.

THESIS BY: FERNANDO RUEDA MARTÍNEZ
LEADERSHIP: DR. MIGUEL TOLEDO VELÁZQUEZ

5th EUROPEAN CONFERENCE
ECONOMICS AND MANAGEMENT
OF ENERGY IN INDUSTRY

Hotel D. Pedro Golf Resort • Vilamoura • Algarve • Portugal • 14-17 April 2009



CALCULATION OF DROPS DISTRIBUTION IN STEAM TURBINES BLADES

Rueda Martínez F.¹, Toledo Velázquez M.^{1,a},
Sánchez Silva F.¹, Rueda Martínez Aldo A.¹

¹Applied Thermal and Hydraulic Engineering Laboratory
National Polytechnic Institute of Mexico
SEPI-ESIME-IPN Unidad Profesional "Adolfo López Mateos"
Av. IPN s/n, Col. Lindavista, 07738, México, D.F.
Tel. & Fax: 57296000 ext. 54754
^ae-mail: mtv49@yahoo.com

ABSTRACT

This paper presents the calculation of the drops distribution in the exit of blades that have flow conditions of wet steam, in order to understand the causes that originate the erosion on the blades of the last stages in the low pressure section of steam turbines. Into the calculation of the velocity distribution for the stream frictionless, the boundary layer on the blade surfaces and the drops in the flow line, on the basis of the stationary, frictionless, two-dimensional, transonic and homogenous flow is found. In this work an approximate movement of the droplets in the blade cascades, flowing through the steam and, in particular, the accumulation of droplets on the stator blades is identified.

KEYWORD: Steam turbine, homogeneous nucleation, drop distribution, erosion stator-rotor blade, transonic flow, mesh pressure-suction side.

1. INTRODUCTION.

The energy in the heated water can be transferred to a thermodynamic working fluid to generate electrical power. Because of the water is only under moderately high temperature and pressure, the working fluids often operate in the two-phase region (water and steam together, for example). The two-phase turbines have moderate efficiencies but a very high blade erosion rate due to impingement by high velocity, unsteady, individual liquid droplets.

Steam turbines are one of the most versatile and oldest prime mover technologies still in general production. Power generation using steam turbines has been in use for about 100 years, when they replaced reciprocating steam engines due to their higher efficiencies and lower costs. The capacity of steam turbines can range from 50 kW to several hundred MWs for large utility power plants. Steam turbines are widely used for combined heat and power applications. Due to the erosion of steam turbine blades has been one of the important technological problems in power generation systems, is necessary the analysis of path and collision of droplets that have brought severe erosion problems in steam turbine blades, causing a high cost of maintenance and repair as well as a safety problem and low efficiency of power generation.

1.1 Droplets by nucleation in steam turbines

Nucleation is the energy necessary to form a stable droplet, also named thermodynamic barrier of germination. In a microscopic level, phase fluctuations occur as random events due to the thermal vibration of atoms (collisions). In terms of classical nucleation theory, the spontaneous fluctuations lead to the formation of small embryonic droplet that can grow beyond

HEFAT2010
7th International Conference on Heat Transfer, Fluid Mechanics and Thermodynamics
19-21 July 2010
Antalya, Turkey

**HUMIDITY DISTRIBUTION IN A TWO DIMENSIONAL STATOR
BLADE CASCADE OF STEAM TURBINE**

Rueda Martínez Fernando, Toledo Velázquez Miguel, Sánchez Silva Florencio,
Ortega Herrera José Ángel, Rueda Martínez Aldo Antonio

Instituto Politécnico Nacional
Laboratorio de Ingeniería Térmica e Hidráulica Aplicada
Edif. 5, 3er piso. ESIME Zacatenco
Av. IPN s/n Col. Lindavista C.P. 07738, México, D.F.
Tel. 57296000 Ext. 54754; Fax: 57296000 Ext. 54783
E-mail: mtv49@yahoo.com

ABSTRACT

One of the most important properties of matter is its capacity to take different physical forms for different values of parameters such as temperature or pressure; for example, the condensation of the vapor forming droplets and that affect the behavior of the velocity triangles. A practical situation where the existence of water droplets creates problems is the behavior of steam in turbines. The temperature and pressure gradients are such that these droplets cause changes on the vector of absolute velocity and give, as a consequence, many problems with undesirable effects on the performance of the machine, including the erosion of the turbine blades due to the repeated impact on them. In this paper the calculation of the humidity distribution from input information about the streamline by means of physical characters of drops moving in a flow lines and by the boundary contact point is presented.

HEFAT2011
8th International Conference on Heat Transfer, Fluid Mechanics and Thermodynamics
26 June – 1 July 2011
Pointe Aux Piments, Mauritius

**THE DENSITY AND MOMENTUM DISTRIBUTIONS OF
2-DIMENSIONAL TRANSONIC FLOW IN AN LP-STEAM TURBINE**

¹Rueda Martínez A. A., ¹Rueda Martínez F. ²Toledo Velázquez M.,

³Sanchez Silva F., ⁴Jiménez Bernal J. A.

Laboratorio de Ingeniería Térmica e Hidráulica Aplicada (LABINTHAP),
SEPI-ESIME-Instituto Politécnico Nacional, México D.F.

¹ Doctor Engineering Student. Author. E-MAIL: aldo_rueda2@hotmail.com

¹ Doctor Engineering Student. Coauthor. E-MAIL: ing.fernandorueda@yahoo.com

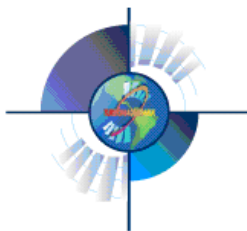
² Doctor Engineering Professor. Author. E-MAIL: mtv49@yahoo.com

³ Doctor Engineering Professor. Co-author

⁴ Doctor Engineering Professor. Co-author

ABSTRACT

Within turbine blade rows, particularly for cascades of high deflection angle, cross-channel gradients of steam properties may be appreciable. To determine the effects on spontaneous condensation of gradients of supersaturation normal to streamlines, the conservation equations can be incorporated in a two dimensional calculation procedure. With the help of program FORTRAN 90 a developed computational program of calculations is accomplished, whose results are communicated to the pressure and Mach number distribution, direction of flow and streamlines in the field and the drops distribution in the outlet of the stator blade mesh. The procedure contains a program section, which avoids difficulties in the strongly curved profile of the leading and trailing edge by a developed computational mesh construction.



**XII CONGRESO Y EXPOSICIÓN
LATINOAMERICANA DE
TURBOMAQUINARIA**

22 al 25 de febrero de 2011
Querétaro, Qro.

**EROSION ANALYSIS BY DROPLETS IN BLADES
OF LOW PRESSURE STEAM TURBINES**

AUTOR

Fernando Rueda Martínez
Estudiante de Doctorado en
Ingeniería Mecánica.
Laboratorio de Ingeniería Térmica
e Hidráulica Aplicada
Sección de Estudios de Posgrado e
Investigación
Escuela Superior de Ingeniería
Mecánica y Eléctrica.
INSTITUTO POLITÉCNICO
NACIONAL
Edificio 5, 3er. piso. Av. IPN s/n,
Colonia Lindavista, 07738, México
D.F.
Tel. 57296000 ext. 54754

AUTOR

Miguel Toledo Velázquez
Profesor Investigador Miembro
SNI, AMC.
Laboratorio de Ingeniería
Térmica e Hidráulica Aplicada
Sección de Estudios de Posgrado
e Investigación
Escuela Superior de Ingeniería
Mecánica y Eléctrica.
INSTITUTO POLITÉCNICO
NACIONAL
Edificio 5, 3er. piso. Av. IPN s/n,
Colonia Lindavista, 07738,
México D.F.
Tel. 57296000 ext. 54754
mtv49@yahoo.com

COAUTOR

Florencio Sánchez Silva
Profesor Investigador Miembro
SNI, AMC.
Laboratorio de Ingeniería Térmica
e Hidráulica Aplicada
Sección de Estudios de Posgrado e
Investigación
Escuela Superior de Ingeniería
Mecánica y Eléctrica.
INSTITUTO POLITÉCNICO
NACIONAL
Edificio 5, 3er. piso. Av. IPN s/n,
Colonia Lindavista, 07738, México
D.F.
Tel. 57296000 ext. 54754

COAUTOR

José Ángel Ortega Herrera
Profesor Investigador Miembro
SNI, AMC.
Sección de Estudios de Posgrado e
Investigación
Escuela Superior de Ingeniería
Mecánica y Eléctrica.
INSTITUTO POLITÉCNICO
NACIONAL
Edificio 5, 3er. piso. Av. IPN s/n,
Colonia Lindavista, 07738, México
D.F.
Tel. 57296000 ext. 54754

COAUTOR

Aldo Antonio Rueda Martínez
Estudiante de Doctorado en
Ingeniería Mecánica.
Laboratorio de Ingeniería
Térmica e Hidráulica Aplicada
Sección de Estudios de Posgrado
e Investigación
Escuela Superior de Ingeniería
Mecánica y Eléctrica.
INSTITUTO POLITÉCNICO
NACIONAL
Edificio 5, 3er. piso. Av. IPN s/n,
Colonia Lindavista, 07738,
México D.F.
Tel. 57296000 ext. 54754

ABSTRACT

The calculation of drops distribution in the exit of blades that have flow conditions of wet steam, in order to understand the causes that originate the erosion on the blades of the last stages in the low pressure section of steam turbines, is presented. Into the calculation of boundary layer on the blade surfaces, the velocity distribution for the stream frictionless and the drops in the flow line, on the basis of the frictionless, two-dimensional, stationary, transonic and homogenous flow is found. In this section, with help of a computational code for the generation of a stator blade mesh, an approximate movement of the droplets in blade cascades and the accumulation of droplets on the stator blades, flowing through the steam, is identified.

**THESIS BY: FERNANDO RUEDA MARTÍNEZ
LEADERSHIP: DR. MIGUEL TOLEDO VELÁZQUEZ**

Energy and Power Engineering, 2011, *, **

doi:****/epe.2011.***** Published Online ** 2011 (<http://www.scirp.org/journal/epe>)



Theoretical and Numerical Analysis of the Mechanical Erosion in Steam Turbine Blades. Part I

Rueda Martínez Fernando; Toledo Velázquez Miguel; Rueda Martínez Aldo Antonio; Sánchez Silva Florencio; Alcántara Montes Samuel; Huerta Chávez Oliver Marcel

*Applied Thermal and Hydraulic Engineering Laboratory
SEPI-ESIME-IPN Unidad Profesional "Adolfo Lopez Mateos"*

Av. IPN s/n, Col. Lindavista, 07738, México, D.F.

Tel.: 57296000 ext. 54783 / Fax 57296000 ext. 54754 E-mail: mtv49@yahoo.com

Abstract

The methodology of calculation of the velocity distribution for the stream frictionless and the drops in the flow line, on the basis of the frictionless, two-dimensional, stationary, transonic and homogenous flow is established. The knowledge of conditions that govern the low pressure section of steam turbines in the last stage to have an approximate movement of the droplets in the blade cascades and the accumulation of droplets on the stator blades, flowing through the steam, is presented. This study is used for developing a code in Fortran about the velocity distribution in the output of stator blades that have flow conditions of wet steam, in order to understand the causes that originate the erosion on the blades of the last stages in the low pressure section of steam turbines.

Keywords: Steam turbine, drop distribution, erosion stator-rotor blade, transonic flow.

Energy and Power Engineering, 2011, *, **
doi:****/epe.2011.***** Published Online ** 2011 (<http://www.scirp.org/journal/epe>)



Theoretical and Numerical Analysis of the Mechanical Erosion in Steam Turbine Blades. Part II

Rueda Martínez Fernando; Toledo Velázquez Miguel; Abugaber Francis Juan;
Carvajal Mariscal Ignacio; Polupan Giorgiy; Ortega Herrera José Ángel;
Rueda Martínez Aldo Antonio.

Applied Thermal and Hydraulic Engineering Laboratory, Lindavista, Mexico
E-mail: mtv49@yahoo.com

Received April 1, 2100; revised April 22, 2011; accepted April 30, 2011

Abstract

In the low pressure section of the steam turbines the damages are pronounced becoming remarkable in all the stages, since the generation of water liquid microparticles implies the impact on the blades having majors problems of erosion in the last stages by the increase of the humidity. In the first part of this work, the calculation presented of the transonic velocity field for the stream frictionless and the drops in the flow line, on the basis of the frictionless, two-dimensional, stationary, transonic and homogenous flow, give an approximate movement of the droplets and its accumulation on the stator blades, flowing through the steam. In order to understand the causes that originate the erosion on the blades of the last stages in low pressure section of steam turbines, the previous procedure is developed in a code in Fortran and the obtained results of velocity distribution in the output of blades that have flow conditions of wet steam are presented.

Keywords: Numerical Code, Mesh Blade, Erosion Blade, Steam Turbine, Drop Distribution.

Energy and Power Engineering, 2011, *, **
doi:****/epe.2011.***** Published Online ** 2011 (<http://www.scirp.org/journal/epe>)



Evaluation of the Gas Turbine Inlet Temperature with Relation to the Excess Air

**Fernando Rueda Martínez, Aldo Antonio Rueda Martínez, Miguel Toledo Velázquez,
Pedro Quinto Diez, Guilibaldo Tolentino Eslava, Juan Abugaber Francis**

Researching and Graduate Section
Applied Hydraulics and Thermal Engineering Laboratory
ESIME – IPN, mtv49@yahoo.com
Professional Unit “Adolfo López Mateos”, Edif. 5, 3^{er} piso SEPI-ESIME, 07738, Col.
Lindavista, México; D.F.
Tel. 729-6000 ext. 54356

Abstract

This paper shows the effect of excess air on combustion gas temperature at turbine inlet, and how it determines power and thermal efficiency of a gas turbine at different pressure ratios and excess air. In such a way an analytic equation that allows calculating the turbine inlet temperature as a function of excess air, pressure ratio and relative humidity is given. Humidity Impact on excess air calculation is also analyzed and presented. Likewise it is demonstrated that dry air calculations determine a higher level for calculations that can be performed on wet air.

Keywords: gas turbine, excess air, turbine inlet temperature, Dry air, Wet air.